Inelastic X-Ray Scattering & Lattice Dynamics

Esen **Ercan** Alp
Advanced Photon Source, Argonne National Laboratory

alp@anl.gov

NX School 2019
June 24, 2019, Argonne National Laboratory, Argonne, IL

Thanks : T. S. Toellner, J. Zhao, M. Y. Hu, A. Alatas, W. Bi, A. Said, T. Gog

Lattice dynamics for beginners

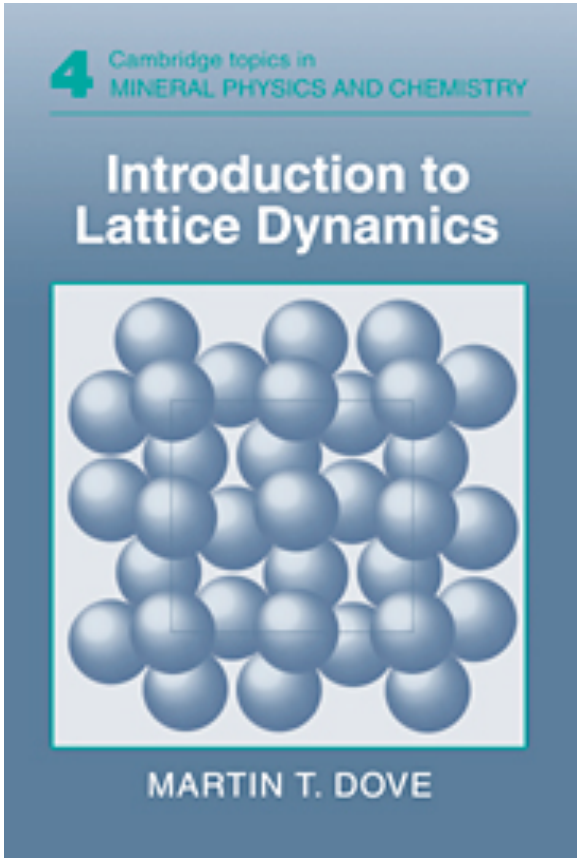

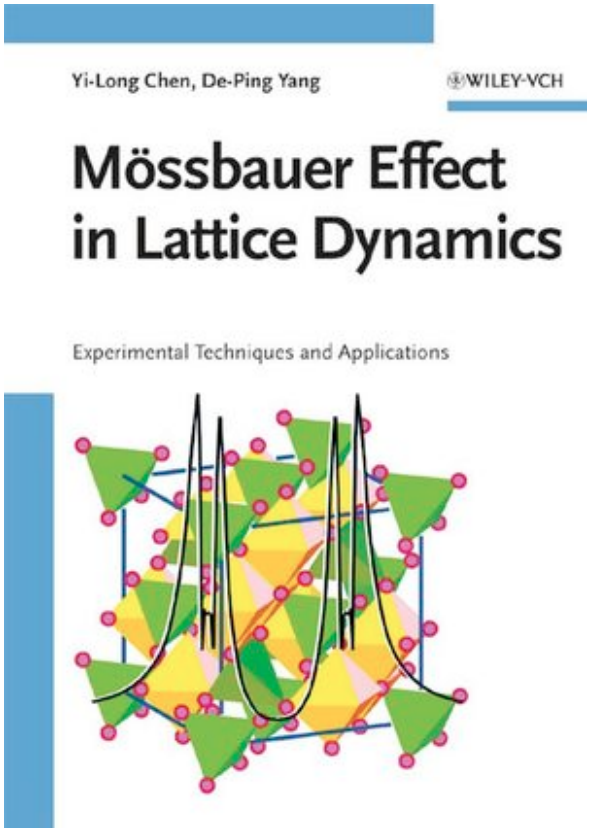

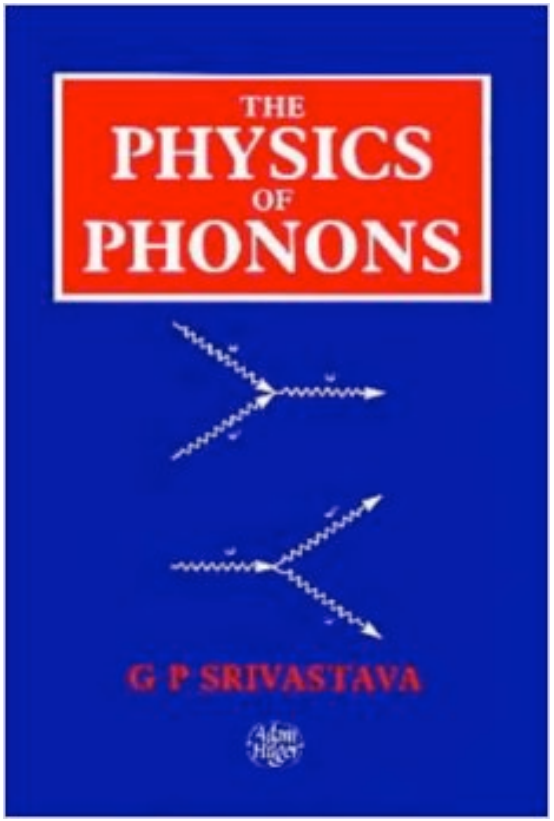

Inelastic X-Ray Scattering & Spectroscopy @ APS

IXS

MCS

RIXS

NRIXS

XRS

XES

NRIS

Compton

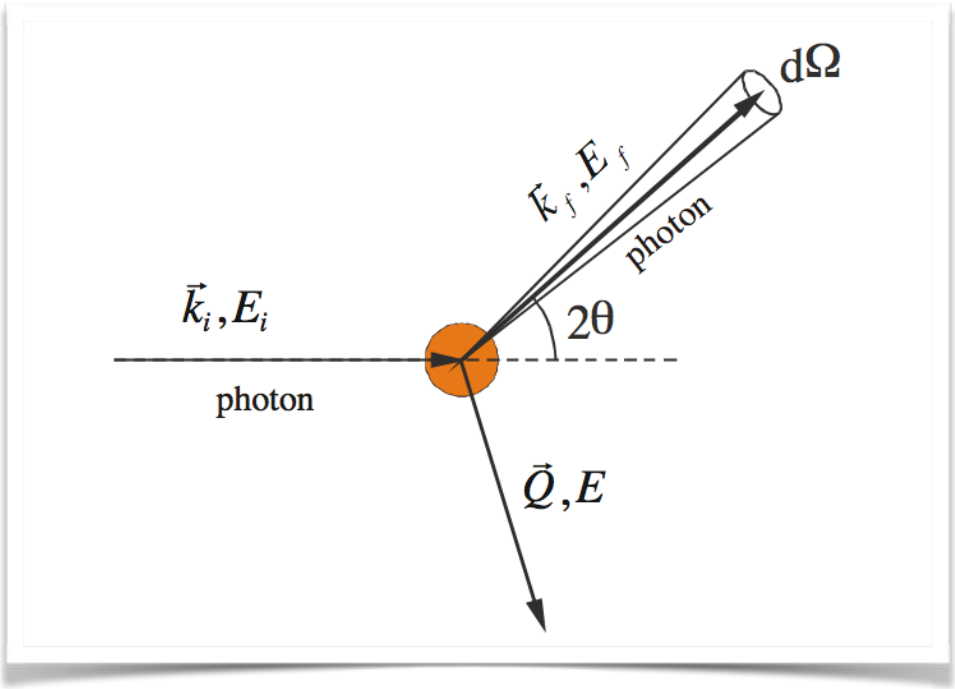

- Nuclear Resonant Inelastic X-Ray scattering, NRIXS: Sectors 3, 16, 30
- Momentum Resolved High Energy Resolution IXS (HERIX) Sectors 3, 30
- Resonant Inelastic X-Ray Scattering, RIXS : Sector 27
- X-Ray Raman Scattering, XRS : Sectors 13, 16, 20
- X-Ray Emission Spectroscopy, XES: Sectors 6, 13, 16, 17

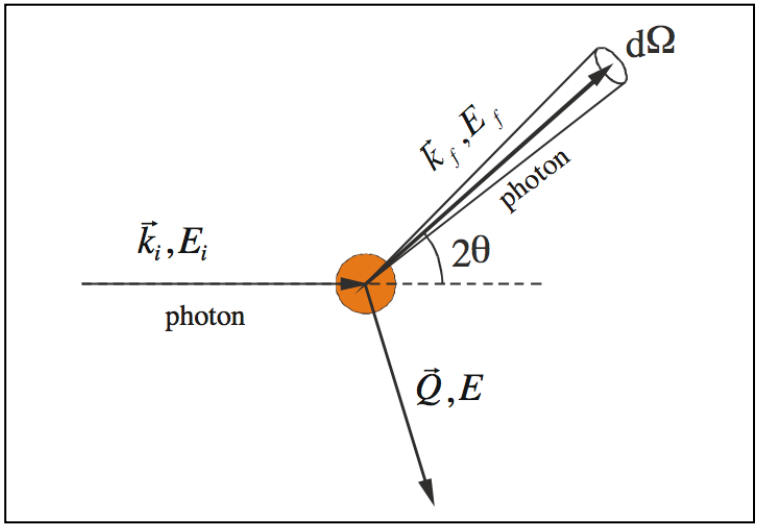

$E_i = E_f$: Elastic scattering

$E_i \neq E_f$: Inelastic scattering

The cause and magnitude of inelastic scattering determines which method to use.

The change in energy could be as little as nano-eV or as high as keV.

X-rays are quite different than other probes because:

i) large and small energy transfers are possible
ii) large momentum transfers at low energy is possible
iii) avoid multiple scattering by being a gentle probe
iv) polarization sensitivity
v) large energy tunability
vi) small beam size

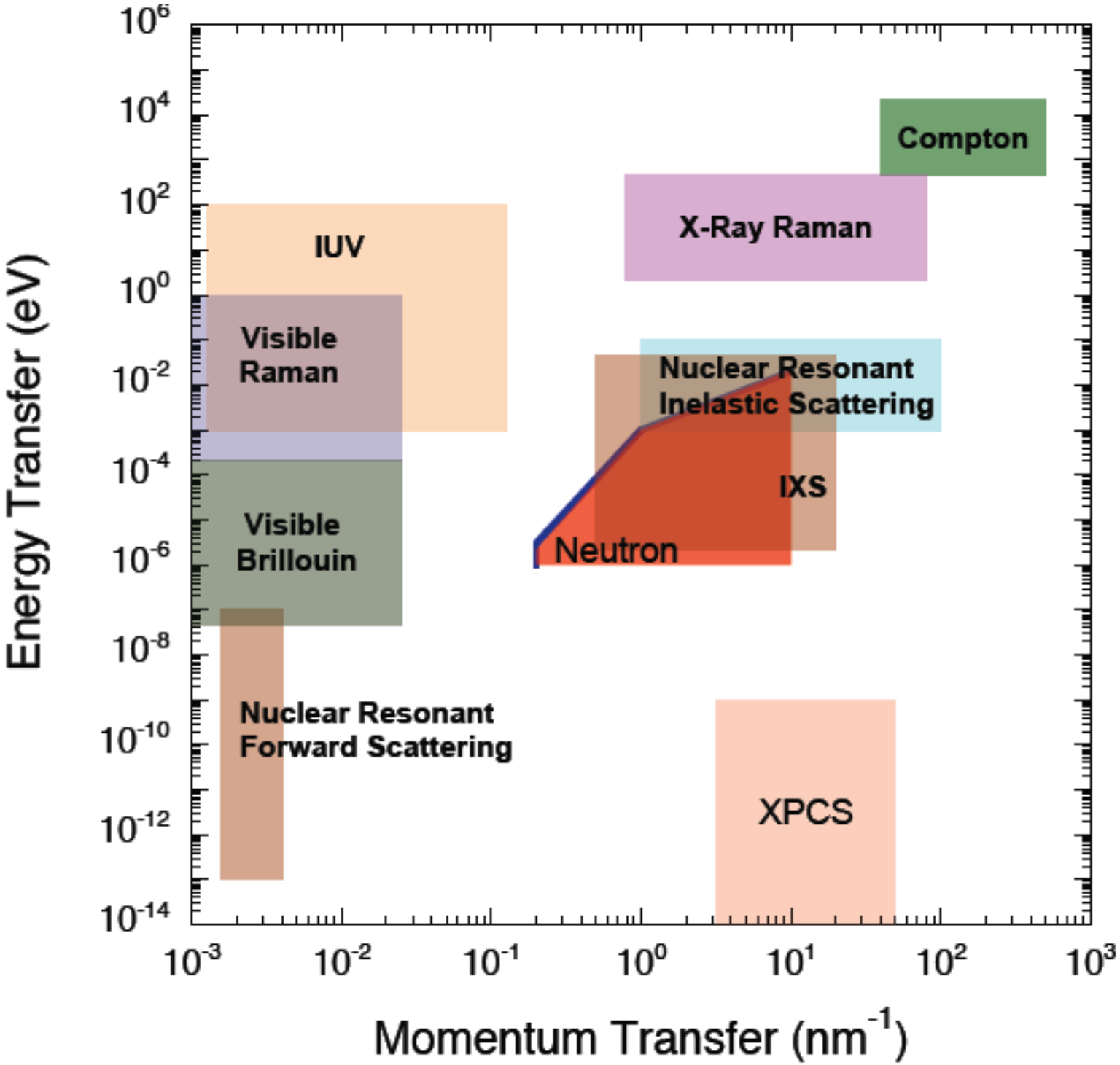
Energy Transfer (eV)
Momentum Transfer (nm^{-1})
10^{6}
10^{4}
10^{2}
10^{0}
10^{-2}
10^{-4}
10^{-6}
10^{-8}
10^{-10}
10^{-12}
10^{-14}
10^{-3}
10^{-2}
10^{-1}
10^{0}
10^{1}
10^{2}
10^{3}
Compton
X-Ray Raman
IUV
Visible Raman
Nuclear Resonant Inelastic Scattering
IXS
Neutron
Visible Brillouin
Nuclear Resonant Forward Scattering
XPCS

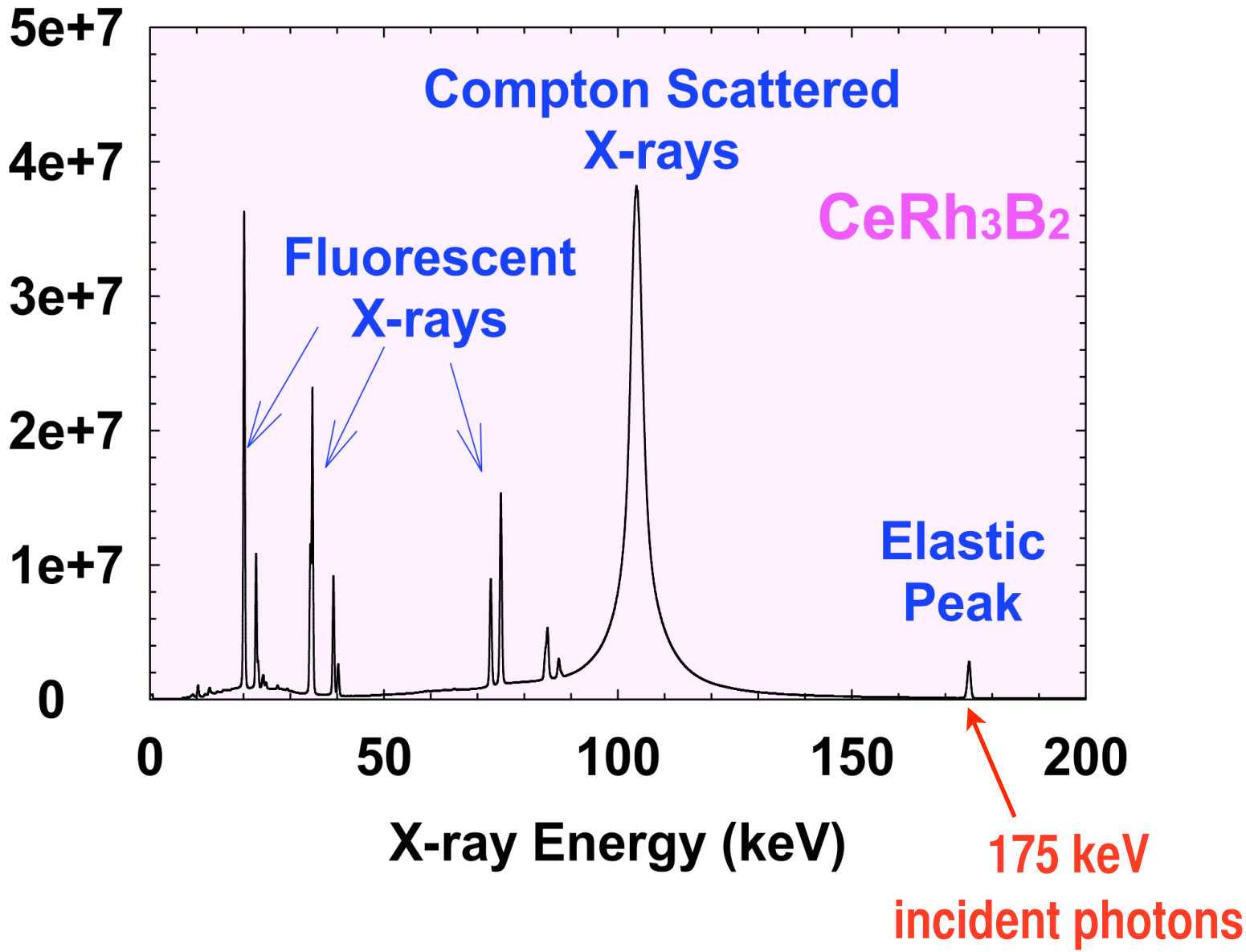

Courtesy: Y. Sakurai, Spring-8

Incident beam energy

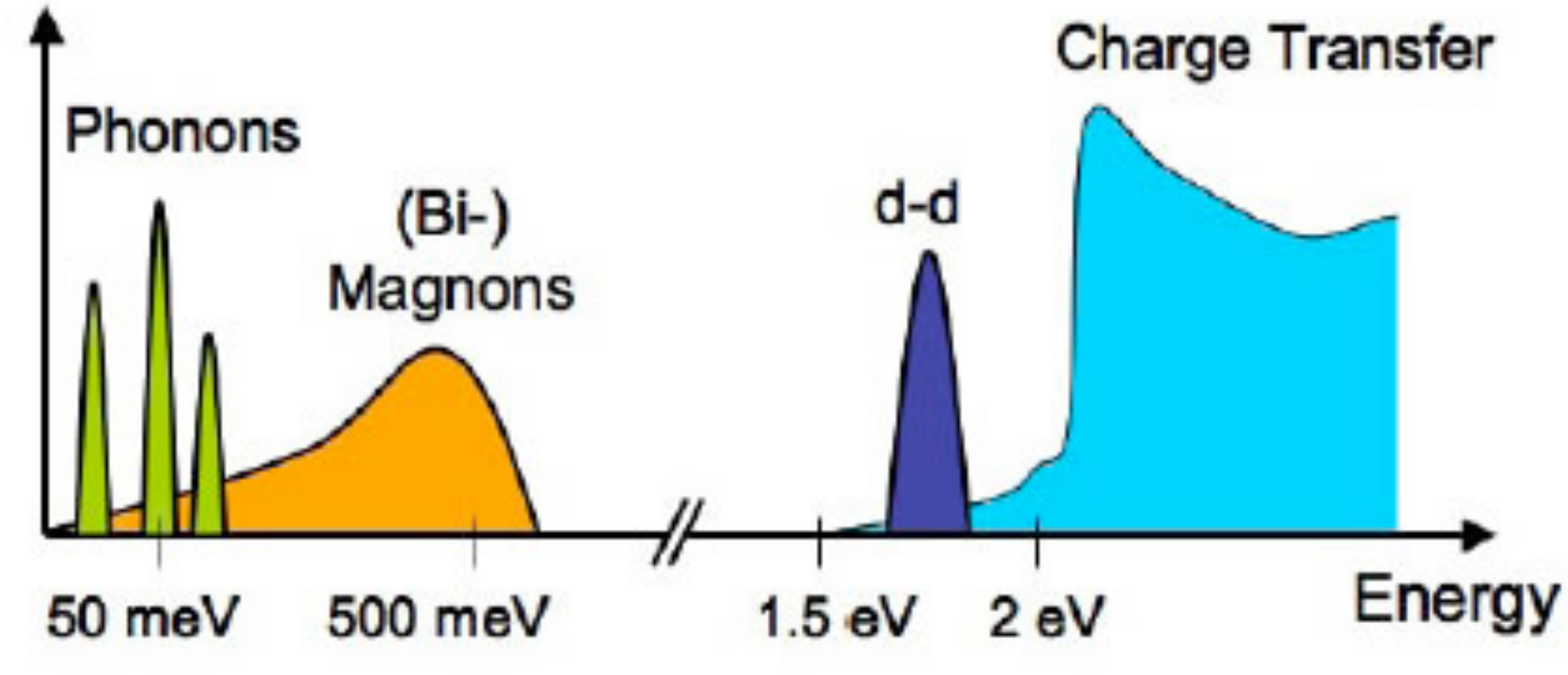

Lattice dynamics for beginners

Lattice dynamics describes vibrations of atoms in condensed matter:

- crystalline solids
- glasses, and
- liquids

However, some of the convenience gained by symmetry or periodic lattice is lost for glasses and liquids. Also, effect of surfaces and defects are glowing short-comings of the classical model.

Lattice dynamics is a reflection of forces acting upon atoms and leads to

- sound velocity: $\mathbf{V_s}$, $\mathbf{V_p}$
- vibrational entropy, $\mathbf{S_v}$
- specific heat, $\mathbf{C_p}$
- force constant, **<F>**
- compression tensor, $\mathbf{c_{11}}$, $\mathbf{c_{12}}$, $\mathbf{c_{44}}$
- Young's modulus, **E**
- Shear modulus, **G**
- stiffness and resilience
- Gruneisen constant, $\boldsymbol{\gamma}$
- viscosity, $\boldsymbol{\nu}$

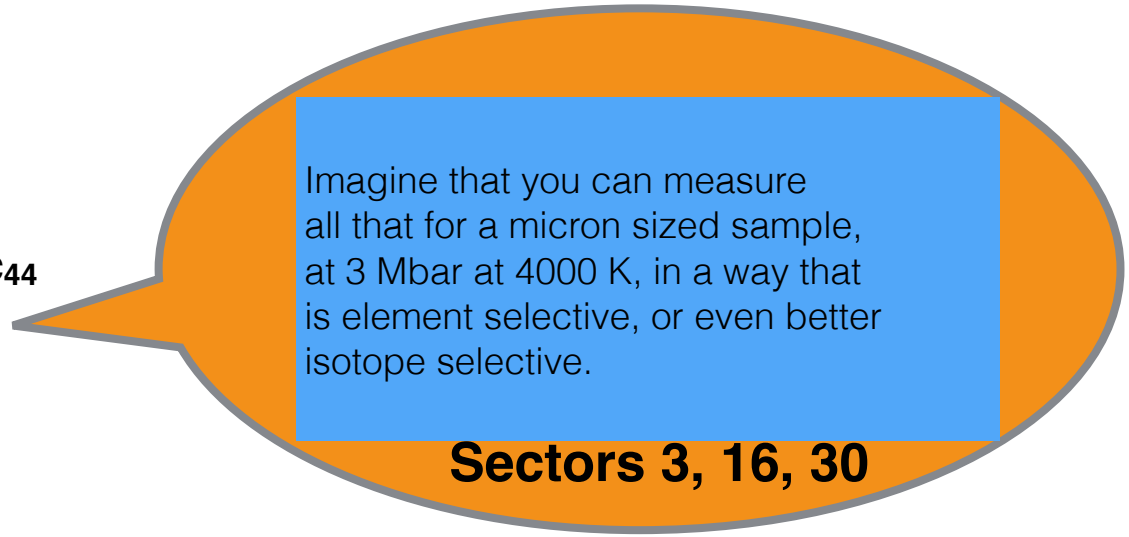

Many experimental techniques exist to study lattice dynamics

- sound velocity, deformation, thermal expansion,heat capacity….
- spectroscopic methods using light, x-rays and neutrons, and electrons
- point contact spectroscopy

Two main approximations should be noticed:

- **Born-Oppenheimer (adiabiatic) approximation**

  - Motion of atoms are independent and decoupled from the electrons.
  - All electrons follow the nuclei. This can be justified by considering the time scales involved: 10^{-15} s (femto) for electrons, 10^{-12} s (pico) for nuclei

- **Harmonic approximation**

  - At equilibrium, attractive and repulsive forces are balanced.
  - When atoms move away from the equilibrium positions, they are forced to come back by restoring forces.
  - Magnitude of atomic displacements are small compared to interatomic distance.
  - All atoms in equivalent positions in every unit cell move together.

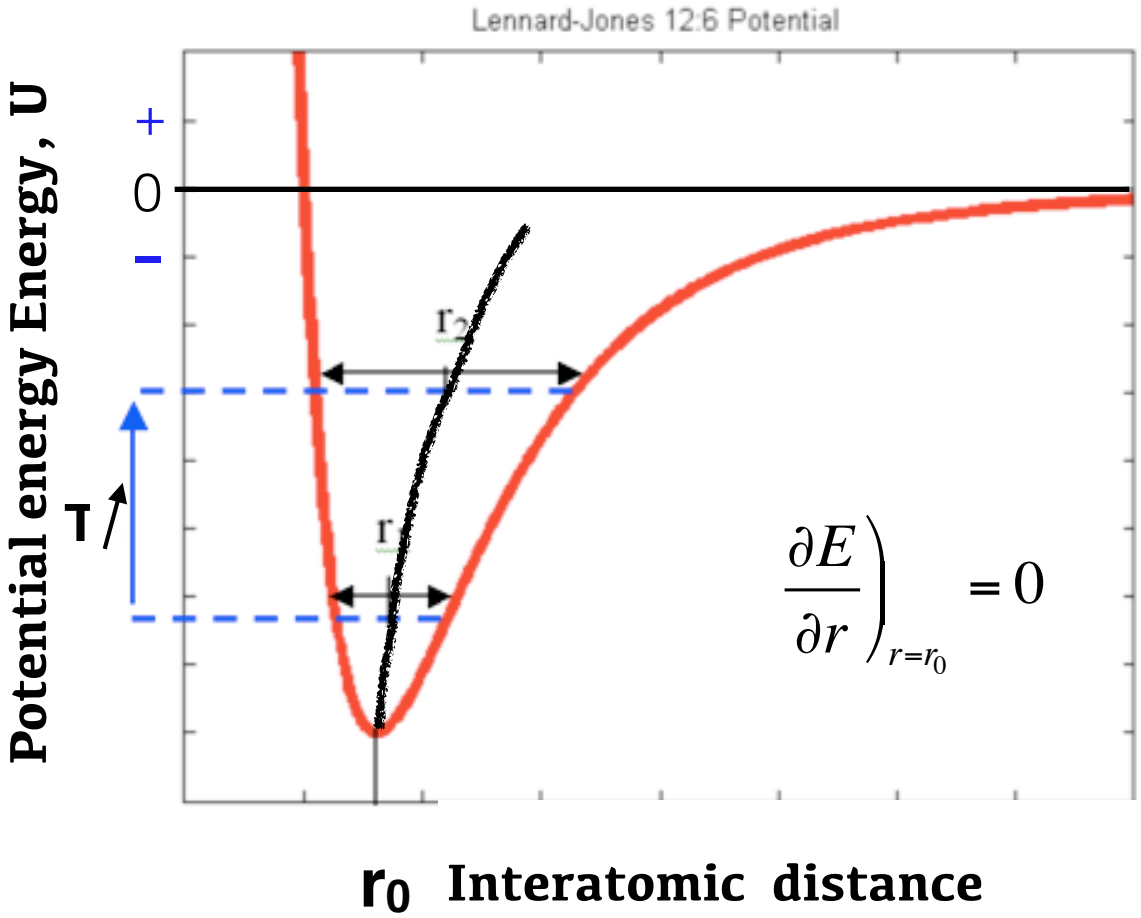

There should be no thermal expansion in the harmonic model.

The fact that there is thermal expansion is an indication that the potential under which the atoms move is not harmonic.

However, harmonic model has so many convenient features that we adopt it to explain many features of atomic vibrations.

$$E(r) = E_0 + \frac{1}{2}\left.\frac{\partial^2 E}{\partial r^2}\right|_{r_0}(r-r_0)^2 + \frac{1}{3!}\left.\frac{\partial^3 E}{\partial r^3}\right|_{r_0}(r-r_0)^3 + \frac{1}{4!}\left.\frac{\partial^4 E}{\partial r^4}\right|_{r_0}(r-r_0)^4 + \cdots$$

ignoring these terms is the harmonic approximation

Diatomic infinite 1-D chain

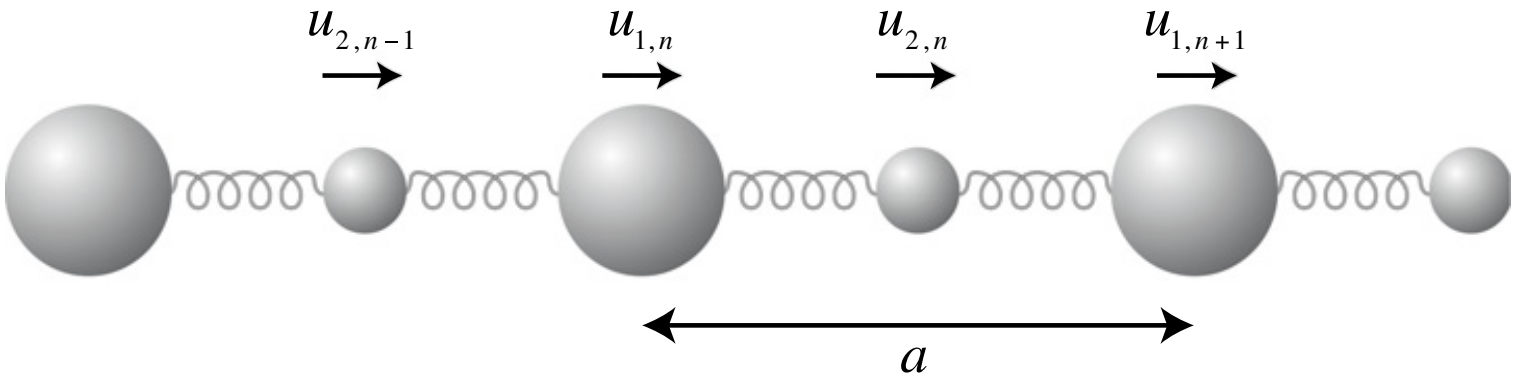

$$E = \frac{1}{2} J \sum_n (u_{1,n} - u_{2,n})^2 + \frac{1}{2} J \sum_n (u_{2,n} - u_{1,n+1})^2$$

$$J = \frac{\partial^2 E}{\partial u_{1,n} \partial u_{2,n}}$$

Force constant (spring constant)

$$u_{1,n}(t) = \tilde{u}_1 \exp\left(i(kna - \omega t)\right)$$

$$u_{2,n}(t) = \tilde{u}_2 \exp\left(i(kna - \omega t)\right)$$

Time dependent displacement of two atoms in terms of relative displacement of each atom

$$E_{1,n} = \frac{1}{2} J(u_{1,n} - u_{2,n})^2 + \frac{1}{2} J(u_{1,n} - u_{2,n-1})^2$$

$$E_{2,n} = \frac{1}{2} J(u_{2,n} - u_{1,n})^2 + \frac{1}{2} J(u_{2,n} - u_{1,n+1})^2$$

Energy

$$f_{1,n} = -\frac{\partial E_{1,n}}{\partial u_{1,n}} = -J(u_{1,n} - u_{2,n}) - J(u_{1,n} - u_{2,n-1})$$

$$f_{2,n} = -\frac{\partial E_{2,n}}{\partial u_{2,n}} = -J(u_{2,n} - u_{1,n}) - J(u_{2,n} - u_{1,n+1})$$

Force as derivative of energy

$$\ddot{u}_{1,n}(t) = -\omega^2 \tilde{u}_1 \exp i\,(kna - \omega t) = -\omega^2 u_{1,n}(t)$$

$$\ddot{u}_{2,n}(t) = -\omega^2 \tilde{u}_2 \exp i\,(kna - \omega t) = -\omega^2 u_{2,n}(t)$$

Acceleration

$$m_1 \ddot{u}_{1,n}(t) = -m_1 \omega^2 u_{1,n}(t) = -J(2u_{1,n}(t) - u_{2,n}(t) - u_{2,n-1}(t))$$

$$m_2 \ddot{u}_{2,n}(t) = -m_2 \omega^2 u_{2,n}(t) = -J(2u_{2,n}(t) - u_{1,n}(t) - u_{1,n+1}(t))$$

Newton's eqⁿ of motion

$$e_1 = m_1^{1/2}\tilde{u}_1; \quad e_2 = m_2^{1/2}\tilde{u}_2$$

Mass normalized displacements (real)

$$\omega^2 \begin{pmatrix} e_1 \\ e_2 \end{pmatrix} = \mathbf{D}(k) \cdot \begin{pmatrix} e_1 \\ e_2 \end{pmatrix}$$

Matrix form of Newton's eqⁿ of motion

$$\mathbf{D}(k) = \begin{pmatrix} 2J/m_1 & -J\left(1+\exp(-ika)\right)/\sqrt{m_1 m_2} \\ -J\left(1+\exp(+ika)\right)/\sqrt{m_1 m_2} & 2J/m_2 \end{pmatrix}$$

Eigen solutions

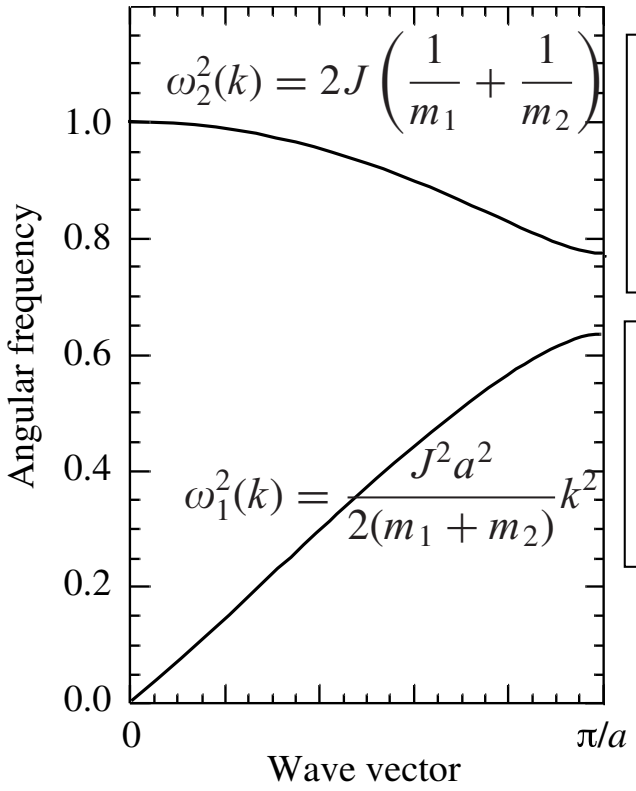

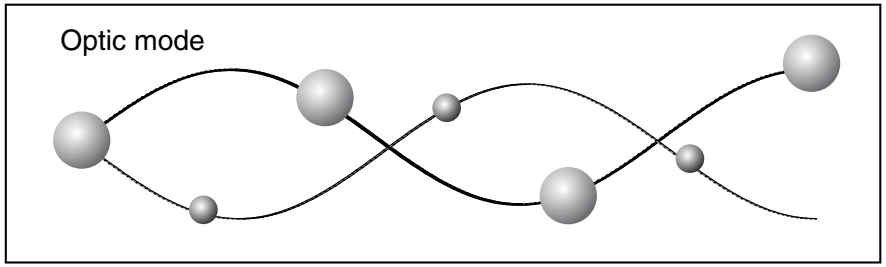

out-of-phase

$$m_1^{1/2} e_1 = -m_2^{1/2} e_2$$

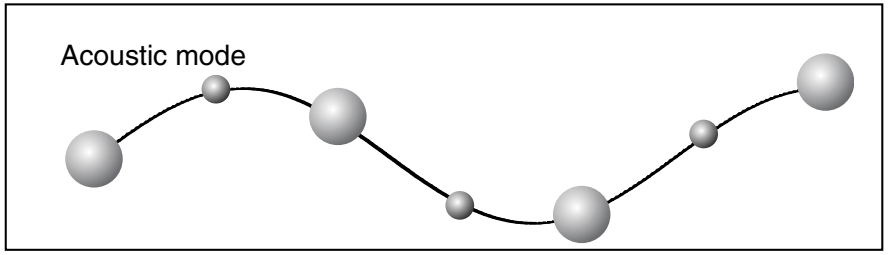

$$m_1^{-1/2} e_1 = m_2^{-1/2} e_2$$

in-phase

Inelastic X-Ray Scattering: A plethora of different techniques

IXS

Non-Resonant

Resonant

ΔE ~ meV
IXS

ΔE ~ 1 meV
Nuclear resonant

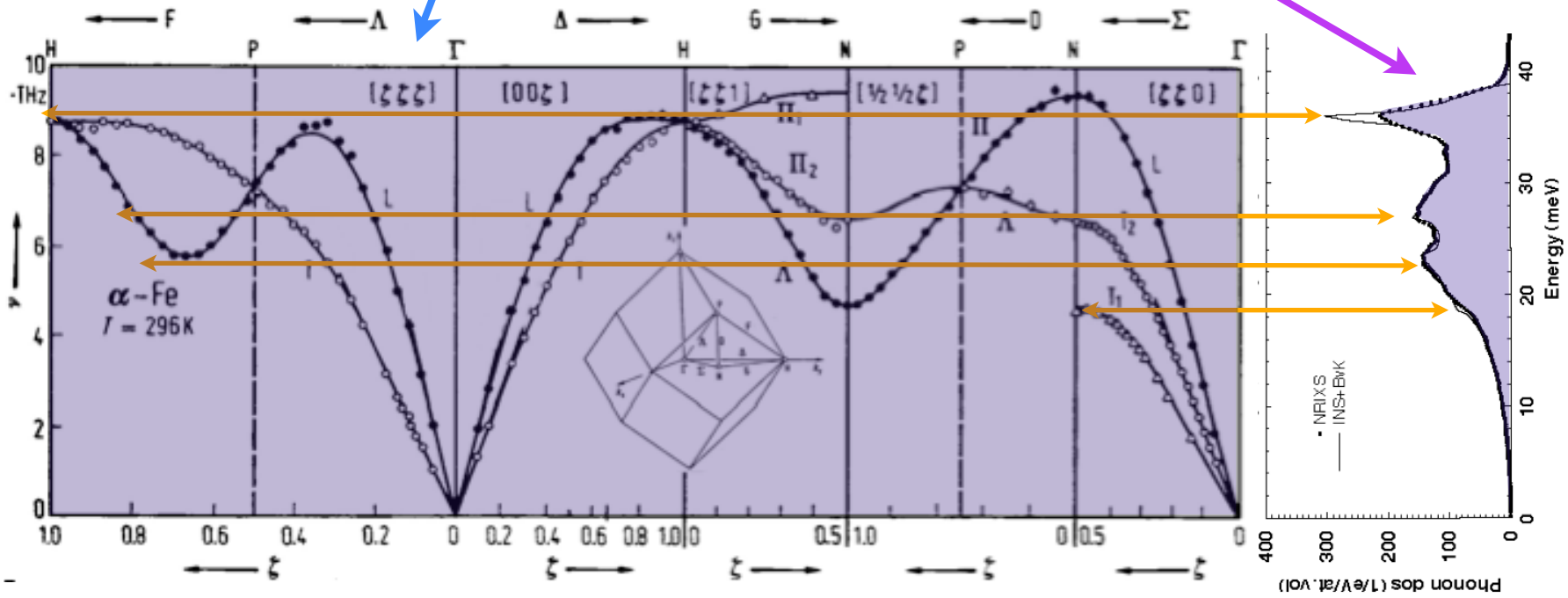

Diamond

Graphene

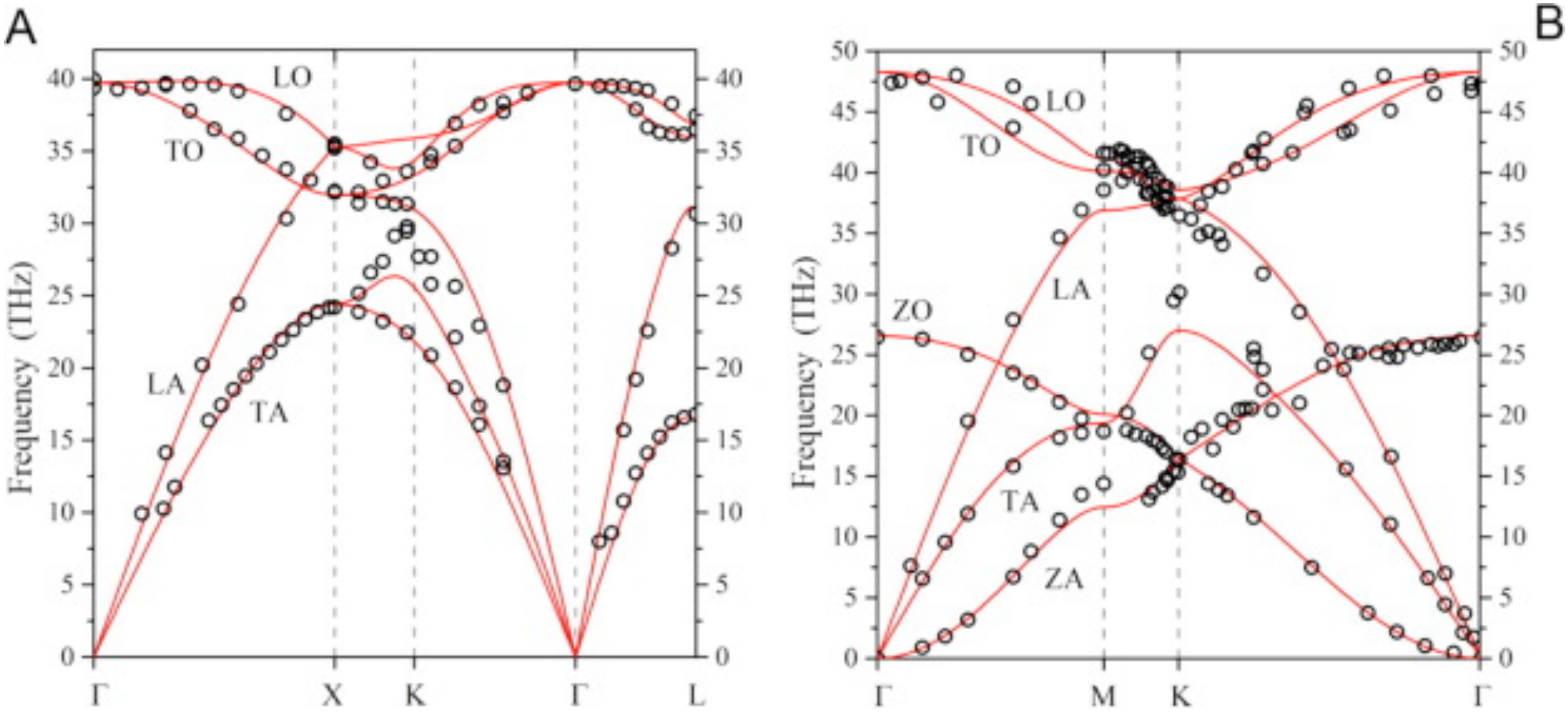

Umberto Monteverde, et al, 2015

HERIX-3 and HERIX-30

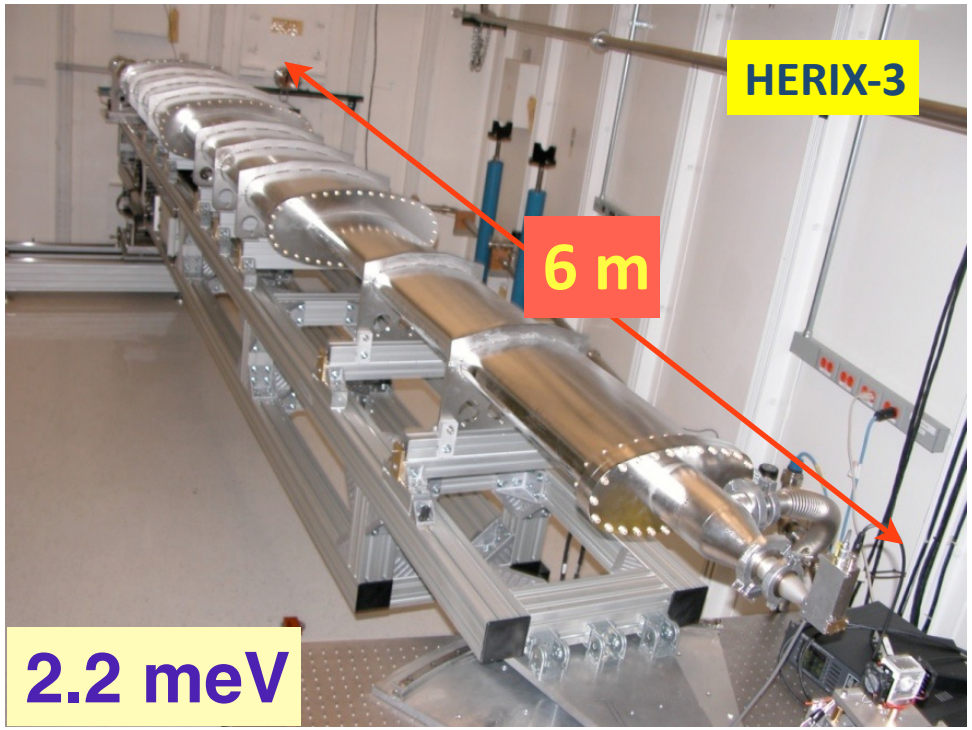

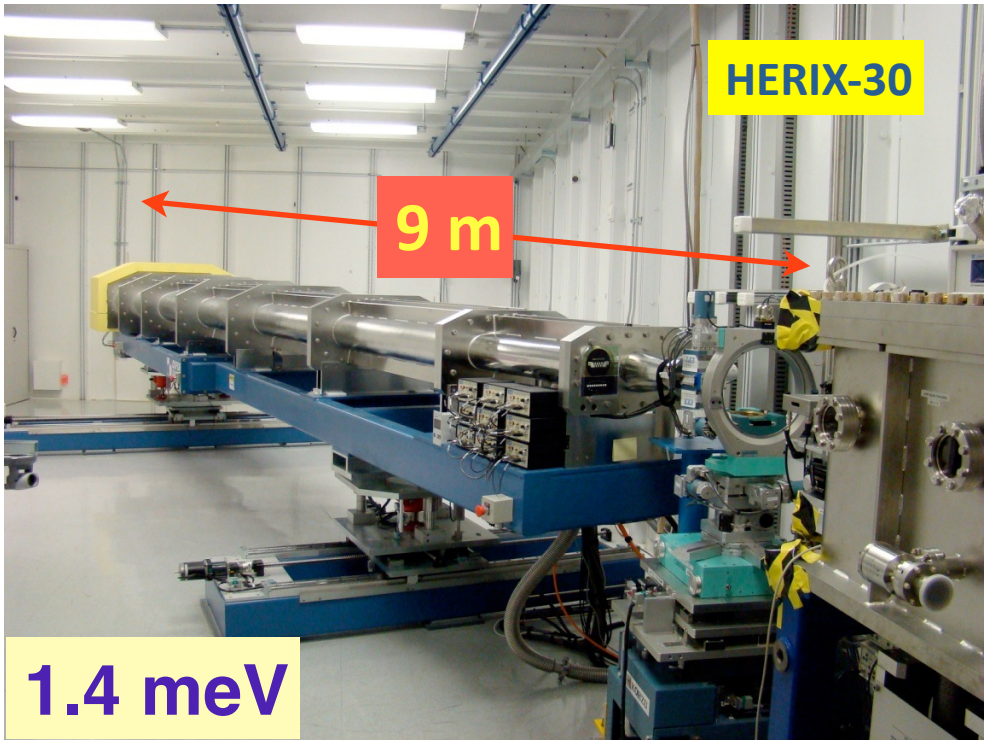

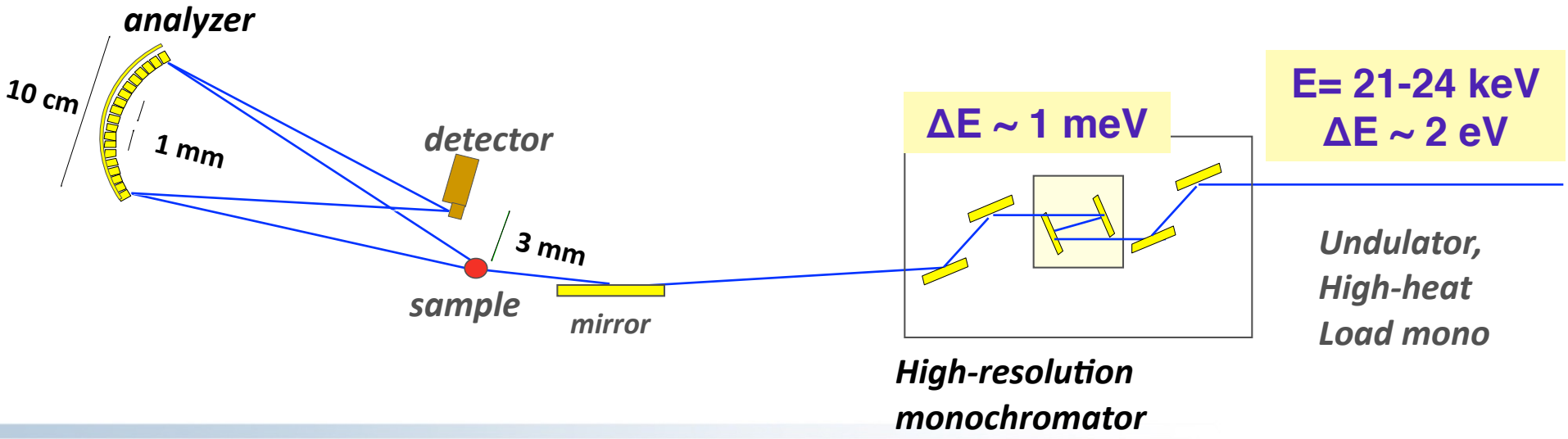

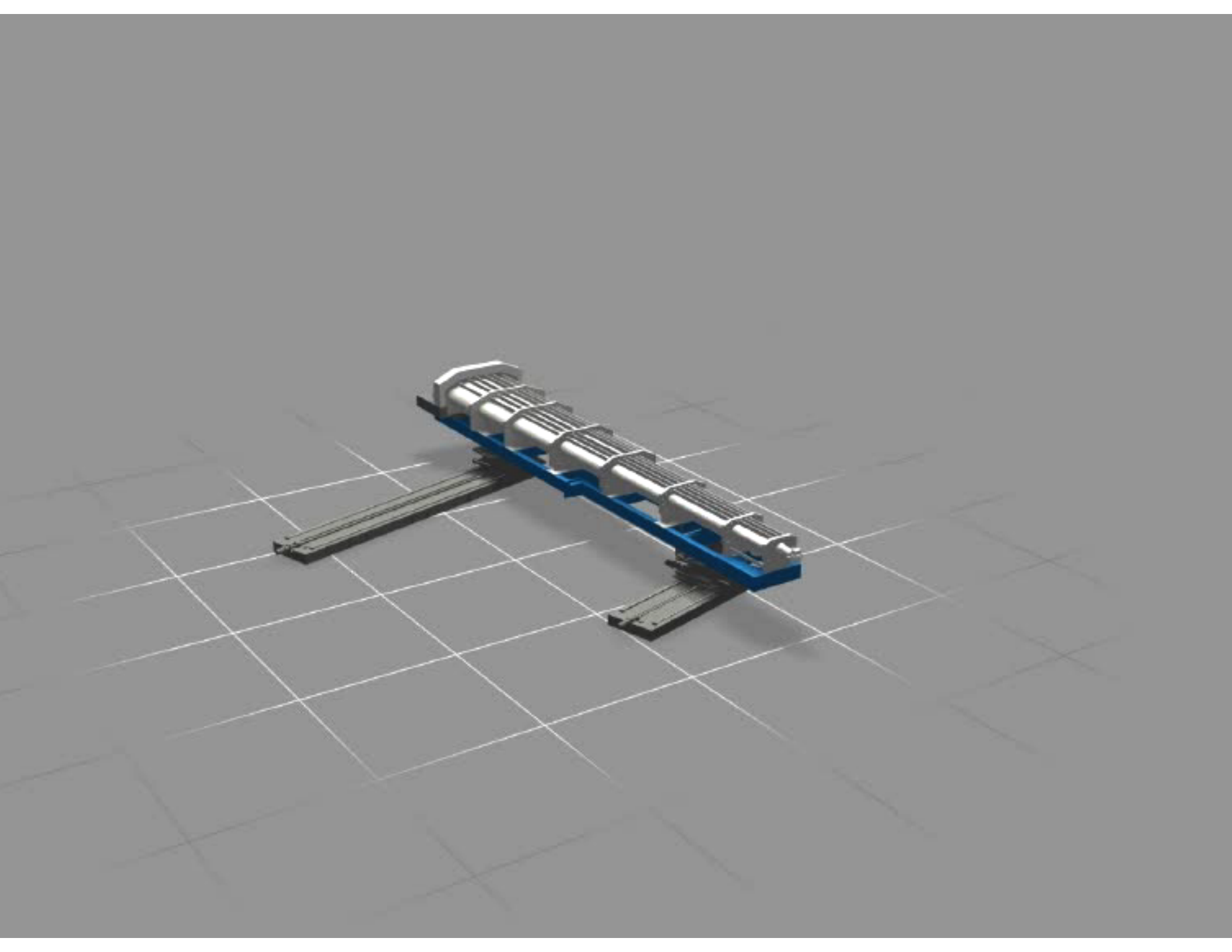

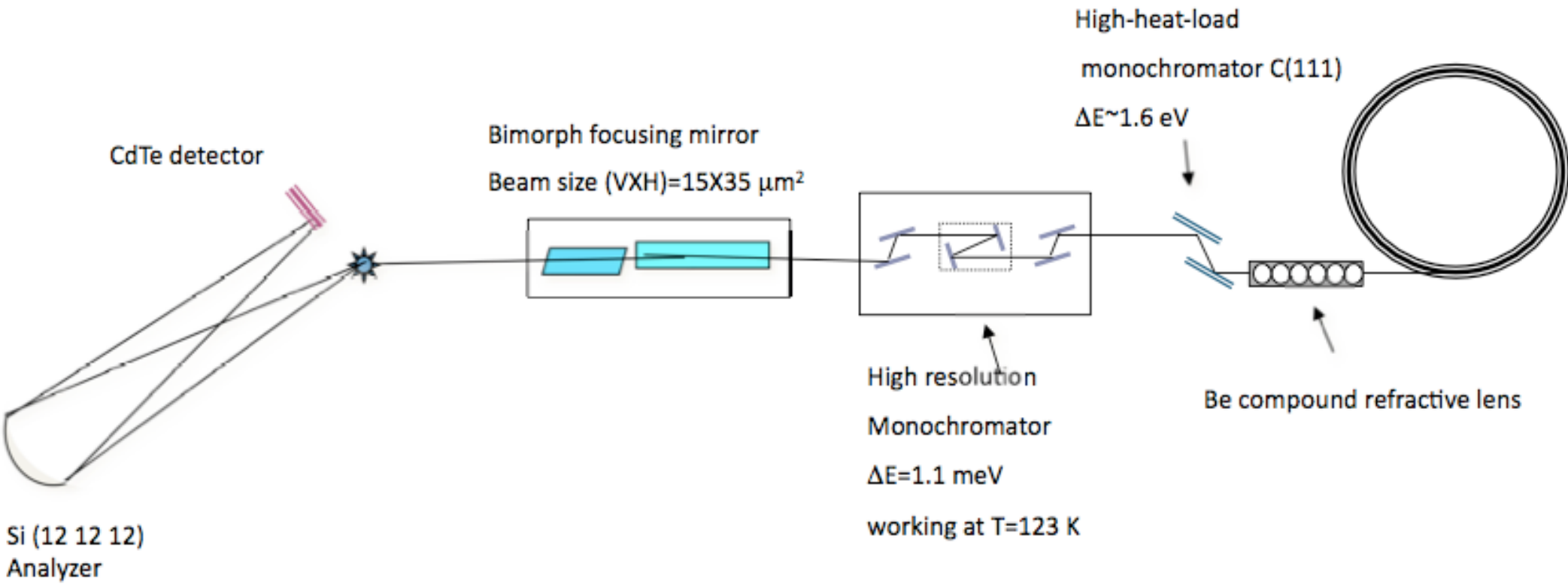
High-heat-load
monochromator C(111)
ΔE~1.6 eV
CdTe detector
Bimorph focusing mirror
Beam size (VXH)=15X35 μm²
High resolution
Monochromator
ΔE=1.1 meV
working at T=123 K
Be compound refractive lens
Si (12 12 12)
Analyzer

Choice of energy

Si Reflection at 90 °	Energy (keV)	Resolution (meV)	Reflectivity (%)
18 6 0	21.657	1.23	78
11 11 11	21.747	0.83	70
13 11 9	21.985	0.81	69
15 11 7	22.685	0.70	68
20 4 0	23.280	0.87	76
12 12 12	23.724	0.80	75
14 14 8	24.374	0.69	74
22 2 0	25.215	0.576	71
13 13 13	25.701	0.37	60

Bent-diced IXS analyzers

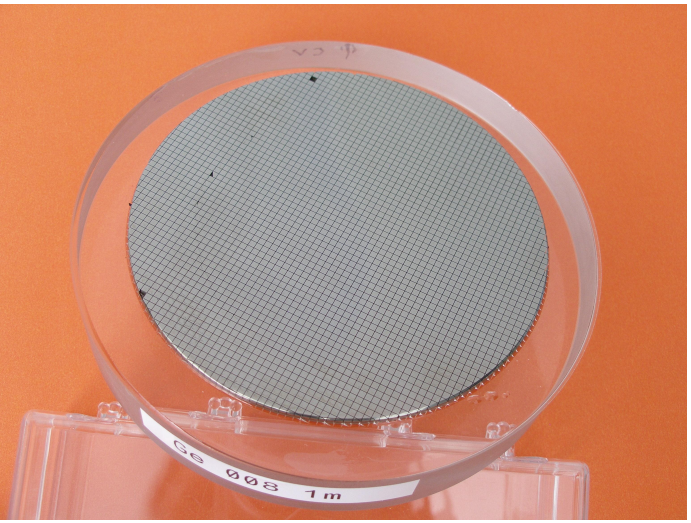

Si

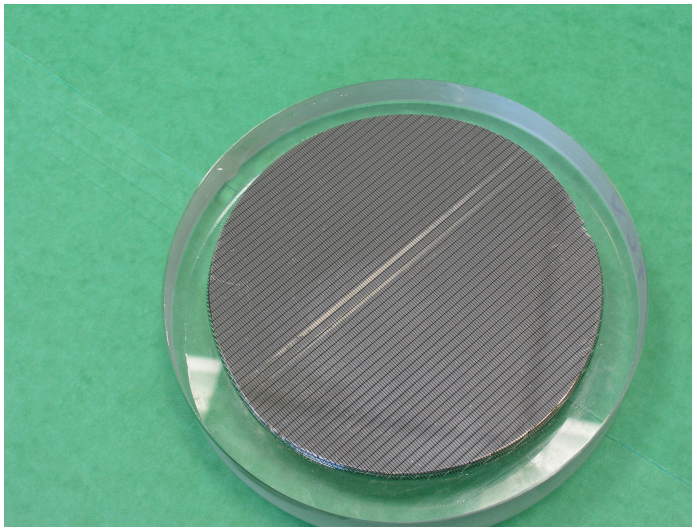

Ge

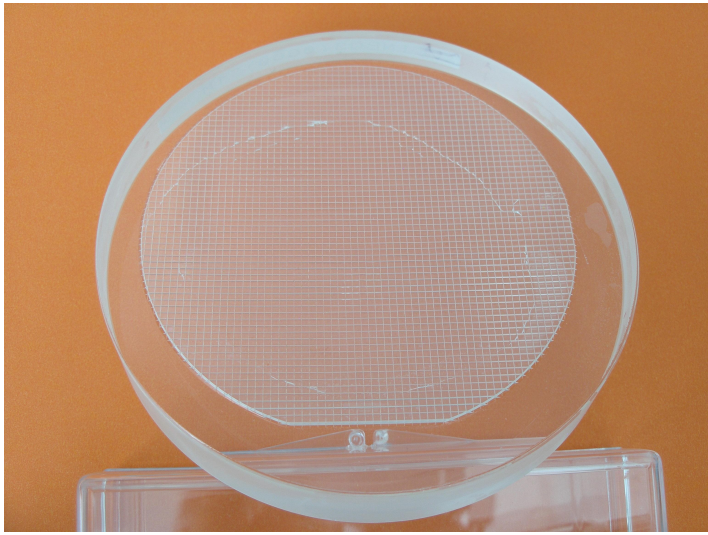

$LiNbO_3$

Generations of high-resolution monochromators

1992

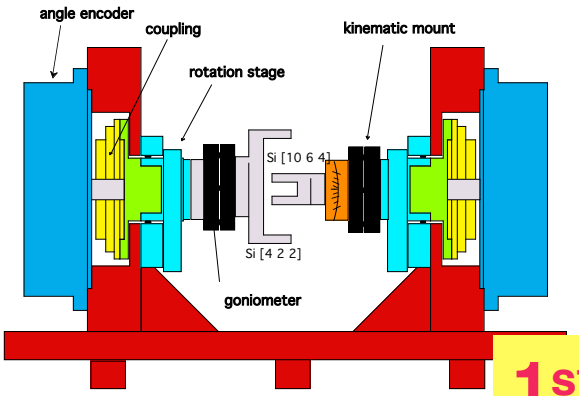

1st

1999

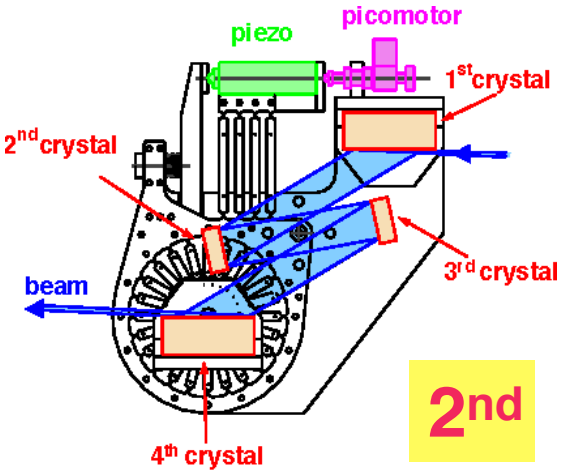

2nd

2002

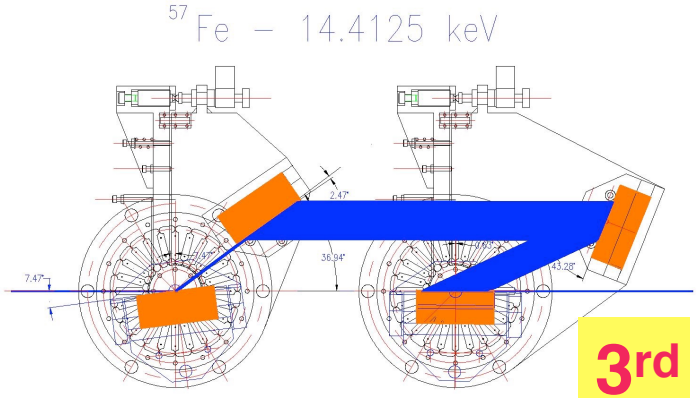

3rd

2004

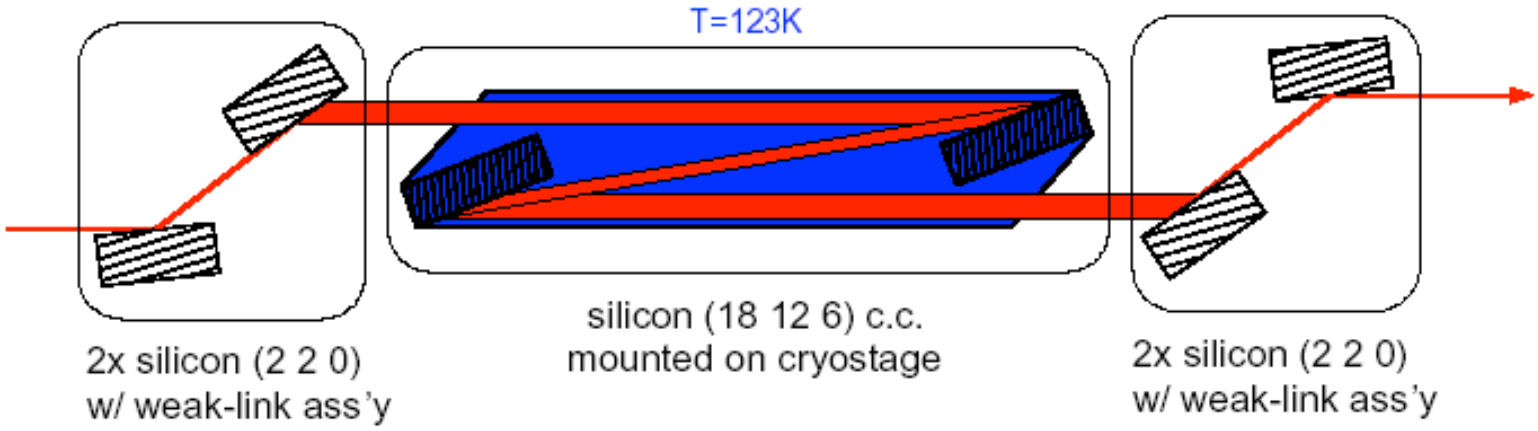

4th

T. Toellner, D. Shu

What is being measured ?

$$\frac{d^2\sigma}{d\Omega\, d\omega} = r_0^2 \frac{\omega_f}{\omega_i} \left|\mathbf{e}_i \cdot \mathbf{e}_f\right| N \sum_{i,f} \left| \left\langle i \left| \sum e^{i\mathbf{Q}\mathbf{r}_j} \right| f \right\rangle \right|^2 \delta(E_f - E_i - \mathbf{h}\omega)$$

Thomson cross section

Dynamical structure factor S(Q,w)

$$S(\mathbf{Q},\omega) = \frac{1}{2\pi} \int dt\, e^{-i\omega t} \left\langle \phi_i \left| \sum_{ll'} f_l(\mathbf{Q}) e^{-i\mathbf{Q}\cdot\mathbf{r}_l(t)} f_{l'}(\mathbf{Q}) e^{i\mathbf{Q}\cdot\mathbf{r}_{l'}(0)} \right| \phi_i \right\rangle$$

Density-density correlations

$$f(Q) = f_{ion}(Q) + f_{valence}(Q)$$

Atomic form factor

Dynamic structure factor

Sum over phonon branch j at reduced momentum transfer, q

Sum over different atoms in the unit cell

Atomic form factor for each atom

scaling with square root of mass

Debye-Waller factor to account for bond strength

phonon occupation probability

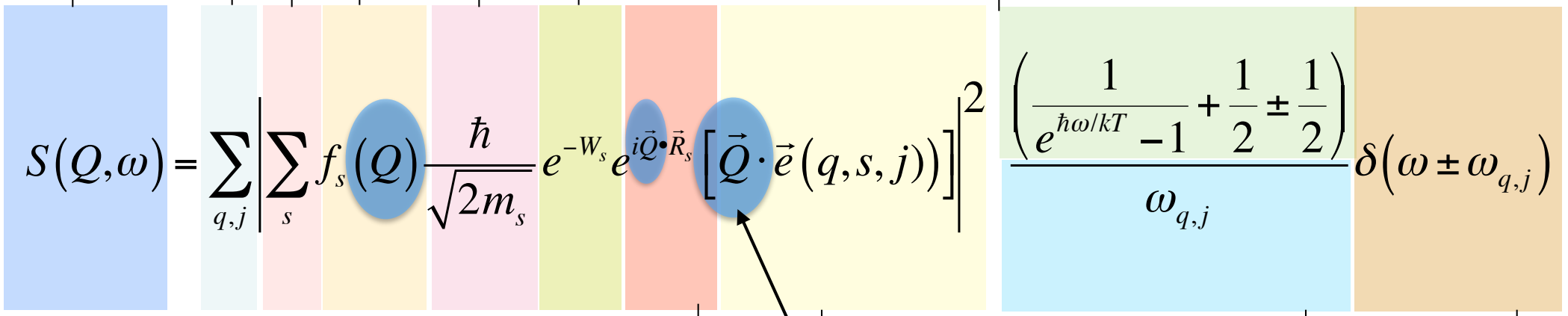

Phase of the scattering amplitude

phonon frequency

Polarization factor between momentum transfer and phonon's polarization vector

delta-function in ω

External probe-photon

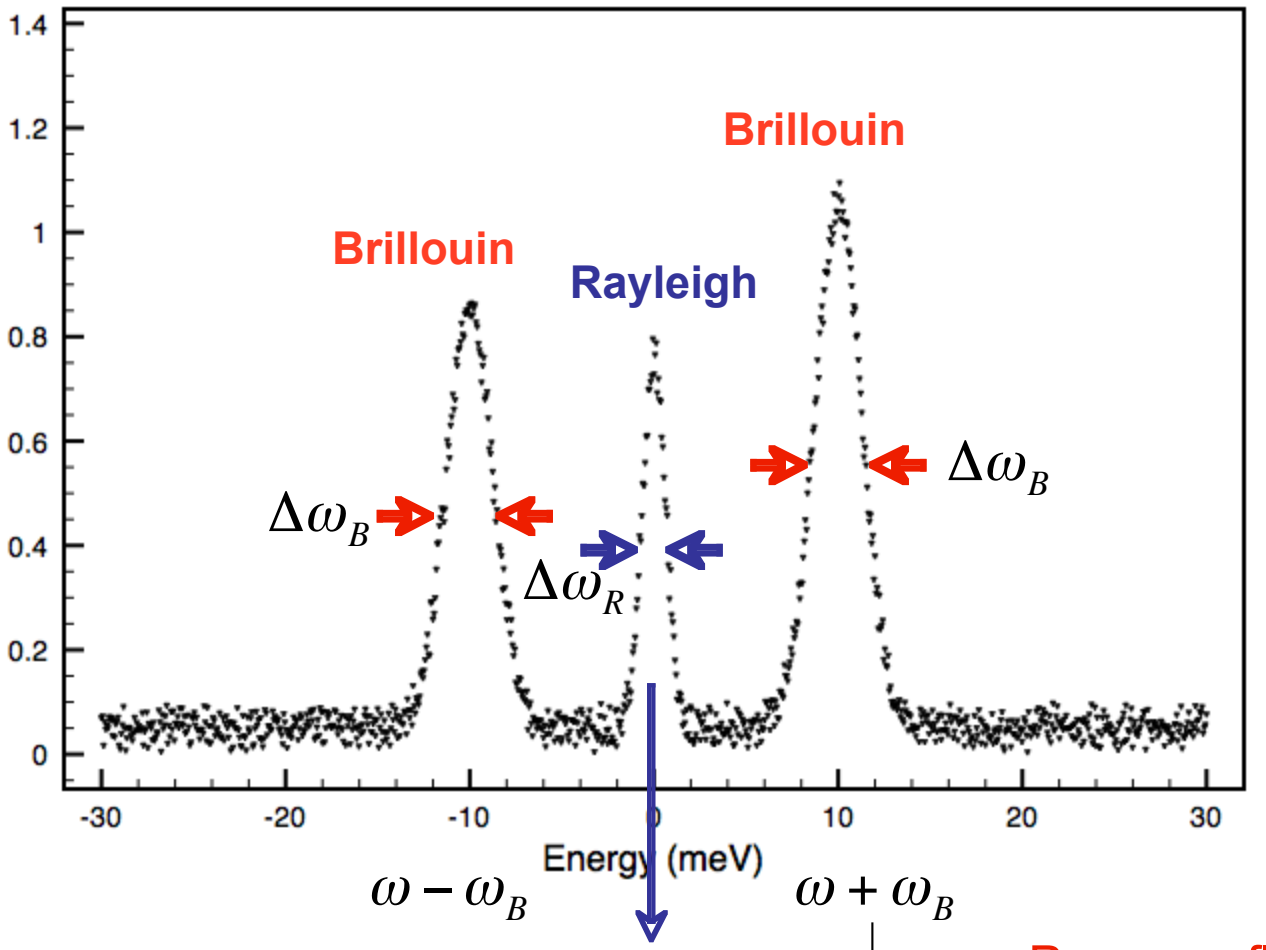

Entropy fluctuations, $\Delta\omega_R \sim \alpha q^2$

Concentration fluctuations $\Delta\omega_R \sim Dq^2$

Pressure fluctuations

$\omega_B(q) = V \cdot q$

$\Delta\omega_B \sim Vq^2$

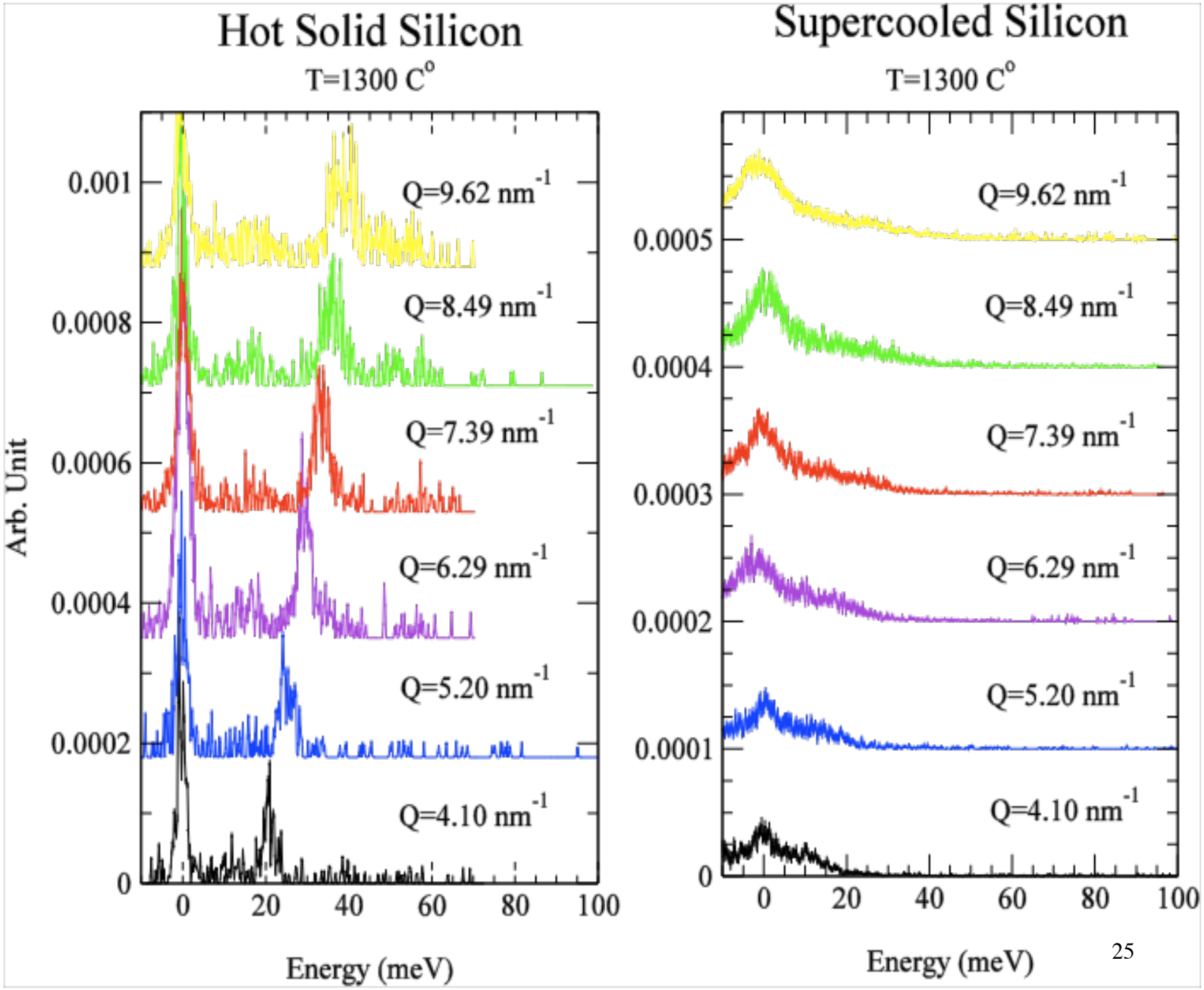
Hot Solid Silicon
T=1300 C°
Supercooled Silicon
T=1300 C°
Arb. Unit
Energy (meV)
Energy (meV)
Q=9.62 nm-1
Q=8.49 nm-1
Q=7.39 nm-1
Q=6.29 nm-1
Q=5.20 nm-1
Q=4.10 nm-1
0.001
0.0008
0.0006
0.0004
0.0002
0
0.0005
0.0004
0.0003
0.0002
0.0001
0
0
20
40
60
80
100

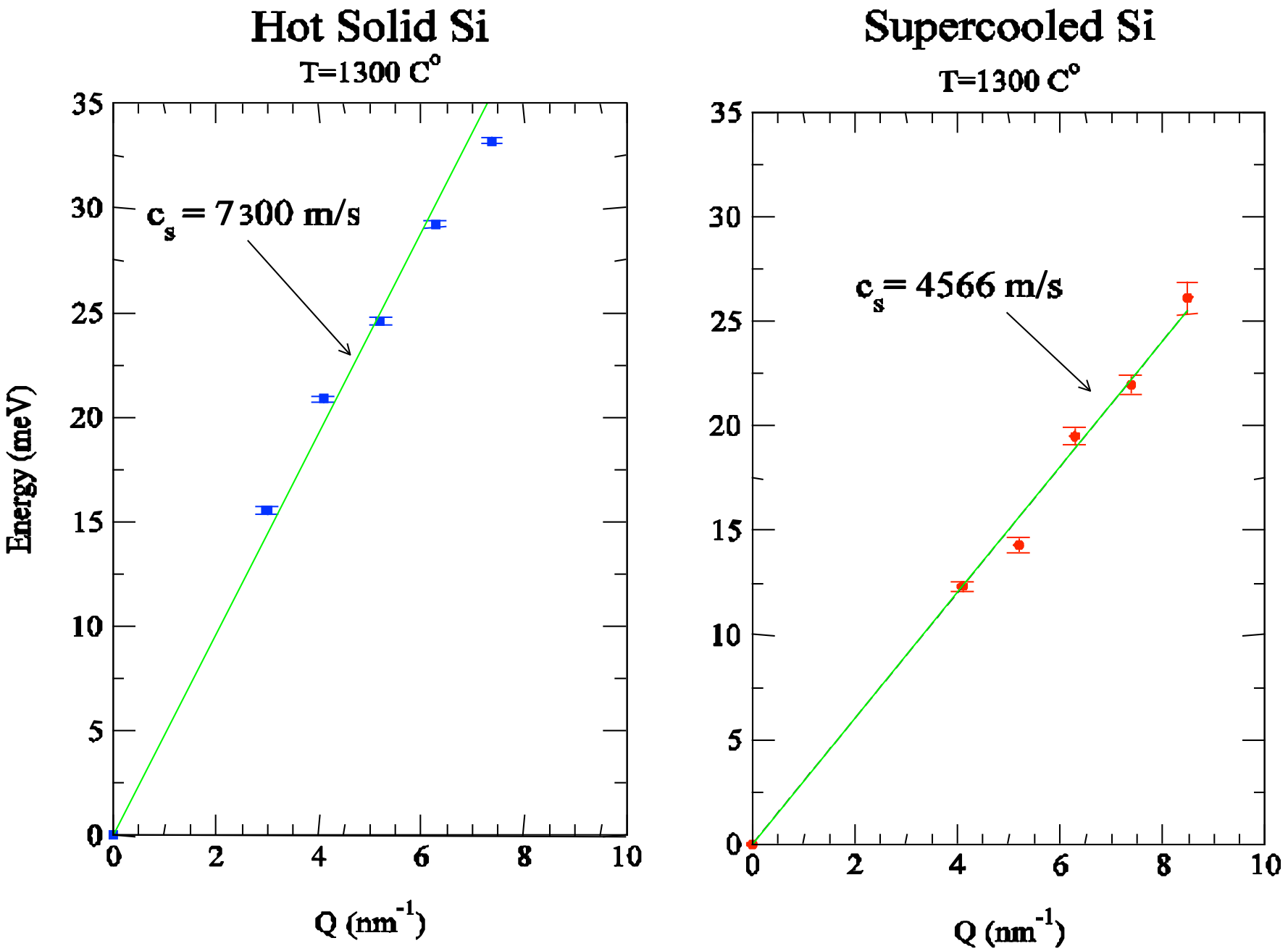
Hot Solid Si
T=1300 C°
c_s = 7300 m/s
Energy (meV)
Q (nm^-1)
Supercooled Si
T=1300 C°
c_s = 4566 m/s
Q (nm^-1)

PHONON's: $\phi\omega\nu\acute{\eta}$ (phonē), *sound*

- Phonons are periodic oscillations in condensed systems.

- They are inherently involved in thermal and electrical conductivity.

- They can show anomalous (non-linear) behavior near a phase transition.

- They can carry sound (acoustic modes) or couple to electromagnetic radiation or neutrons (acoustical and optical).

- Have energy of $\hbar\omega$ as quanta of excitation of the lattice vibration mode of angular frequency ω. Since momentum, $\hbar k$, is exact, they are delocalized, collective excitations.

- Phonons are bosons, and they are not conserved. They can be created or annihilated during interactions with neutrons or photons.

- They can be detected by Brillouin scattering (acoustic), Raman scattering, FTIR (optical).

- Their dispersion throughout the BZ can ONLY be monitored with x-rays (IXS), or neutrons (INS).

- Accurate prediction of phonon dispersion require correct knowledge about the force constants: COMPUTATIONAL TECHNIQUES ARE ESSENTIAL.

$$\omega^2 \mathbf{e} = \mathbf{D}(\mathbf{k}) \cdot \mathbf{e} \quad \Rightarrow \quad \omega^2 = \mathbf{e}^{\mathrm{T}} \cdot \mathbf{D}(\mathbf{k}) \cdot \mathbf{e}$$

Eigenvalue eqⁿ.

$$D_{j,j'}(\mathbf{k}) = \frac{1}{\sqrt{m_j m_{j'}}} \sum_{n'} \Phi_{0,n'}^{j,j'} \exp\left(i\mathbf{k} \cdot (\mathbf{r}_{j,0} - \mathbf{r}_{j',n'})\right)$$

Dynamical matrix

$$\mathbf{e}_\lambda^{\mathrm{T}} \cdot \mathbf{e}_\lambda = 1; \quad \mathbf{e}_{\lambda'}^{\mathrm{T}} \cdot \mathbf{e}_\lambda = \delta_{\lambda',\lambda}$$

Eigenvalues are orthonormal..

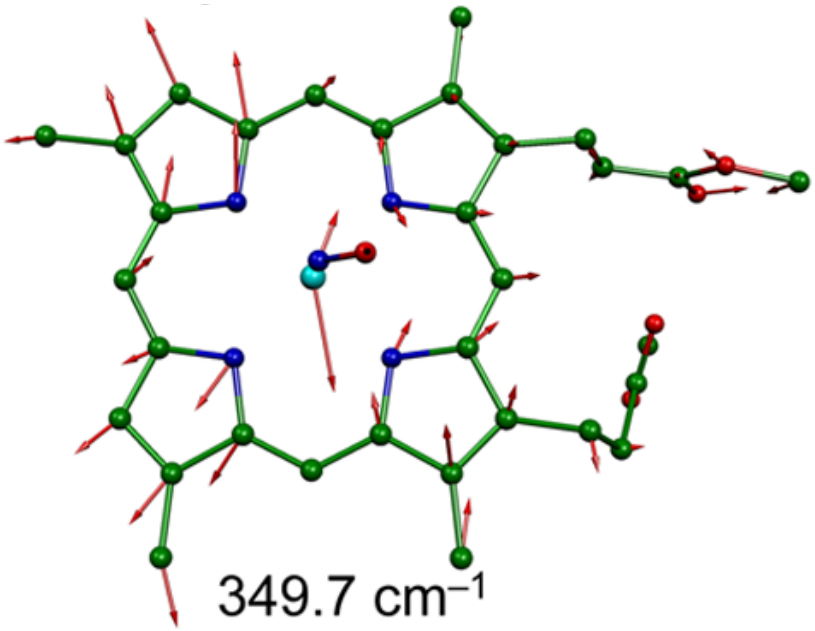

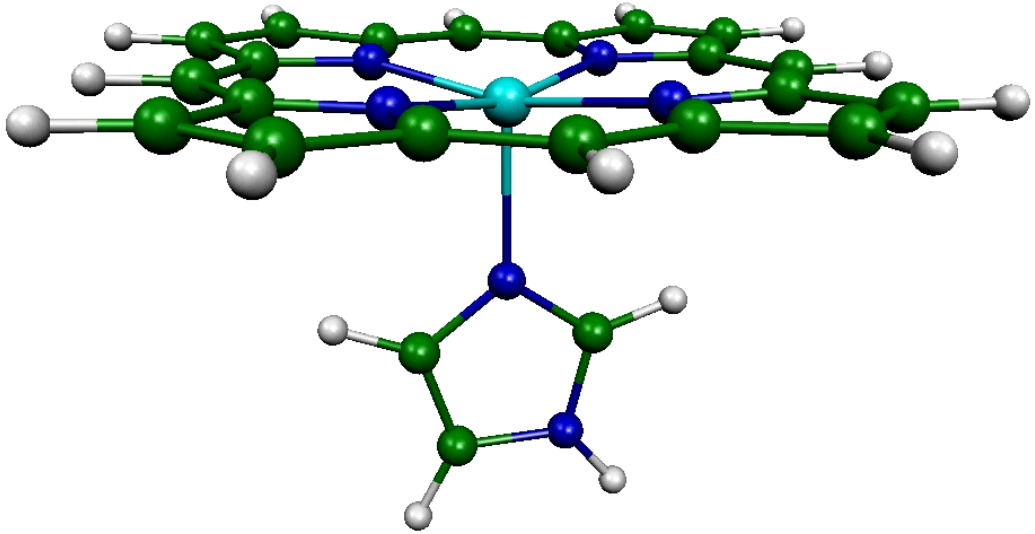

symmetrical stretching

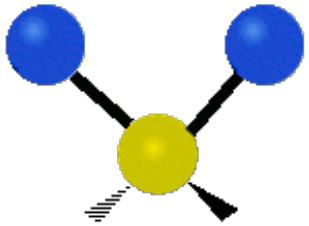

asymmetrical stretching

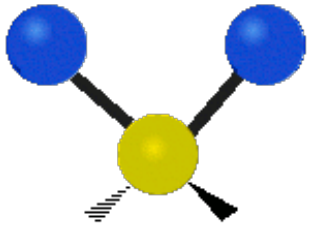

scissoring

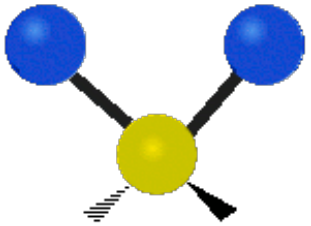

rocking

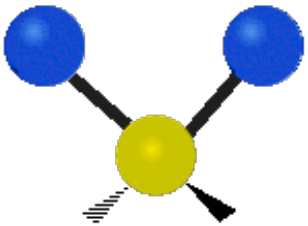

wagging

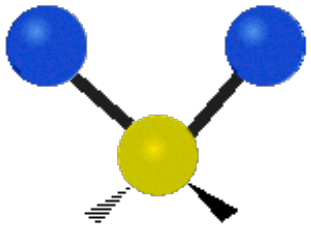

twisting

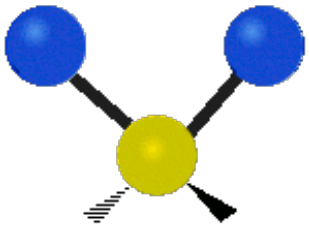

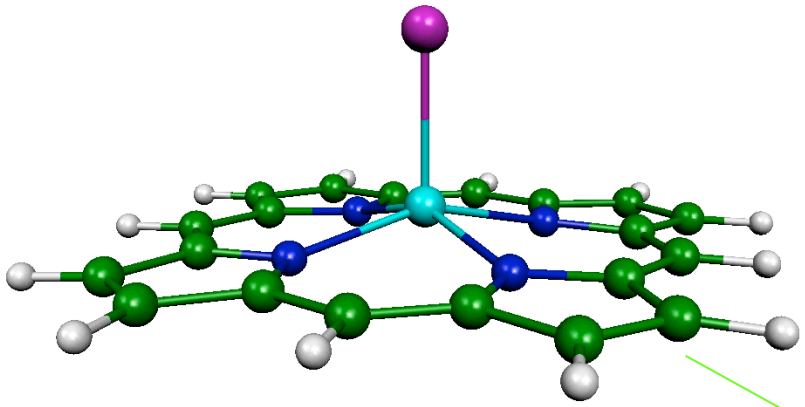

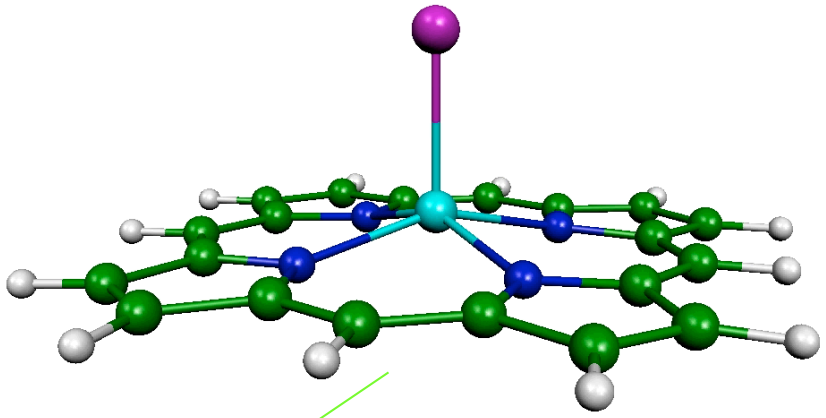

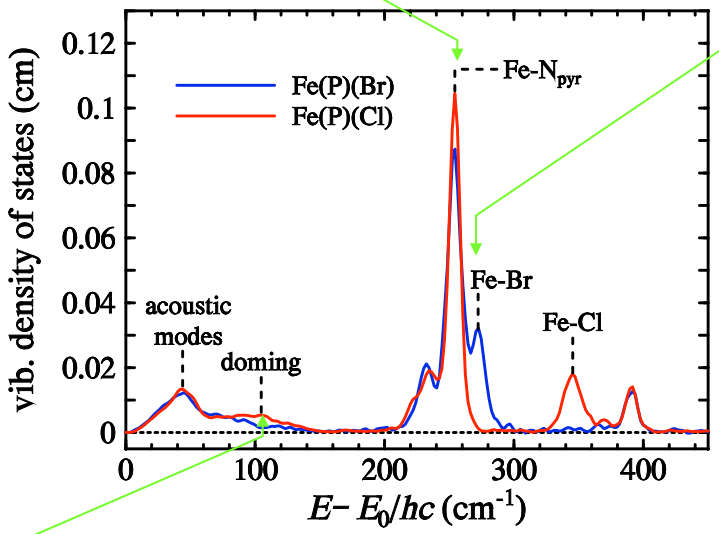
vib. density of states (cm)
0.12
0.1
0.08
0.06
0.04
0.02
0
Fe(P)(Br)
Fe(P)(Cl)
Fe-N$_{pyr}$
Fe-Br
Fe-Cl
acoustic
modes
doming
0
100
200
300
400
$E - E_0/hc$ (cm^{-1})

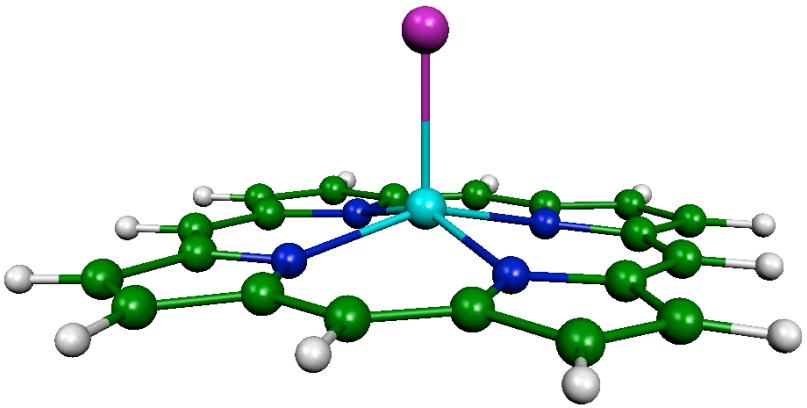

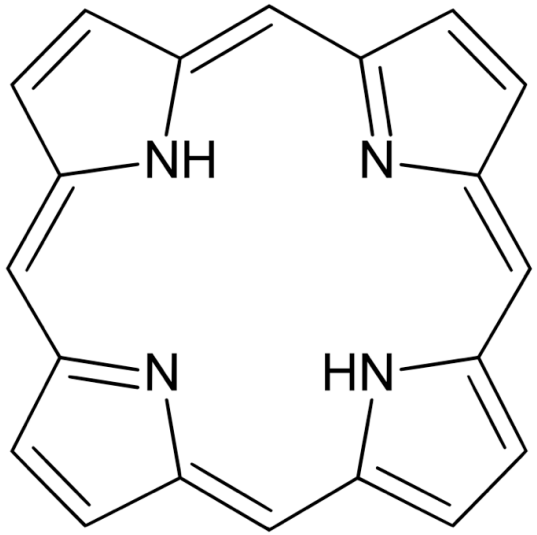
NH
N
N
HN

PHONONS (cont'd)

$$E_n = \left(n + \frac{1}{2}\right)\hbar\omega$$

Energy of a single oscillation as a function of number of phonons. The second term +1/2 is the "zero-point" energy.

$$E = \sum_{\mathbf{k},\lambda} \omega^2_{\mathbf{k},\lambda} \left|Q\left(\mathbf{k},\lambda\right)\right|^2 = \sum_{\mathbf{k},\lambda} \left(n_{\mathbf{k},\lambda} + \frac{1}{2}\right)\hbar\omega_{\mathbf{k},\lambda}.$$

Total energy, in terms of normal mode coordinates

$$\left\langle n(\omega_{\mathbf{k},\lambda})\right\rangle = \frac{1}{\exp(\hbar\omega_{\mathbf{k},\lambda}/k_{\mathrm{B}}T) - 1}$$

Bose-Einstein statistics for average number of modes at a given temperature

$$\mathcal{H} = \frac{1}{2}\sum_{j,\ell} m_j \left|\dot{\mathbf{u}}_{j\ell}\right|^2 + \frac{1}{2}\sum_{\substack{j,j'\\ \ell,\ell'}} \mathbf{u}^T_{j\ell} \cdot \Phi^{j,j'}_{\ell,\ell'} \cdot \mathbf{u}_{j'\ell'}$$

Hamiltonian of the system:

$\mathcal{H}$=Kin. En. + Pot. En

Phonon density of states

Many thermodynamic functions like free energy, specific heat, and entropy are additive functions of phonon density of states.

This stems from the notion that the normal modes do not interact in the harmonic approximation.

Phonon density of states is the number of modes in a unit energy interval.

$$c_v(T) = 3Nk \int \frac{\hbar^2 \omega^2 e^{\hbar\omega/kT}}{(kT)^2 (1 - e^{\hbar\omega/kT})^2} \cdot g(\omega) \cdot d\omega$$

Vibrational specific heat

Phonon density of states is a key ingredient for many thermodynamic properties

If we choose to write in terms of energy, $E = \hbar\omega, \quad \beta = 1/k_B T$

$$c_v(T) = 3k_B \int (\beta E/2)^2 \operatorname{csc} h(\beta E) \cdot g(E) \cdot dE$$

Vibrational specific heat

$$S_v(T) = 3k_B \int_0^\infty \{\beta E/2 \bullet \cot h(\beta E) - \ln[2 \sin h(\beta E)]\} \cdot g(E) \cdot dE$$

Vibrational entropy

$$f_{LM} = e^{-E_R \int \{g(E)/2\}.\coth(\beta E/2) dE}$$

Lamb-Mössbauer factor

$$g(E) = \frac{3m}{2\pi^2 \hbar^3 \rho v_D^3} E^2$$

Debye Sound velocity

$$\langle F \rangle = \frac{M}{\hbar^2} \int_0^\infty E^2 g(E) dE$$

Average restoring force constant

And, some thermodynamics

$$\mathcal{Z} = \frac{1}{1 - \exp(-\beta\hbar\omega)}$$

Partition function

$$F = -k_{\mathrm{B}} T \ln \mathcal{Z}$$

Free energy

$$C = -T \frac{\partial^2 F}{\partial T^2}$$

Heat capacity

$$E = \sum_{\mathbf{k},\lambda} \left(\langle n(\omega_{\mathbf{k},\lambda}) \rangle + \frac{1}{2} \right) \hbar\omega_{\mathbf{k},\lambda} \equiv \int \left(\langle n(\omega) \rangle + \frac{1}{2} \right) \hbar\omega \, g(\omega) \, \mathrm{d}\omega.$$

Energy in terms of
phonon density of states

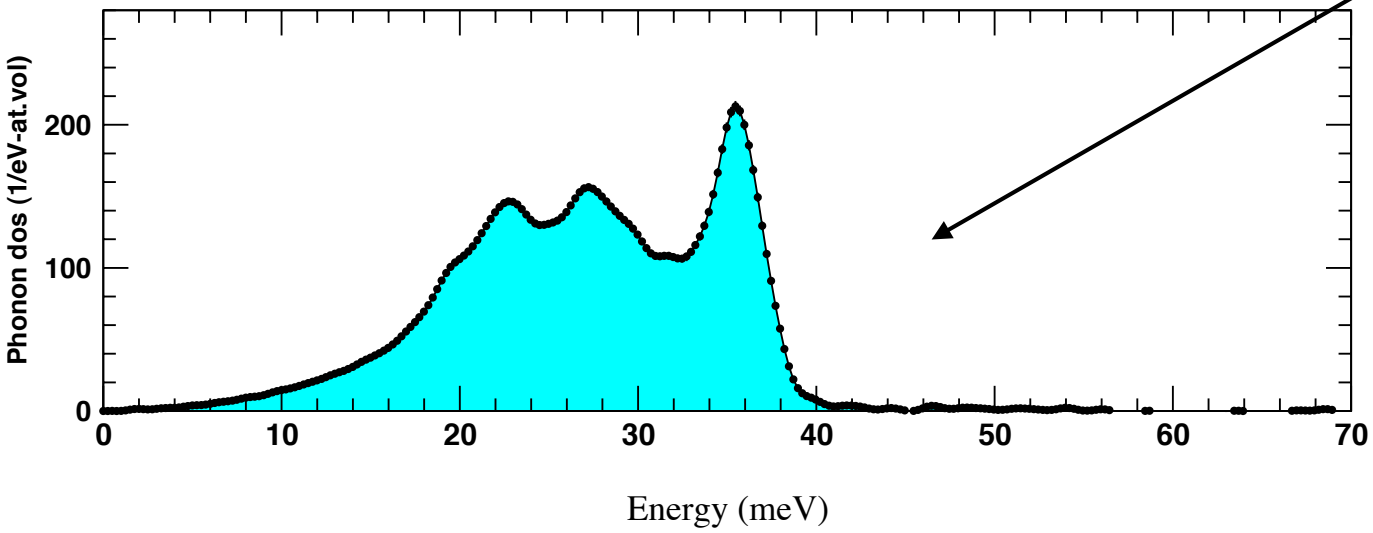

Why x-rays instead of neutrons or visible light ?

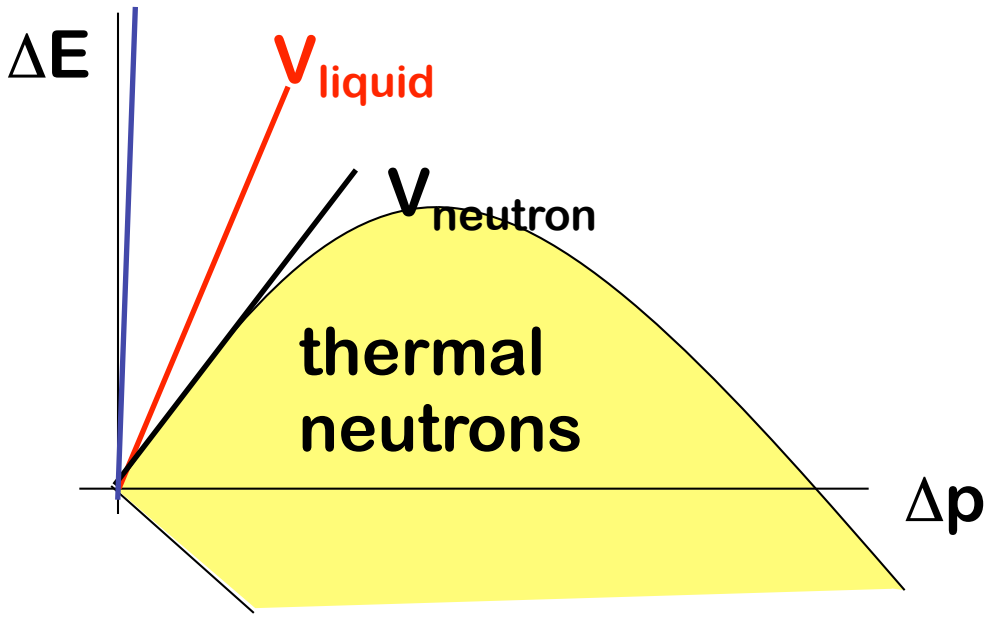

Limited momentum transfer capability of neutrons at low energies favor x-rays to study collective excitations with large dispersion, like sound modes.

When the sound velocity exceeds that of neutrons in the liquid, x-rays become unique. The low-momentum/high-energy transfer region is only accessible by x-rays.

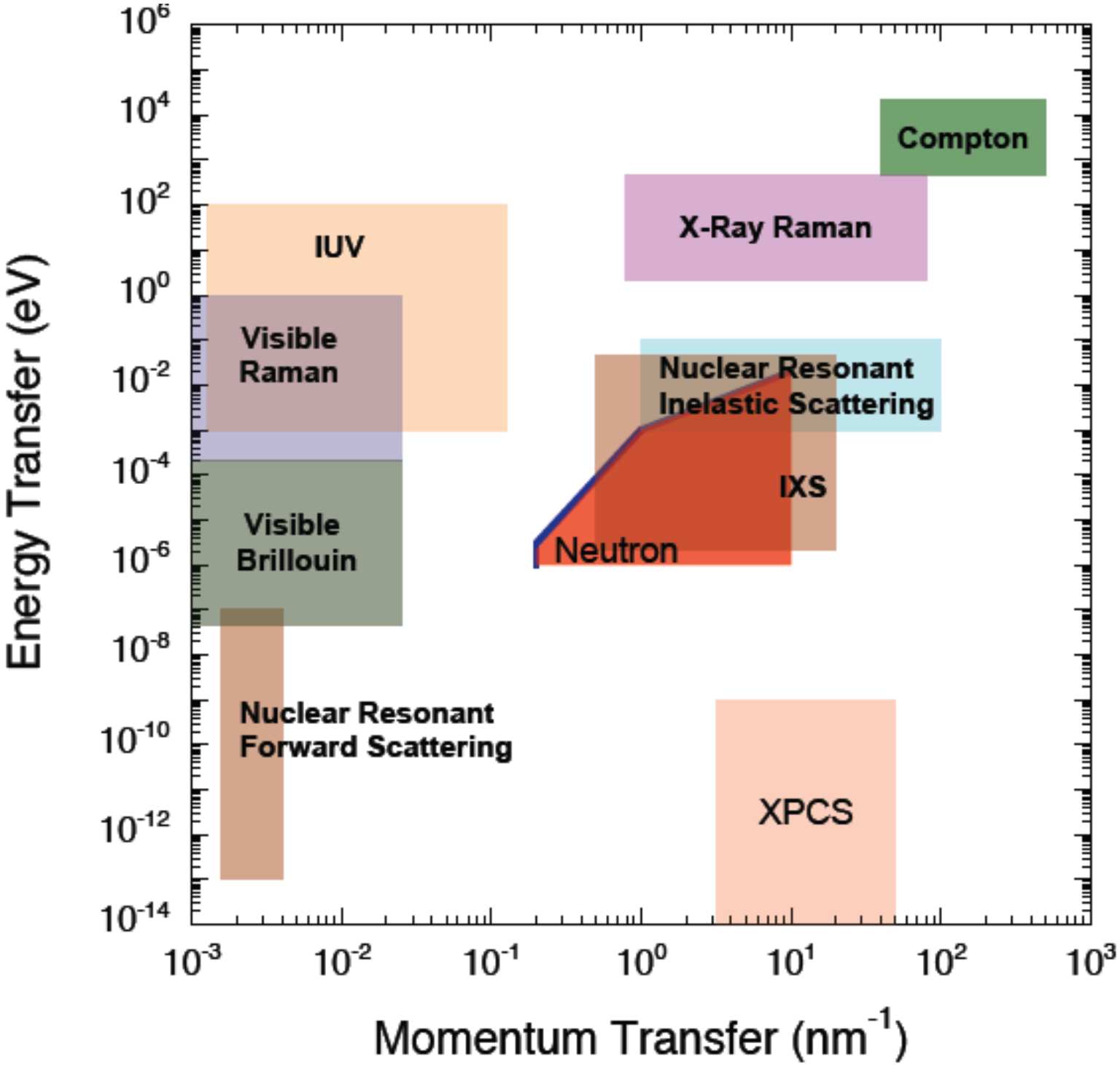
Energy Transfer (eV)
Momentum Transfer (nm^{-1})
10^{6}
10^{4}
10^{2}
10^{0}
10^{-2}
10^{-4}
10^{-6}
10^{-8}
10^{-10}
10^{-12}
10^{-14}
10^{-3}
10^{-2}
10^{-1}
10^{0}
10^{1}
10^{2}
10^{3}
Compton
X-Ray Raman
IUV
Visible Raman
Nuclear Resonant Inelastic Scattering
IXS
Neutron
Visible Brillouin
Nuclear Resonant Forward Scattering
XPCS

Inelastic X-Ray Scattering: two approaches

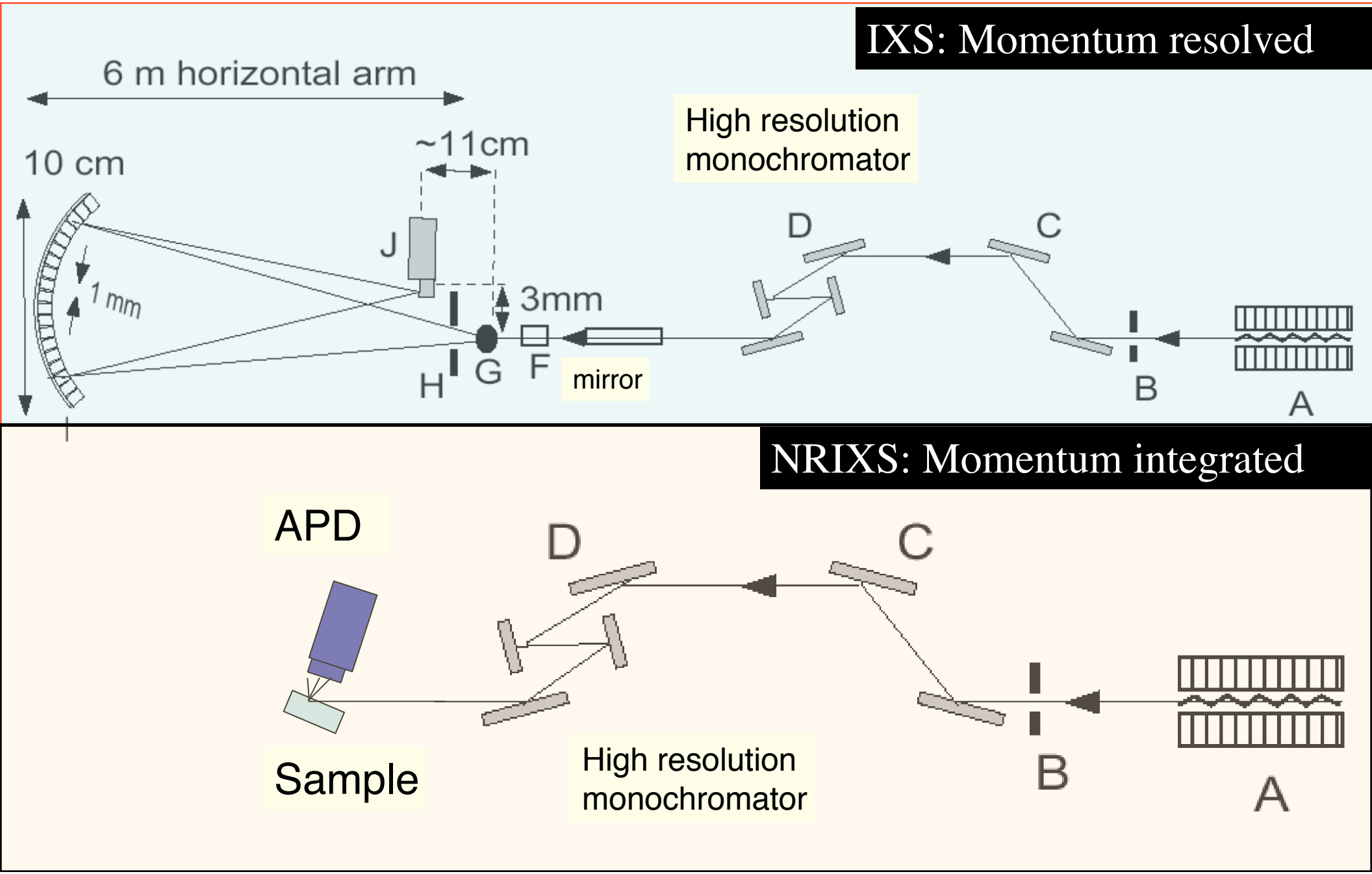

Nuclear Resonant Scattering

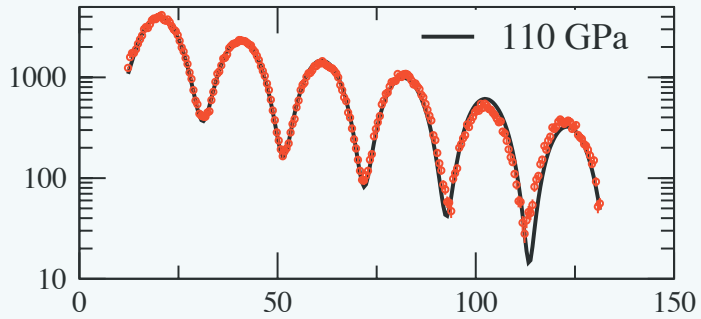

SMS: Synchrotron Mössbauer Spectroscopy
NFS : Nuclear Forward Scattering

Isomer shift
Quadrupole splitting
Magnetic hyperfine field
- -valence state
- -local crystallographic symmetry
- -magnetic ordering
- -relaxation

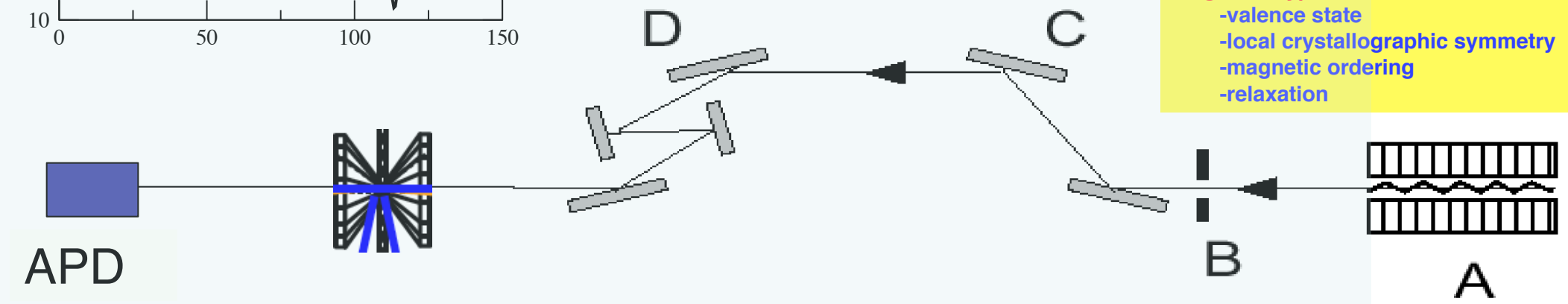

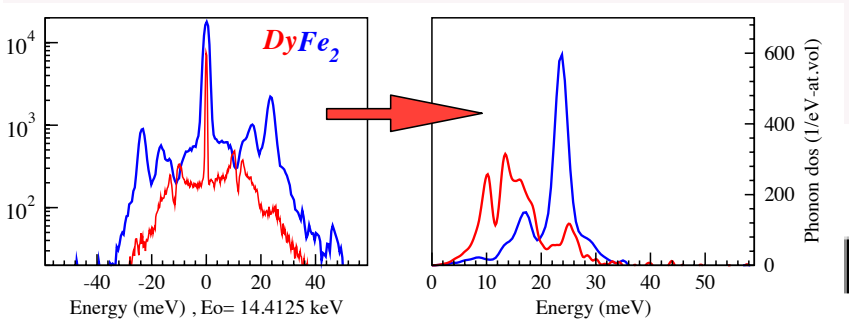

NRIXS: Nuclear Resonant Inelastic X-ray Scattering
NRVS: Nuclear Resonant Vibrational Spectroscopy

Partial phonon density of states
Recoil-free fraction
- -speed of sound
- -vibrational modes
- -entropy and specific heat
- -phonon confinement
- -resilience, compressibility
- -Debye Temperature

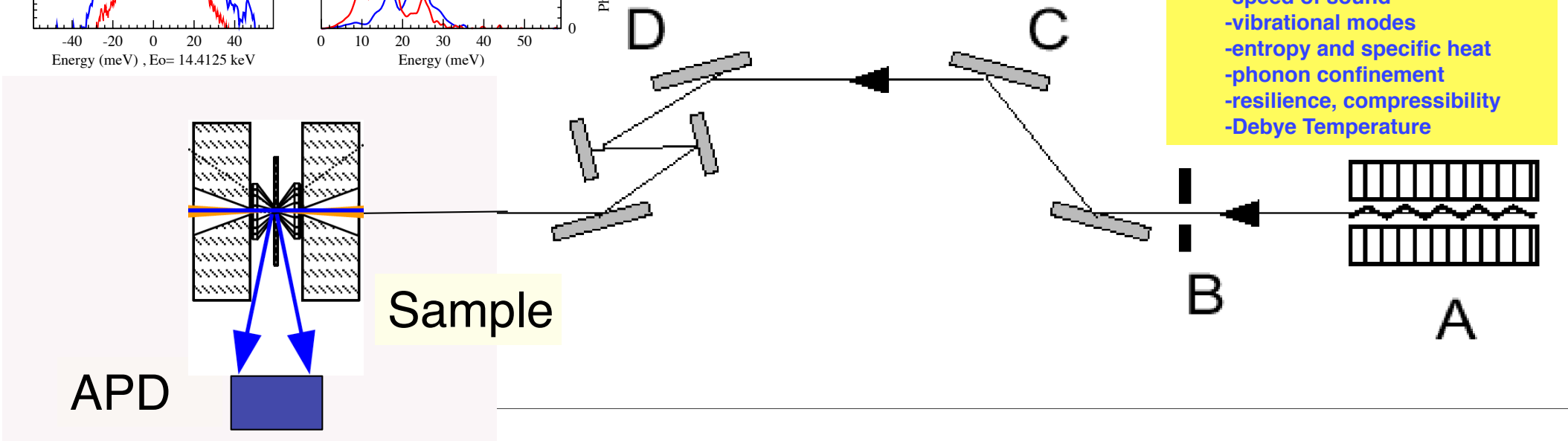

Kernresonanzabsorption von γ-Strahlung in Ir^{191}

Von Rudolf L. Mössbauer

Aus dem Laboratorium für technische Physik der Technischen Hochschule in München
und dem Institut für Physik im Max-Planck-Institut für medizinische Forschung in Heidelberg

(Z. Naturforschg. 14 a, 211—216 [1959]; eingegangen am 5. November 1958)

Bei der Emission und Selbstabsorption von weicher γ-Strahlung in Kernen treten bei tiefen Temperaturen in Festkörpern sehr starke Linien mit der natürlichen Linienbreite auf. Diese Linien erscheinen als Folge davon, daß bei tiefen Temperaturen bei einem Teil der Quantenübergänge der γ-Rückstoßimpuls nicht mehr vom einzelnen Kern aufgenommen wird, sondern von dem Kristall als Ganzes. Da die scharfen Emissions- und Absorptionslinien energetisch an der gleichen Stelle liegen, tritt ein sehr starker Resonanzfluoreszenzeffekt auf. Durch eine „Zentrifugen"-Methode, bei der die Emissions- und Absorptionslinien gegeneinander verschoben werden, läßt sich der Fluoreszenzeffekt unterdrücken und so eine unmittelbare Bestimmung der natürlichen Linienbreite von Resonanzlinien vornehmen. Erste Messungen nach dieser Methode ergeben für die Lebenszeit τ des 129 keV-Niveaus in Ir^{191}: $\tau = \left(1{,}4\ {}^{+0{,}2}_{-0{,}1}\right) \cdot 10^{-10}$ sec.

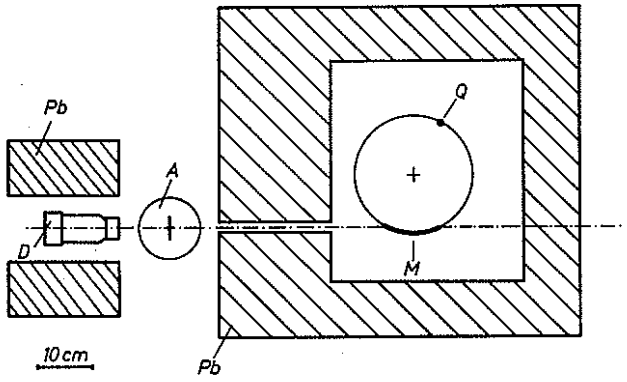

Abb. 2. Versuchsgeometrie. A Absorber-Kryostat; Q rotierender Kryostat mit Quelle; D Szintillationsdetektor. M ist der bei der Messung ausgenützte Teil des Rotationskreises der Quelle.

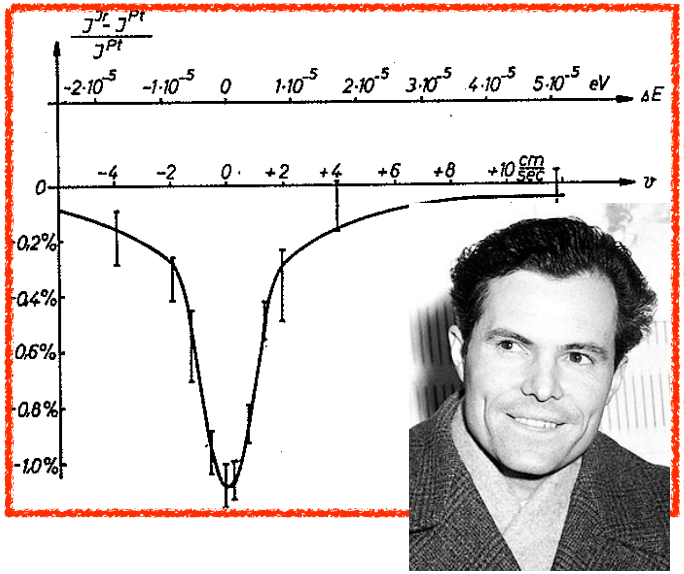

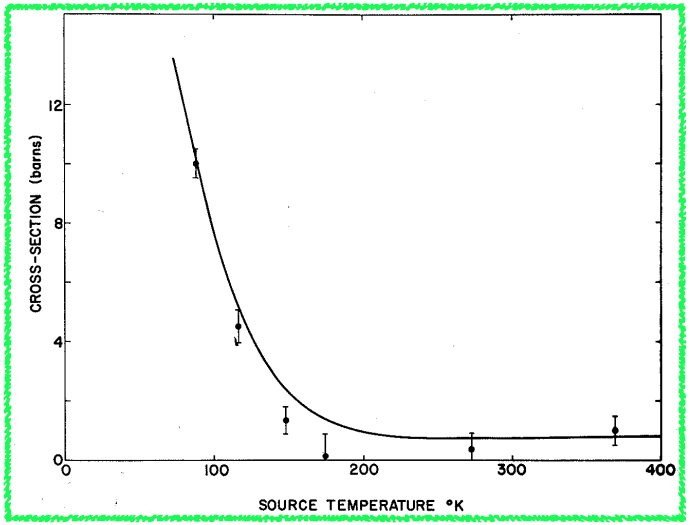

absorption-emission & recoil

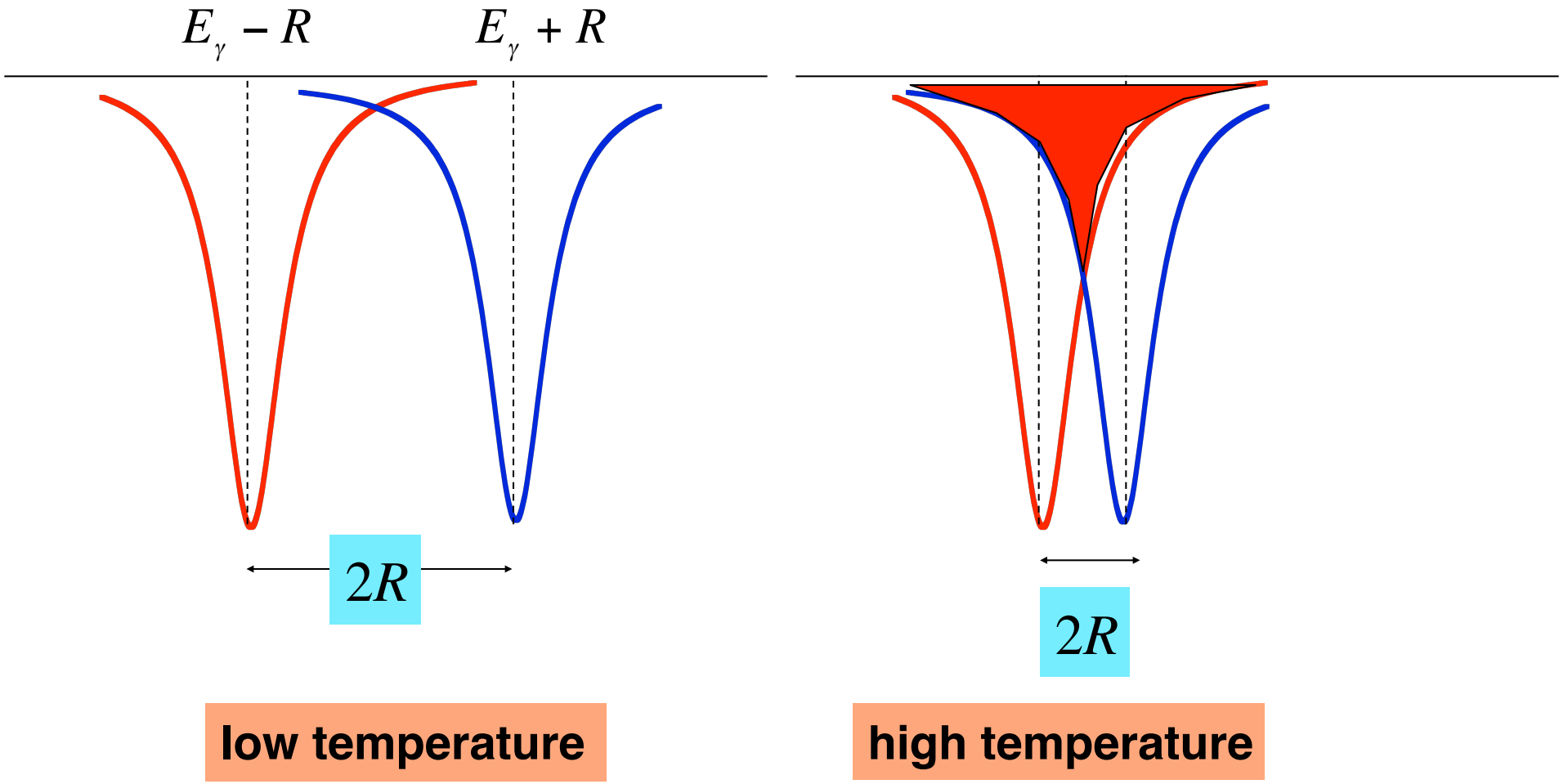

intuitive expectation: large resonance absorption at high temperature

Mossbauer's observation: less absorption at high temperature

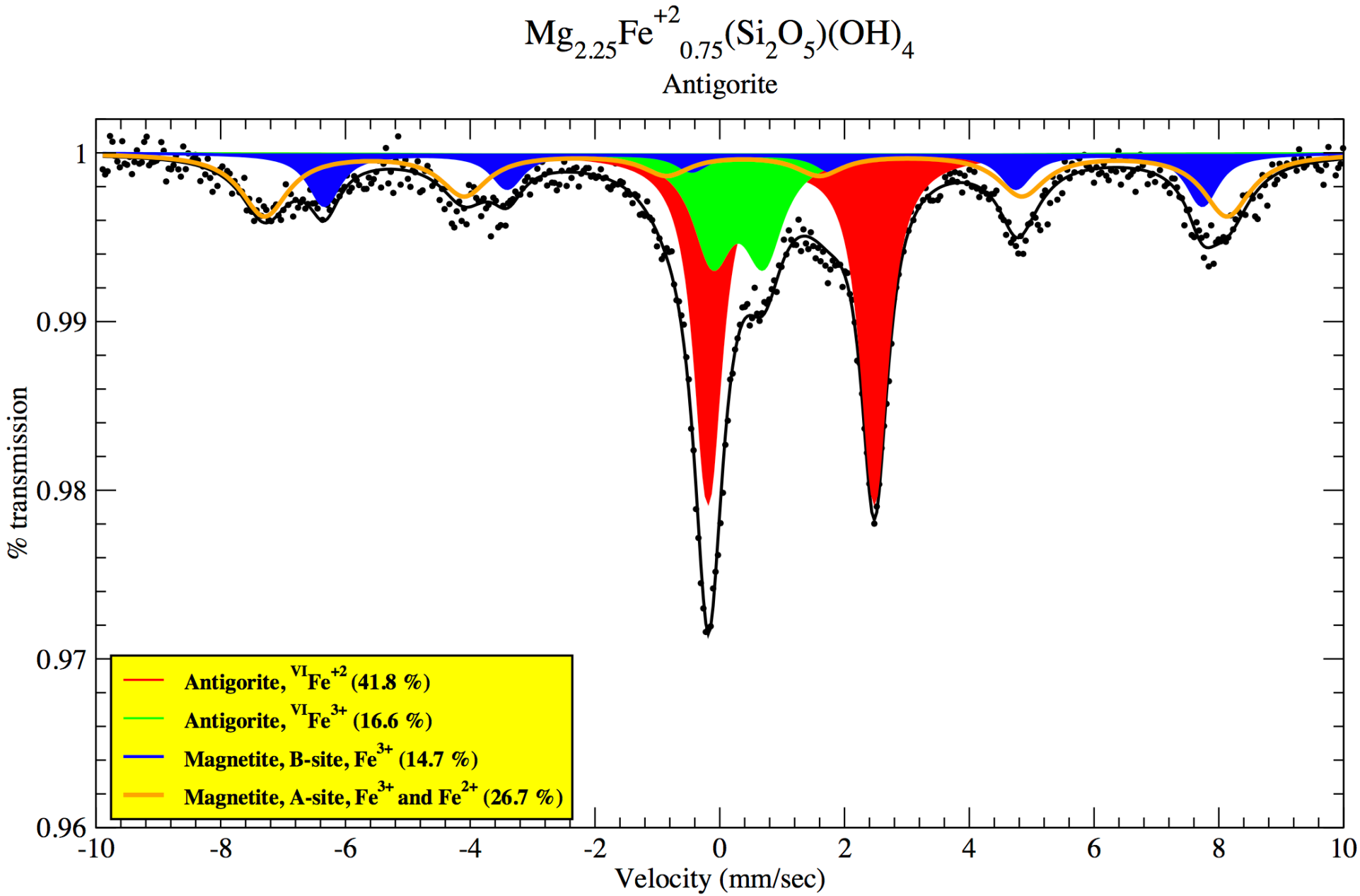
$Mg_{2.25}Fe^{+2}_{0.75}(Si_2O_5)(OH)_4$
Antigorite
1
0.99
0.98
0.97
0.96
% transmission
-10
-8
-6
-4
-2
0
2
4
6
8
10
Velocity (mm/sec)
Antigorite, $^{VI}Fe^{+2}$ (41.8 %)
Antigorite, $^{VI}Fe^{3+}$ (16.6 %)
Magnetite, B-site, Fe^{3+} (14.7 %)
Magnetite, A-site, Fe^{3+} and Fe^{2+} (26.7 %)

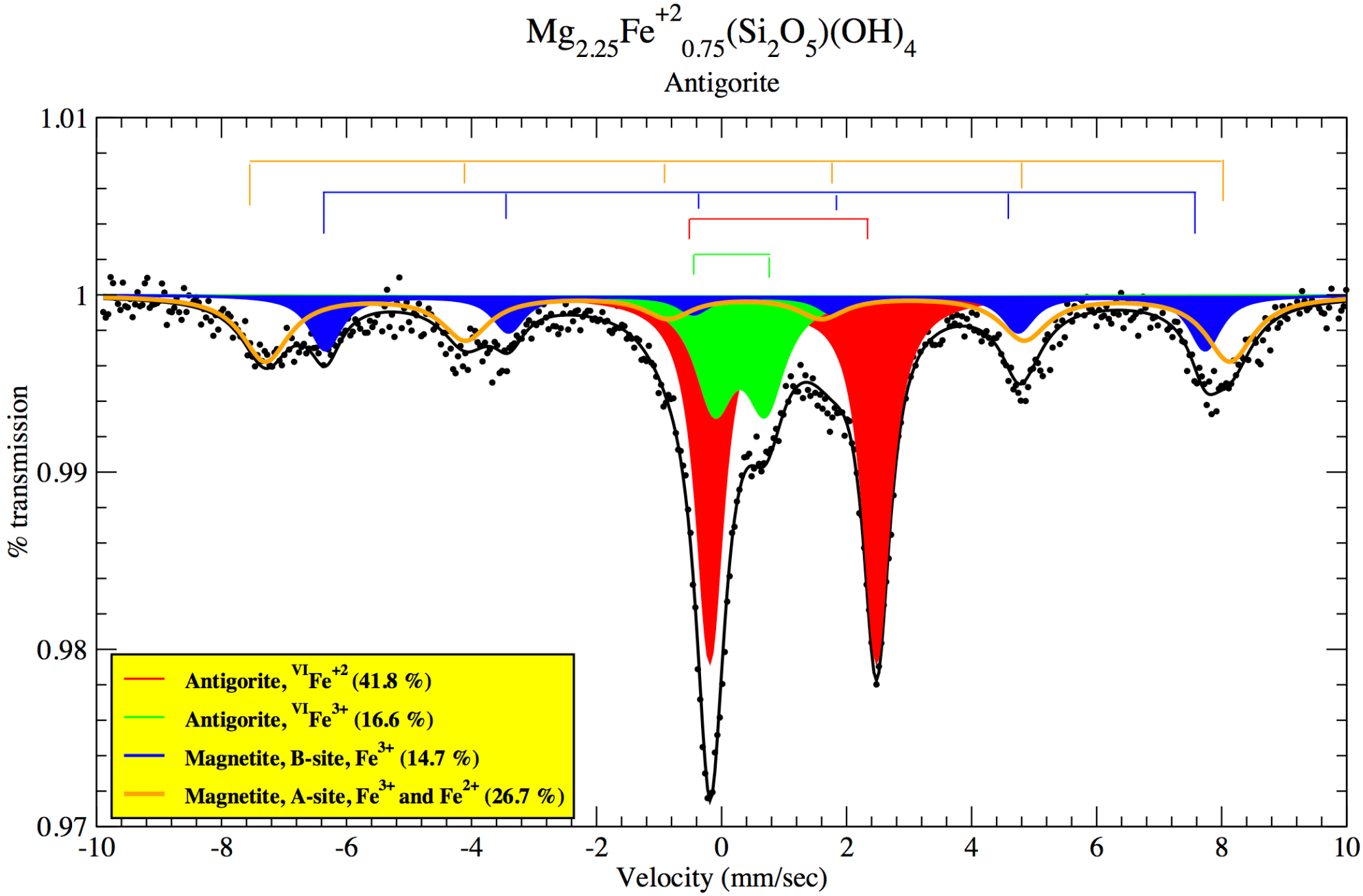
$Mg_{2.25}Fe^{+2}_{0.75}(Si_2O_5)(OH)_4$
Antigorite
1.01
1
0.99
0.98
0.97
% transmission
-10
-8
-6
-4
-2
0
2
4
6
8
10
Velocity (mm/sec)
Antigorite, $^{VI}Fe^{+2}$ (41.8 %)
Antigorite, $^{VI}Fe^{3+}$ (16.6 %)
Magnetite, B-site, Fe^{3+} (14.7 %)
Magnetite, A-site, Fe^{3+} and Fe^{2+} (26.7 %)

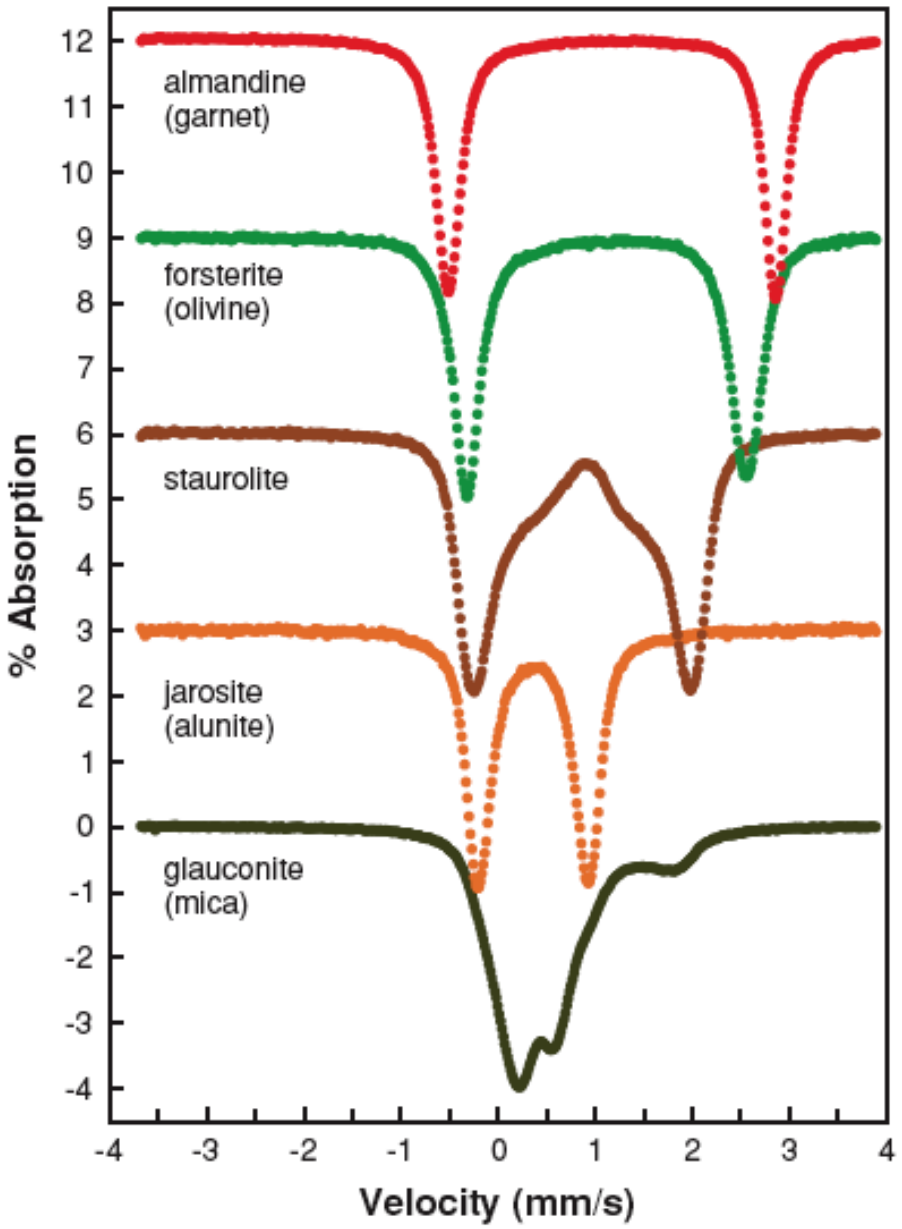

Fe^{2+}, cubic

Fe^{2+}, octahedral

Fe^{2+}, tetrahedral

Fe^{3+}, octahedral

Fe^{3+}, tetrahedral

M. Darby Dyar, et al, Ann. Rev. Earth. Planet. Sci, 34 (2006) 83

How isomer shift & quadrupole splitting are used for valence identification in Mössbauer Spectroscopy ?

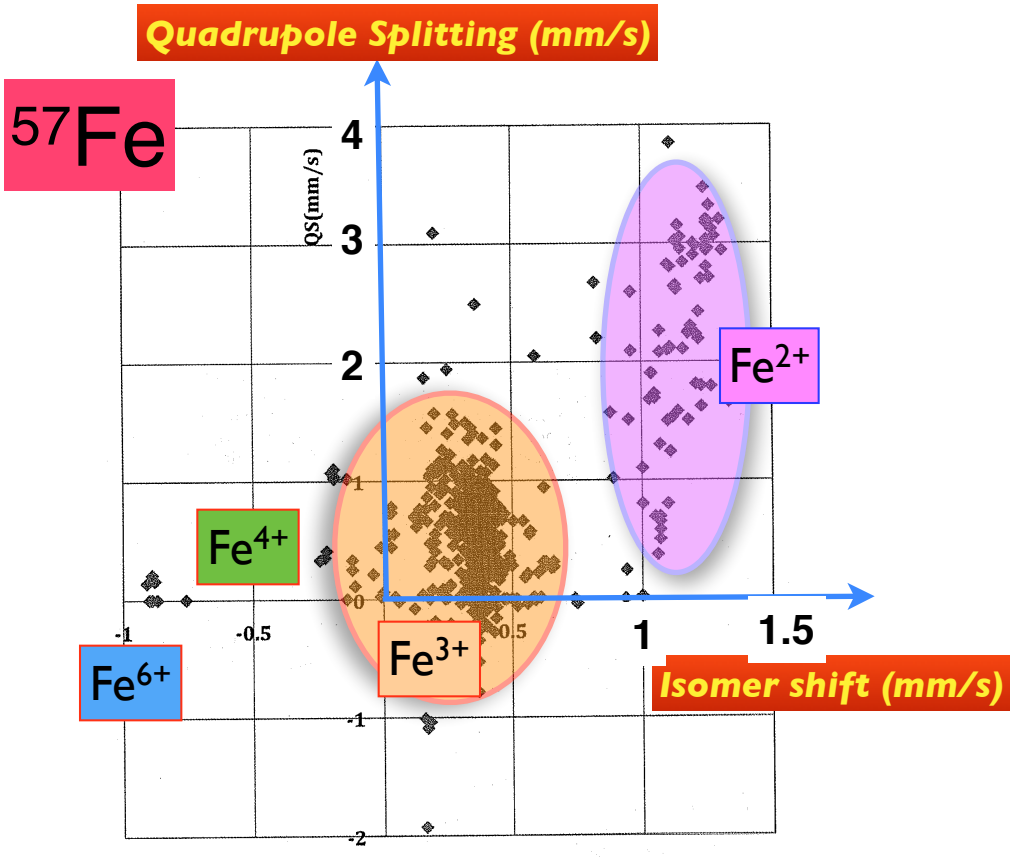

After 50 years of research and more than 10,000 papers, approximately 800 iron compounds have been classified, and the results are disseminated by the Mössbauer Effect Data Center (MEDC).

Given the fact that measured Mössbauer line-widths are typically 0.3 mm/sec, it is common to determine IS and QS with an accuracy of 0.1 mm/sec.

Hence, in many circumstances, this combination of IS-QS values provide valuable guidance into valence issues in minerals, lunar rocks, and meteorite studies.

Ref: Mossbauer Effect Reference and Data Journal, vol 33, No;1 (January 2010)

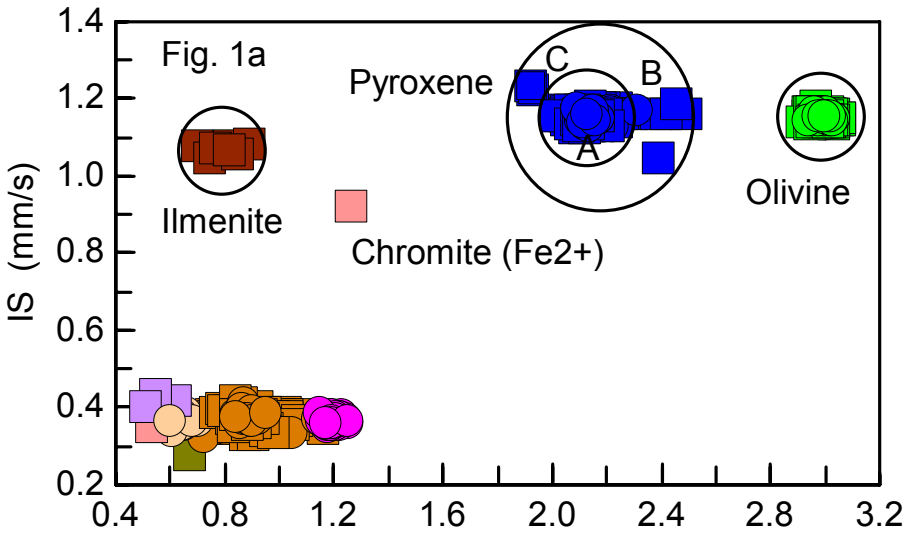
Fig. 1a
Pyroxene
C
B
A
Olivine
Ilmenite
Chromite (Fe2+)
IS (mm/s)
1.4
1.2
1.0
0.8
0.6
0.4
0.2
0.4
0.8
1.2
1.6
2.0
2.4
2.8
3.2

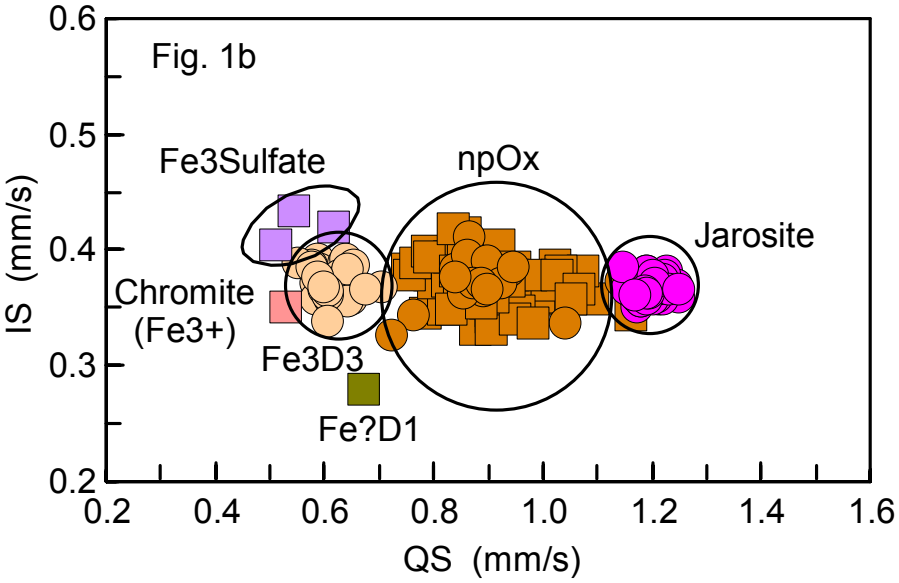
Fig. 1b
Fe3Sulfate
npOx
Jarosite
Chromite
(Fe3+)
Fe3D3
Fe?D1
IS (mm/s)
QS (mm/s)
0.6
0.5
0.4
0.3
0.2
0.2
0.4
0.6
0.8
1.0
1.2
1.4
1.6

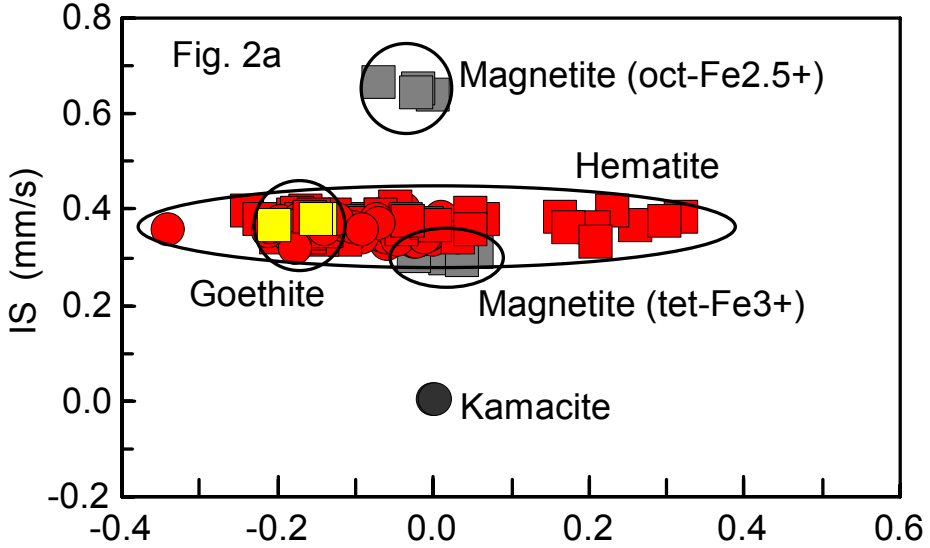
Fig. 2a
Magnetite (oct-Fe2.5+)
Hematite
Goethite
Magnetite (tet-Fe3+)
Kamacite
IS (mm/s)
0.8
0.6
0.4
0.2
0.0
-0.2
-0.4
-0.2
0.0
0.2
0.4
0.6

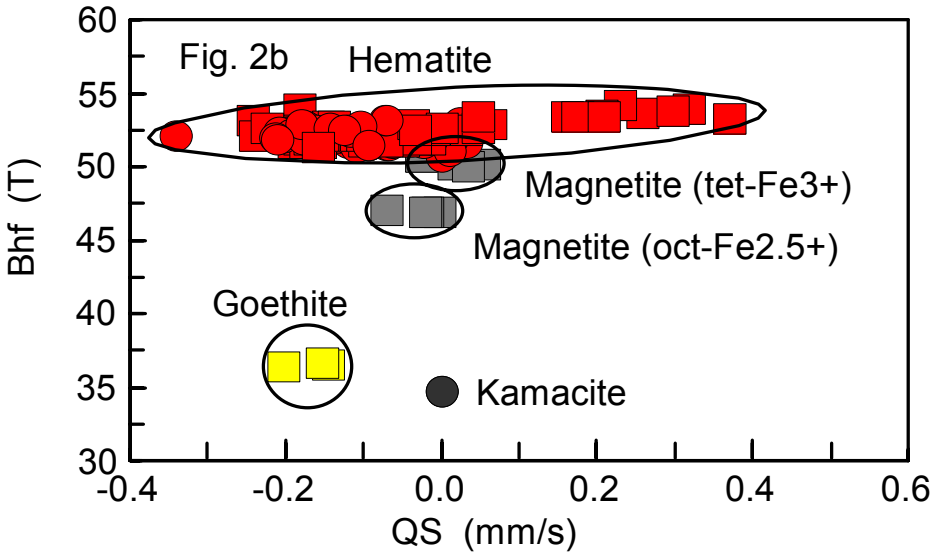
Fig. 2b
Hematite
Magnetite (tet-Fe3+)
Magnetite (oct-Fe2.5+)
Goethite
Kamacite
Bhf (T)
QS (mm/s)
60
55
50
45
40
35
30
-0.4
-0.2
0.0
0.2
0.4
0.6

Standard Time structure @ APS

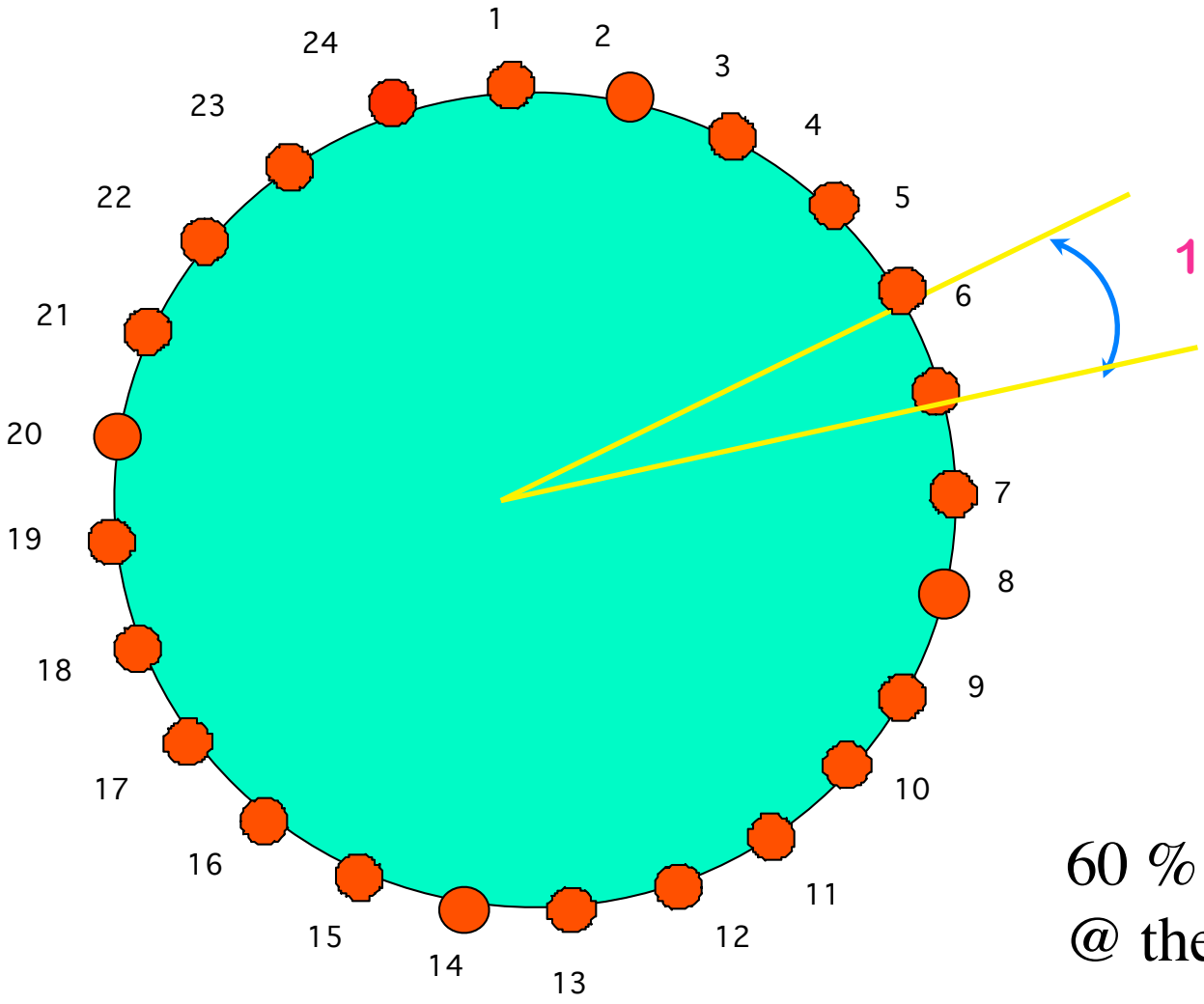

60 % of the time
@ the APS

1 revolution=3.68 μsec =>1296 buckets

Nuclear Resonance and Fallout in ^{57}Fe-decay

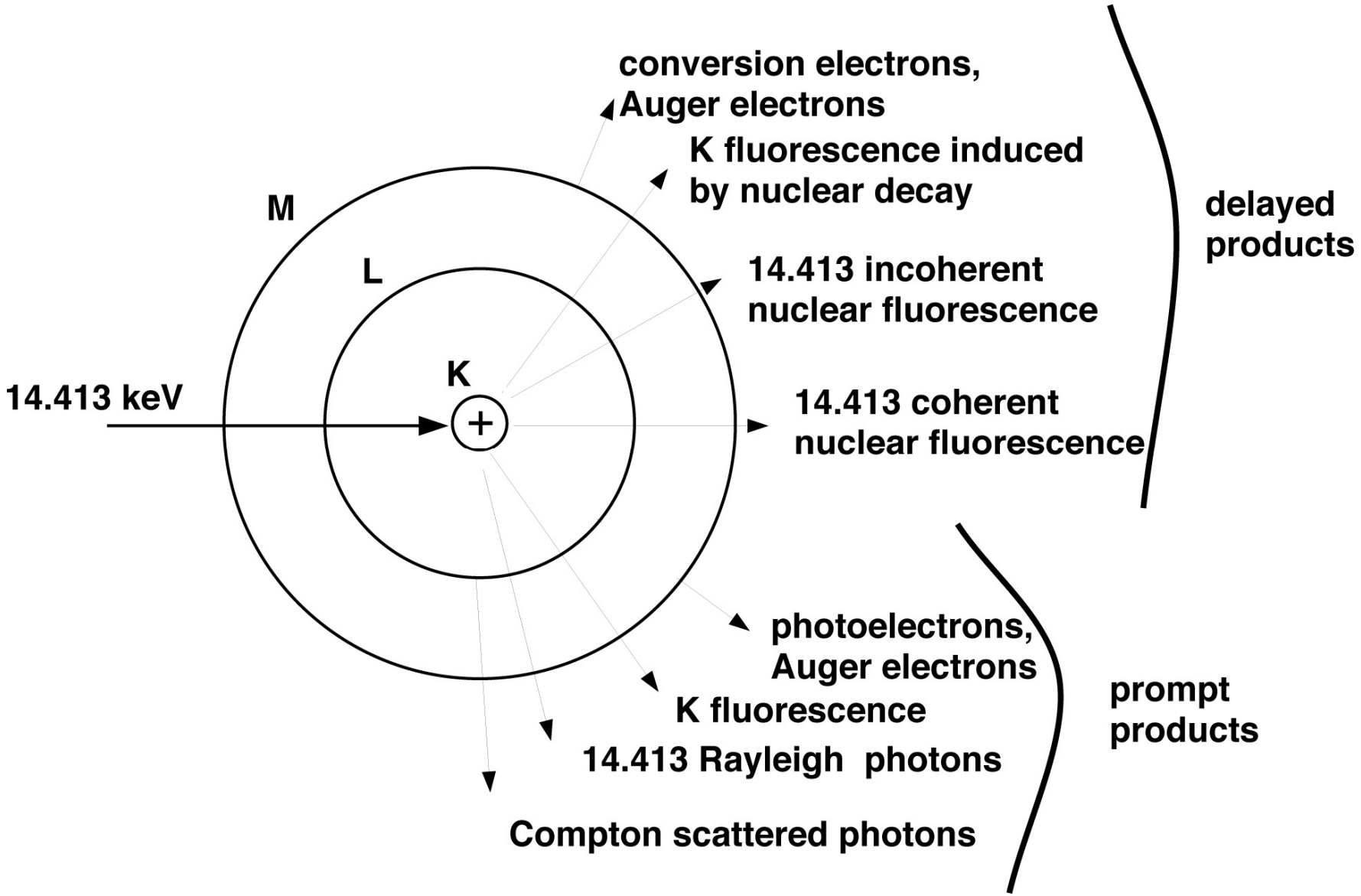

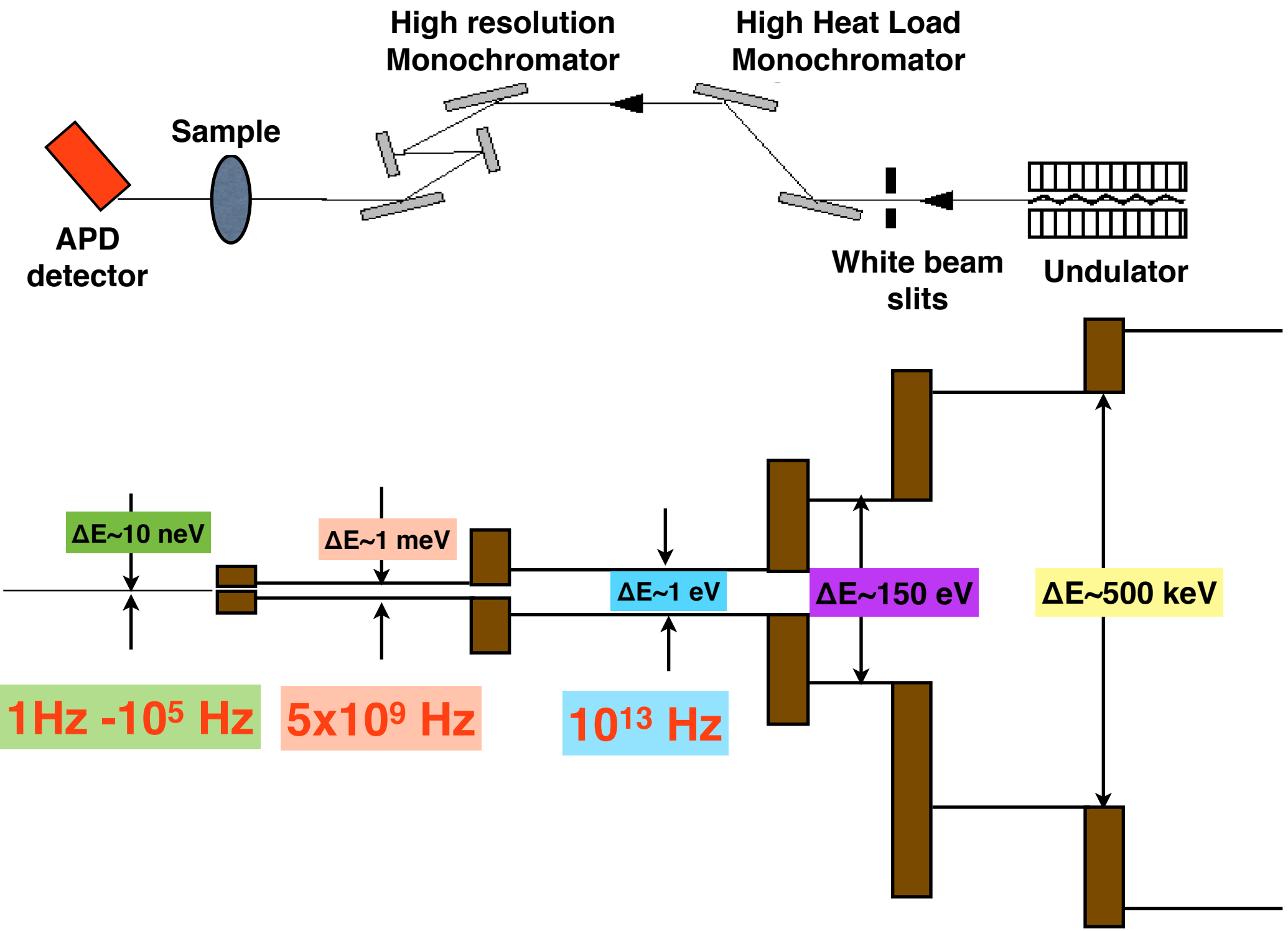
High resolution
Monochromator
High Heat Load
Monochromator
Sample
APD
detector
White beam
slits
Undulator
ΔE~10 neV
ΔE~1 meV
ΔE~1 eV
ΔE~150 eV
ΔE~500 keV
1Hz -10^5 Hz
5x10^9 Hz
10^13 Hz

Detection of nuclear decay

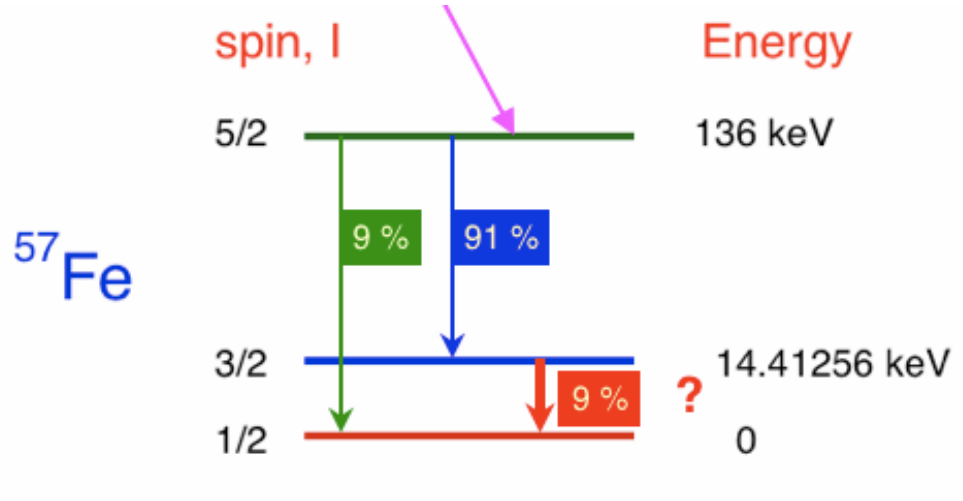

prompt photons

log I

exponential decay

delayed photons

0

time (nsec)

153 nsec

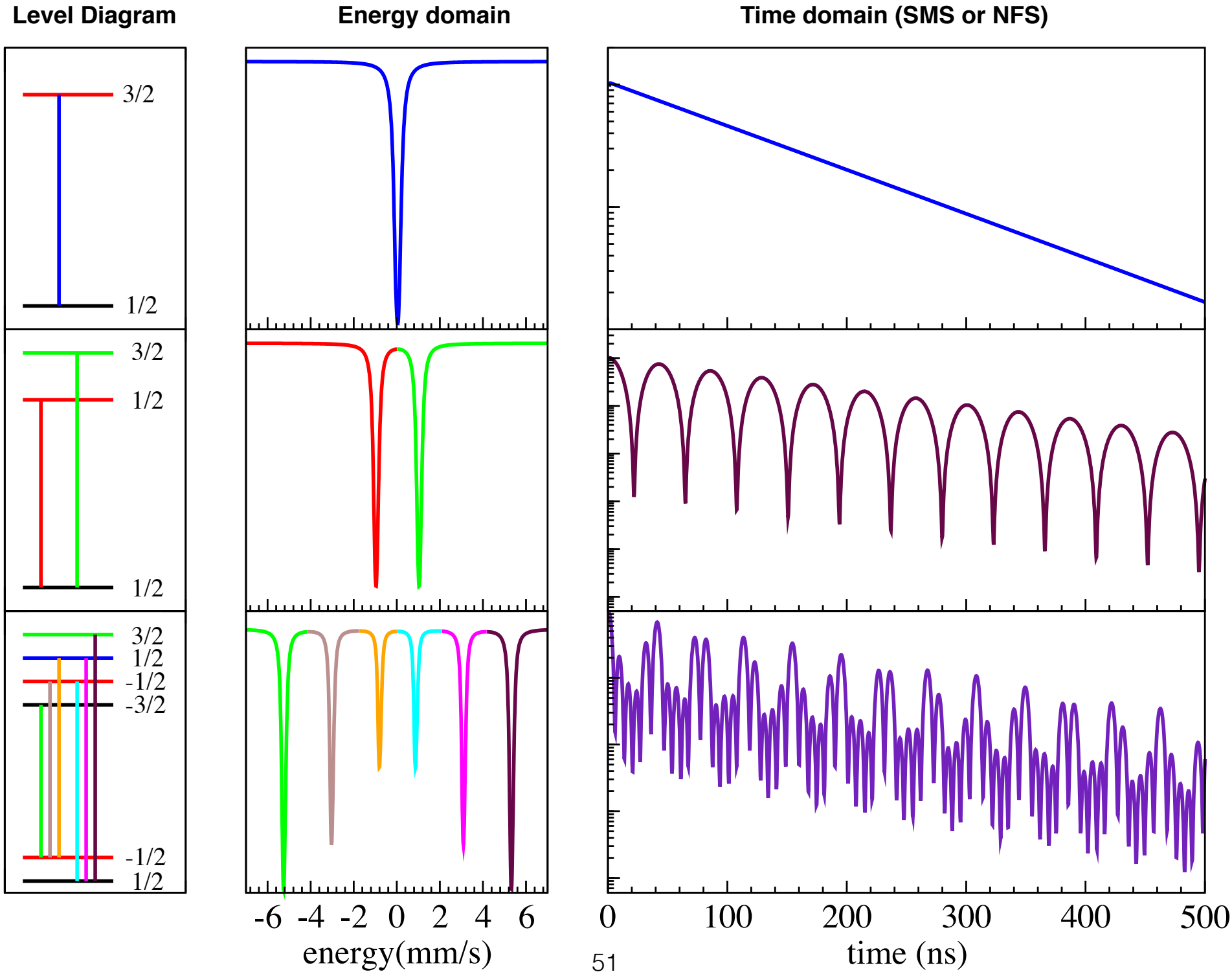
Level Diagram
Energy domain
Time domain (SMS or NFS)
3/2
1/2
3/2
1/2
1/2
3/2
1/2
-1/2
-3/2
-1/2
1/2
-6 -4 -2 0 2 4 6
energy(mm/s)
0 100 200 300 400 500
time (ns)

α (bcc-Fe) to ε (fcc-Fe) transition under pressure by synchrotron Mössbauer spectroscopy

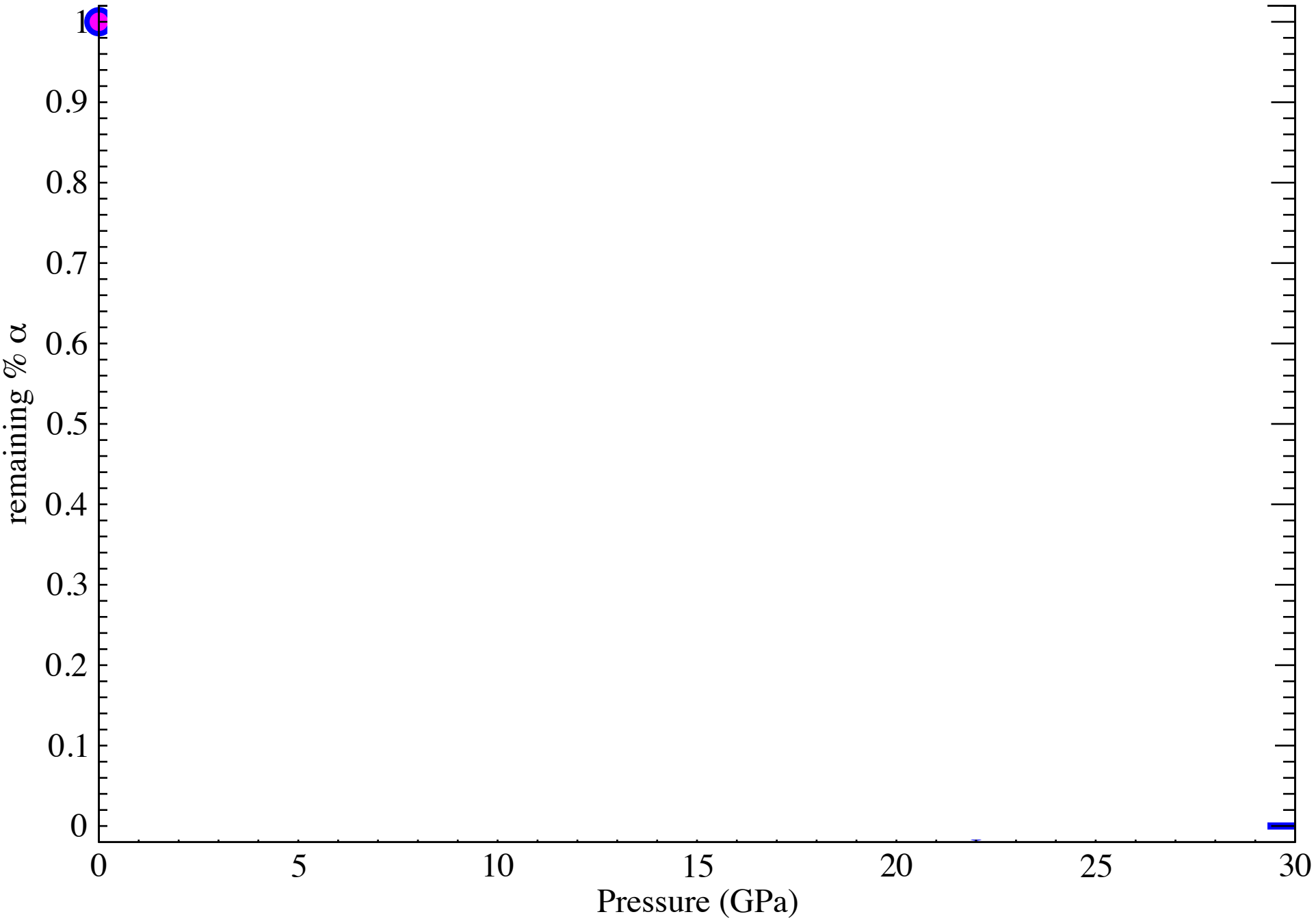

mixed alpha & epsilon phase of pure iron at 15.3 GPa pressure

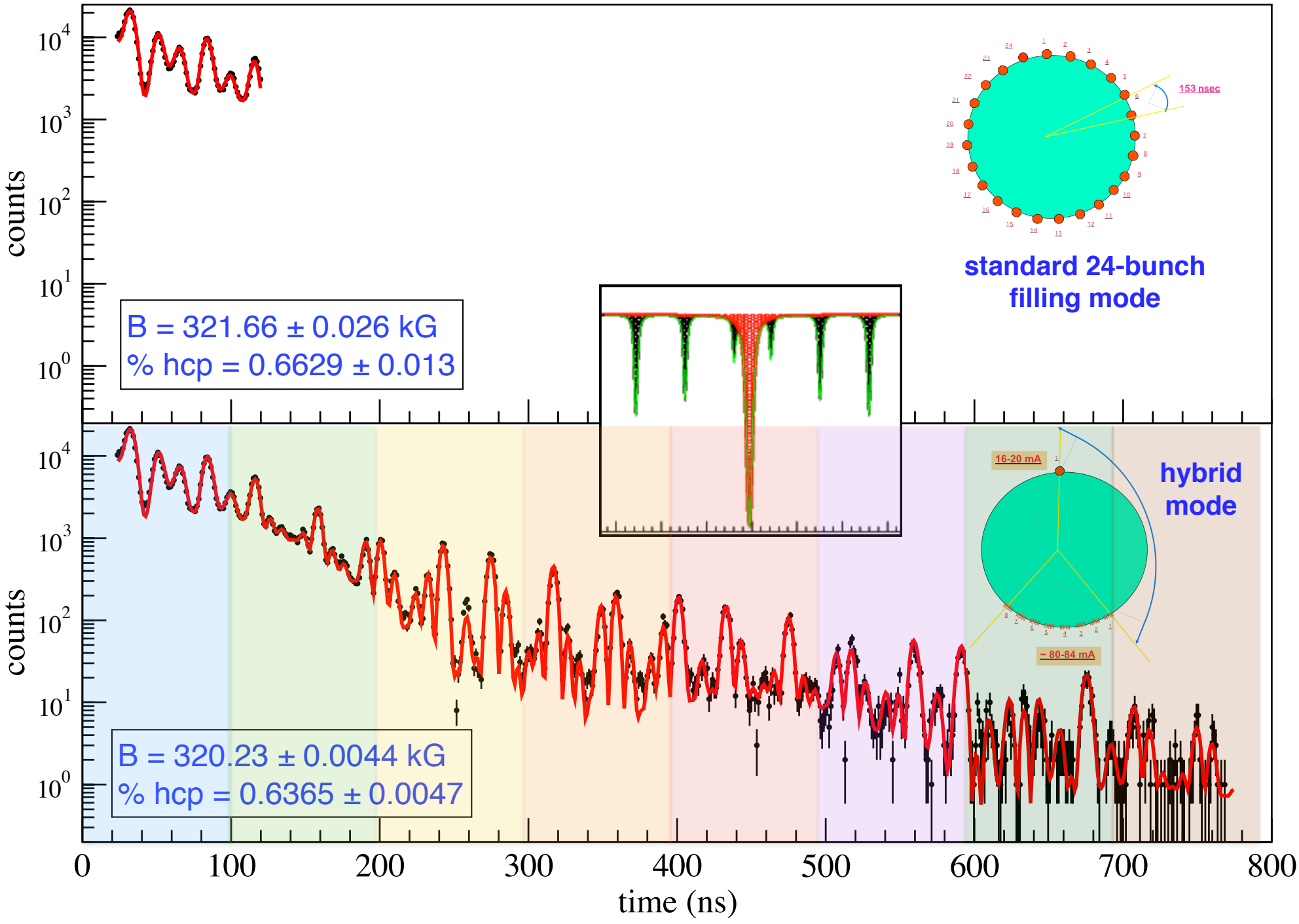

Early dreamers..

Zero phonon "Mössbauer pip"

Visualized by W. Vischer at Los Alamos & K. S. Singwi at Argonne (1960), but only properly observed after synchrotron radiation based tunable monochromators are realized.
(W. Sturhahn et al, PRL , 74 (1995) p. 3832)

Visualized by Stan Ruby (1974) at Argonne and properly observed by E. Gerdau (Hamburg).
(S. L Ruby. J. de Physique 35 (1974) C6-209

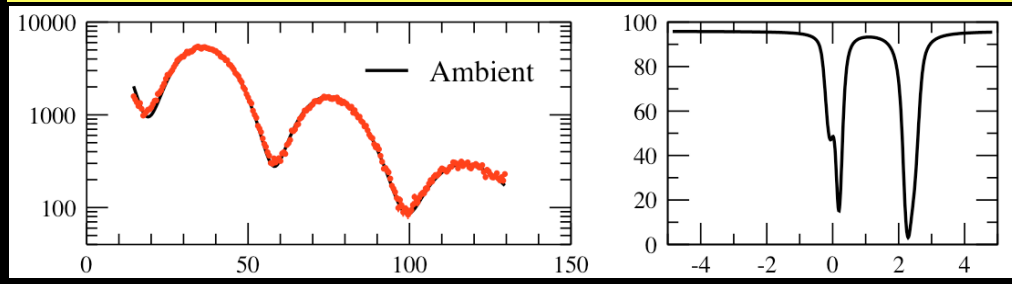

Singwi (1967)

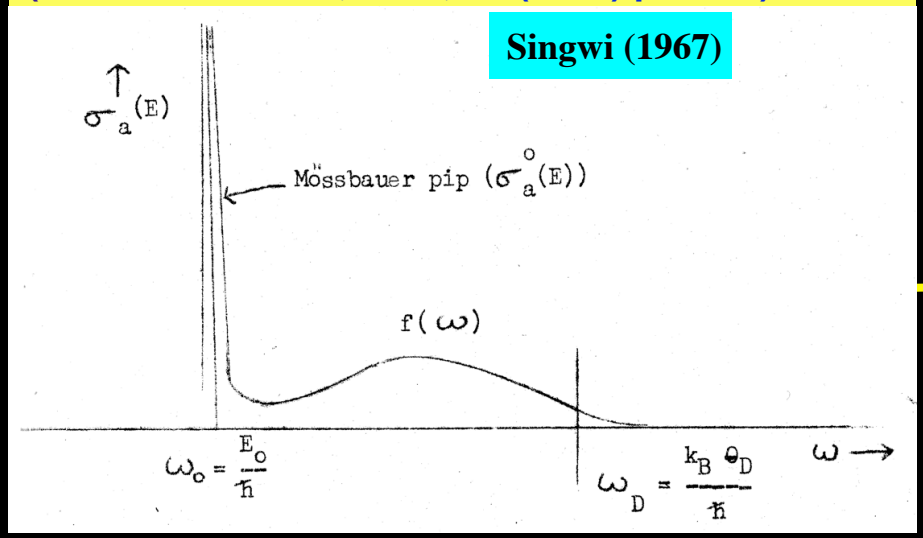

5 neV + mono. resolution

Phonon annihilation

Phonon creation

- 0 +

Energy (~ meV)

Phonon Density of States Measured by Inelastic Nuclear Resonant Scattering

W. Sturhahn, T. S. Toellner, and E. E. Alp
Advanced Photon Source, Argonne National Laboratory, Argonne, Illinois 60439

X. Zhang and M. Ando
Photon Factory, National Laboratory for High Energy Physics, Oho 1-1, Tsukuba, Ibaraki 305, Japan

Y. Yoda and S. Kikuta
Department of Applied Physics, Faculty of Engineering, The University of Tokyo, Hongo 7-3-1, Bunkyo-ku, Tokyo 113, Japan

M. Seto
Research Reactor Institute, Kyoto University, Sennan-gun, Osaka 590-04, Japan

C. W. Kimball and B. Dabrowski
Department of Physics, Northern Illinois University, De Kalb, Illinois 60115
(Received 16 December 1994)

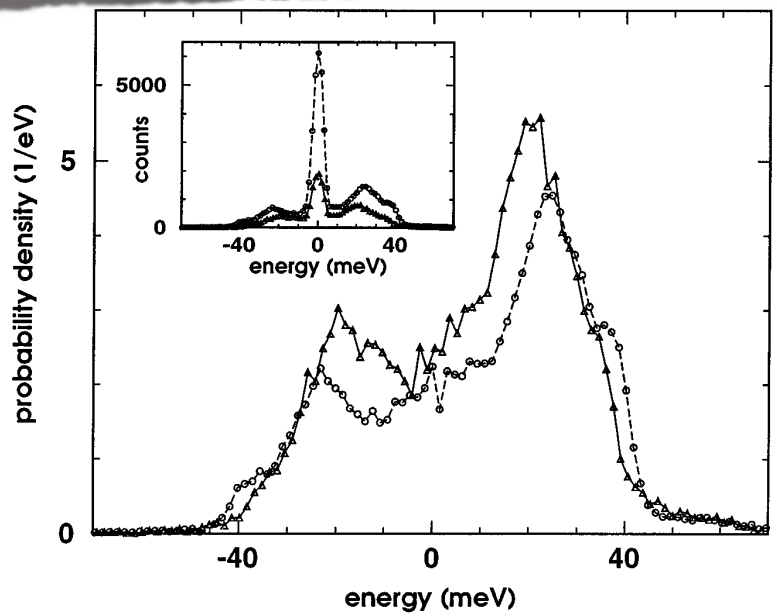

> 400 citations

Phonon excitation probability

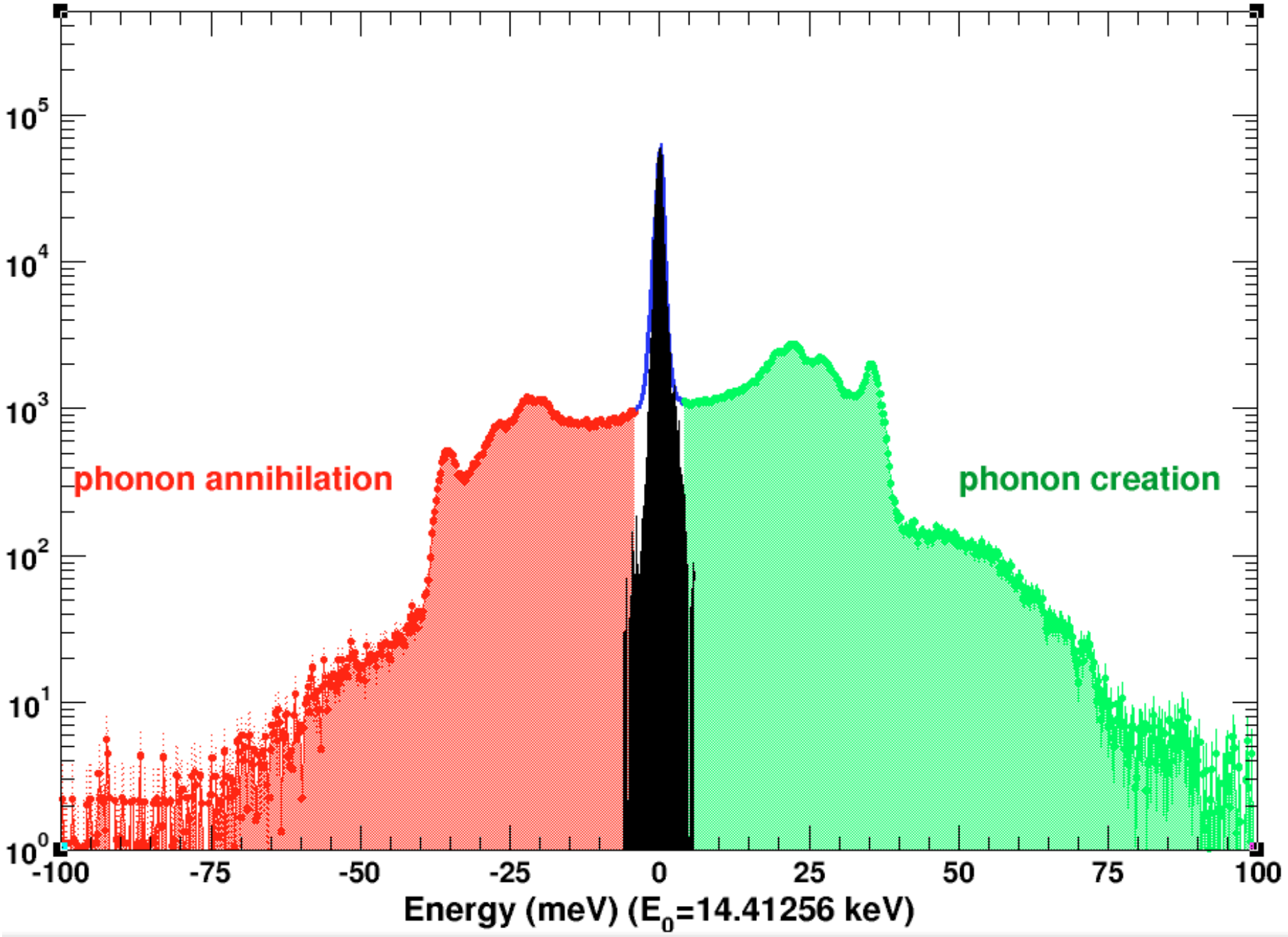

Multi-phonon decomposition

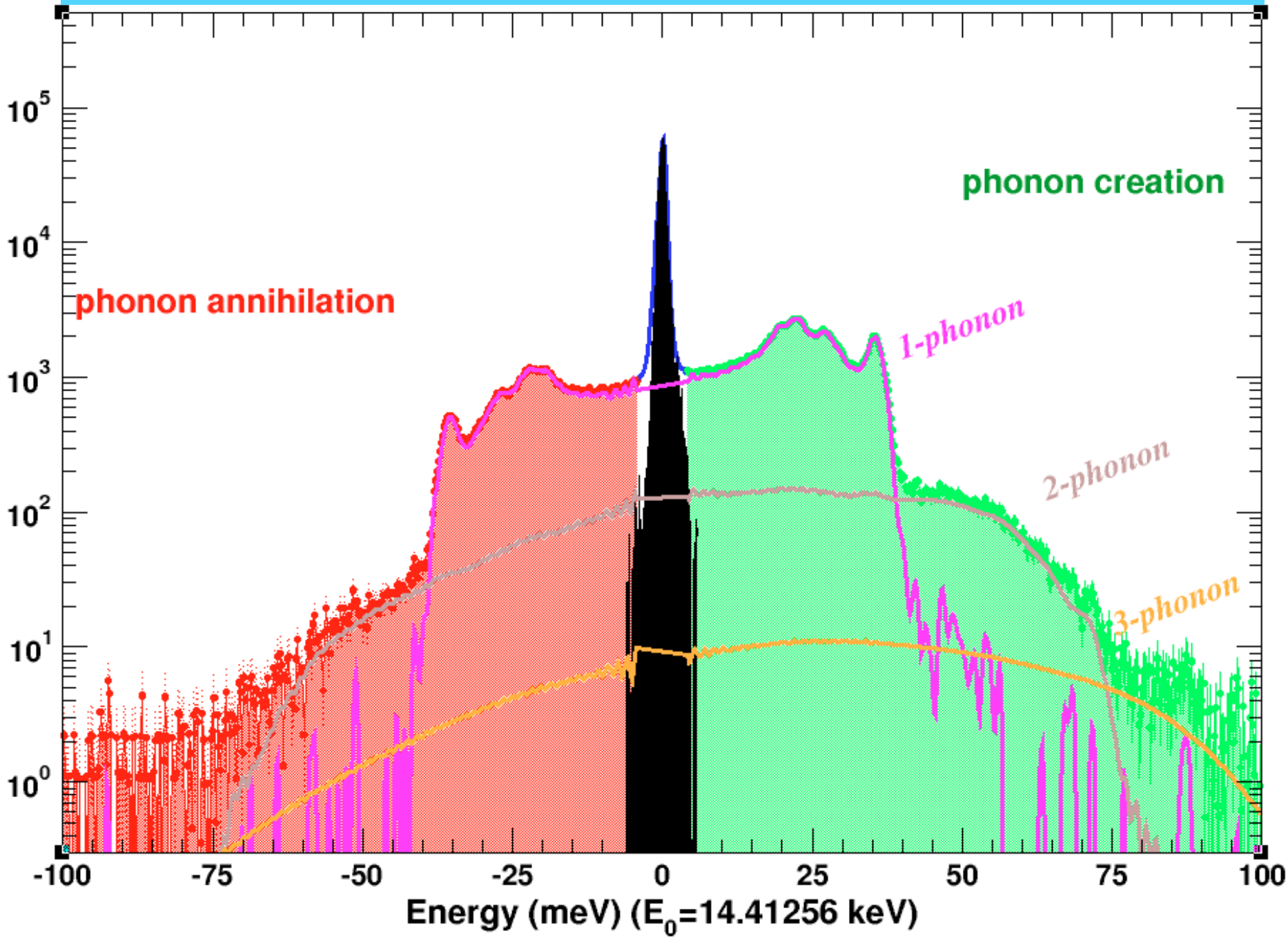

Lipkin's sum rules related to phonon excitation probability

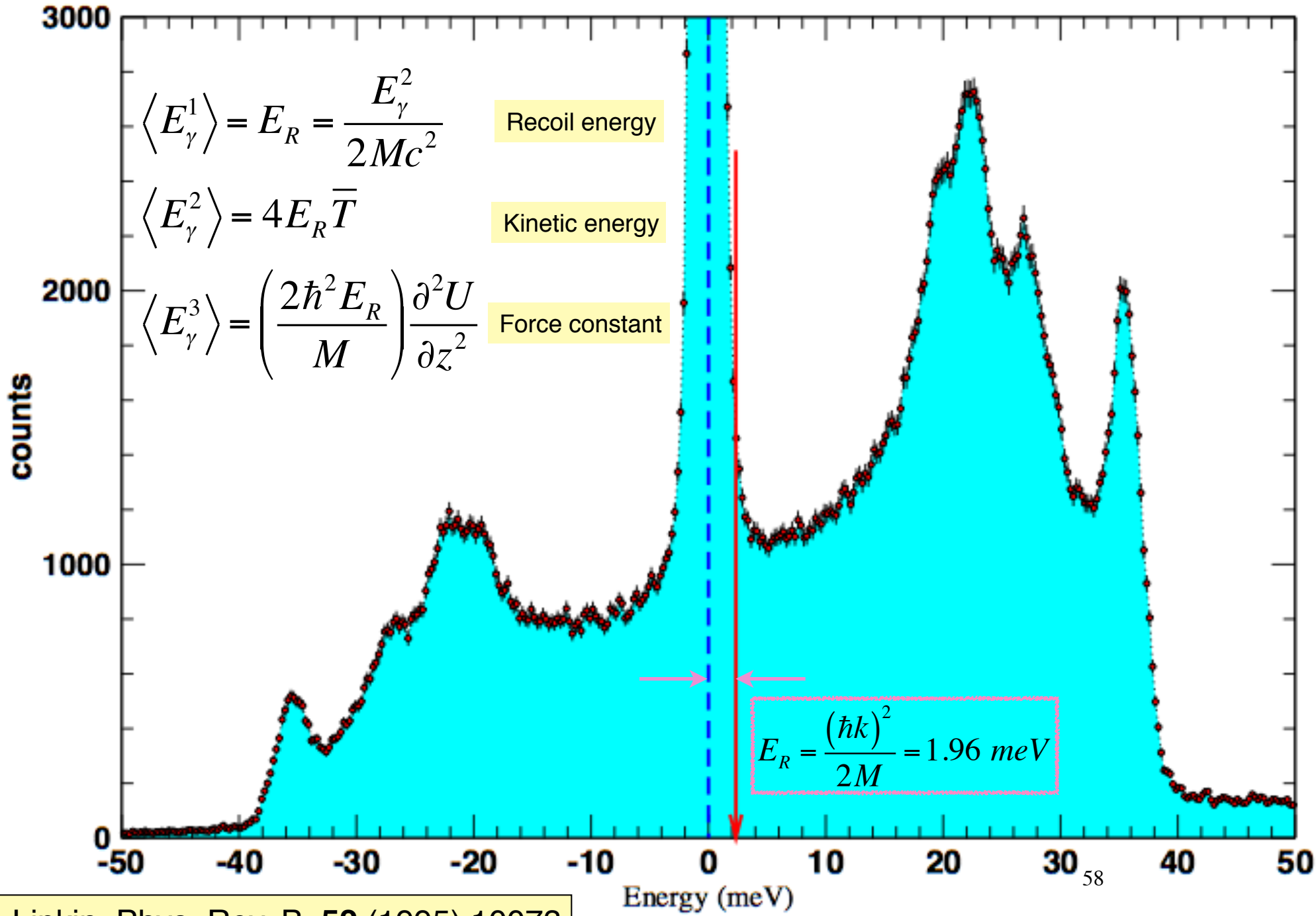

H. Lipkin, Phys. Rev. B, **52** (1995) 10073

Detailed Balance

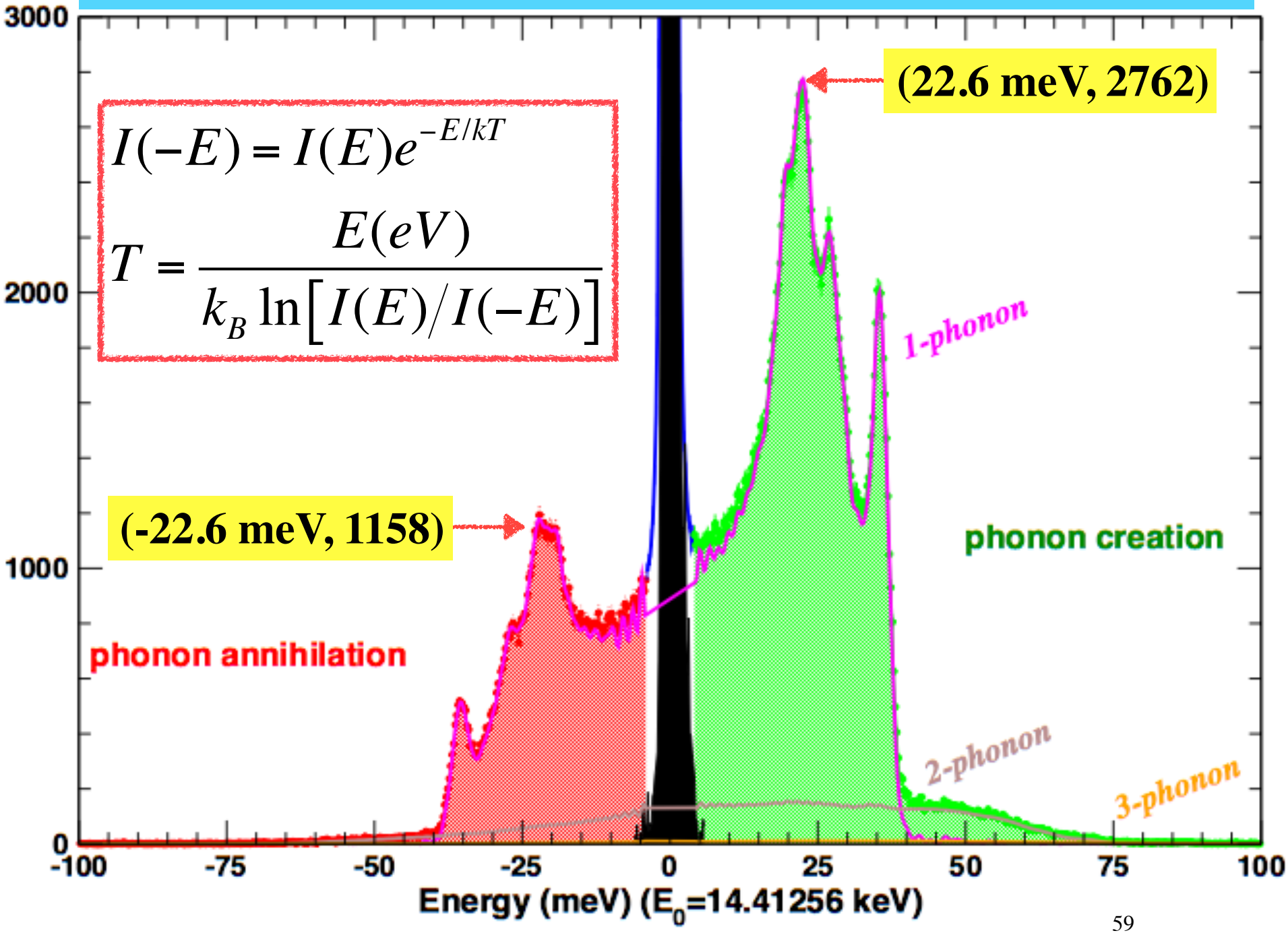

Detailed Balance

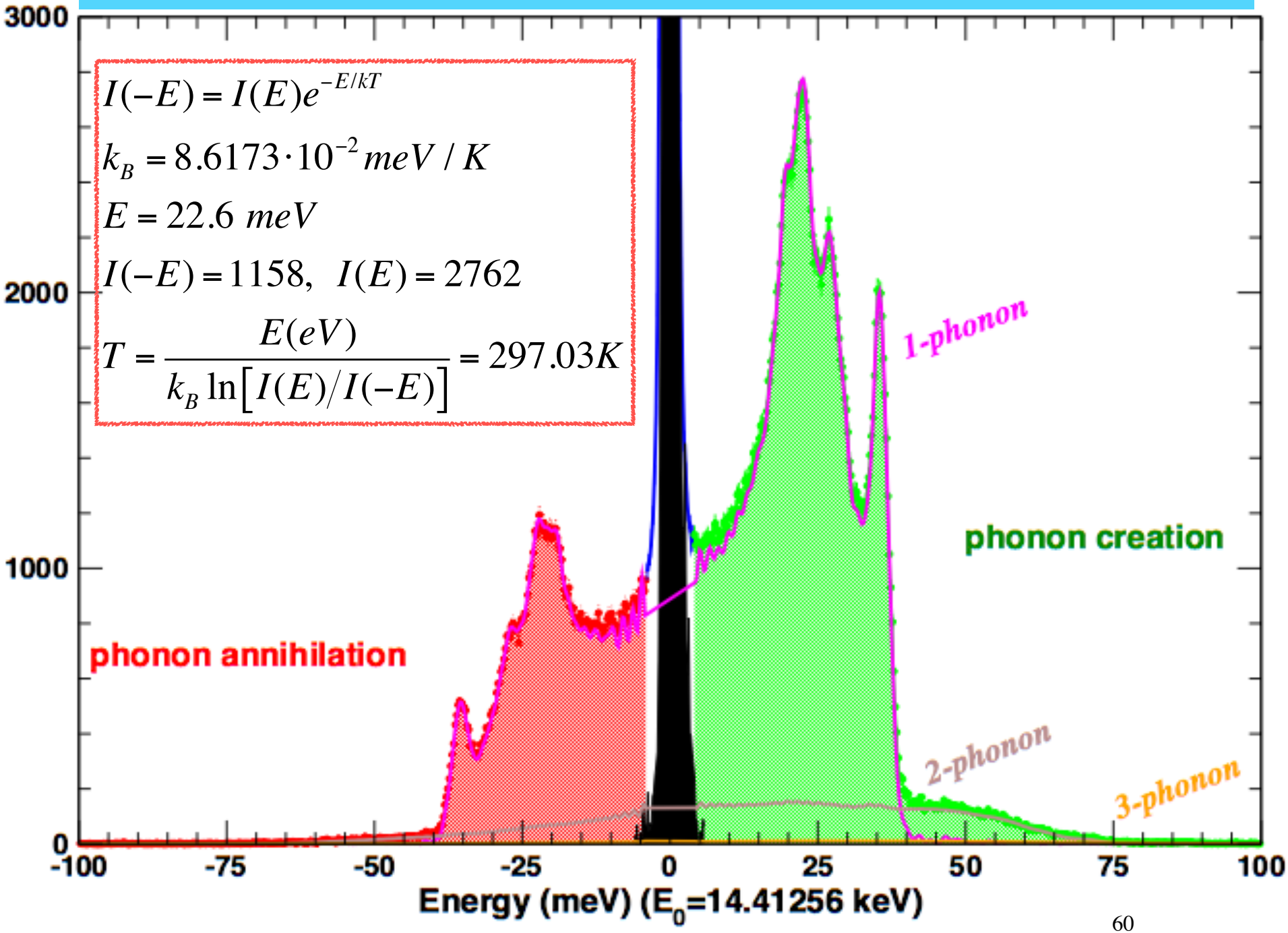

Temperature dependence of phonon excitation probability

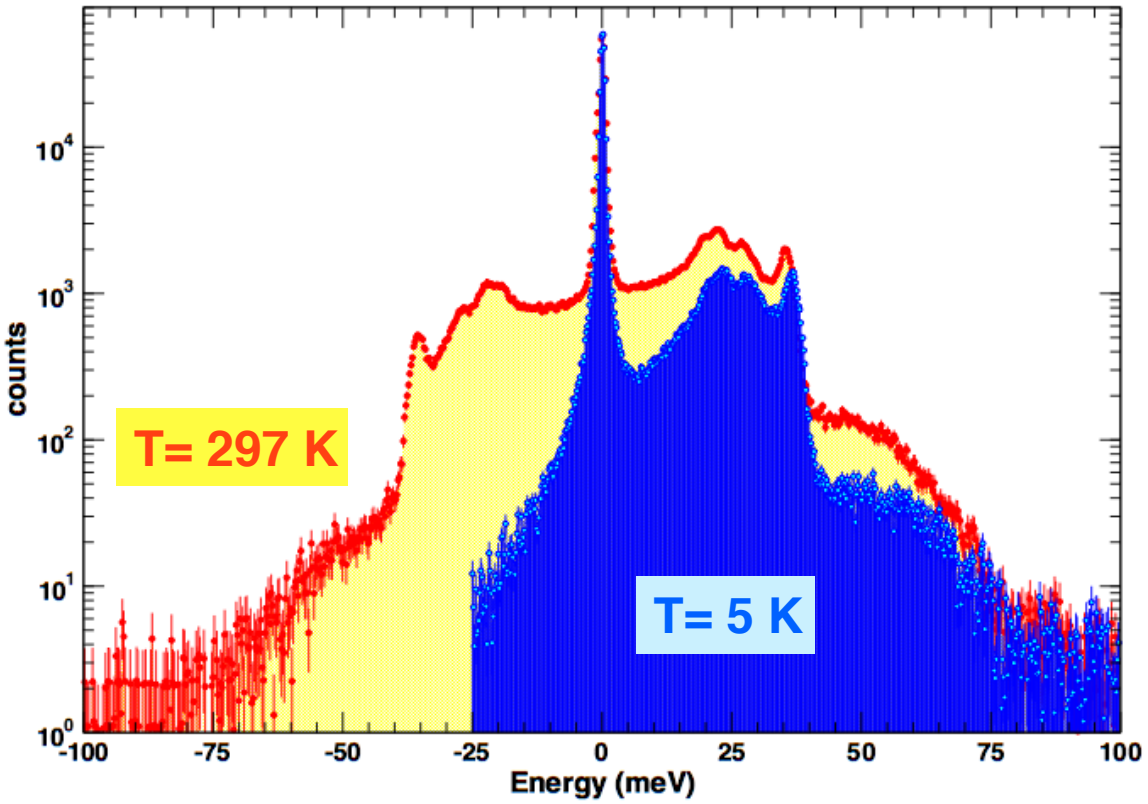

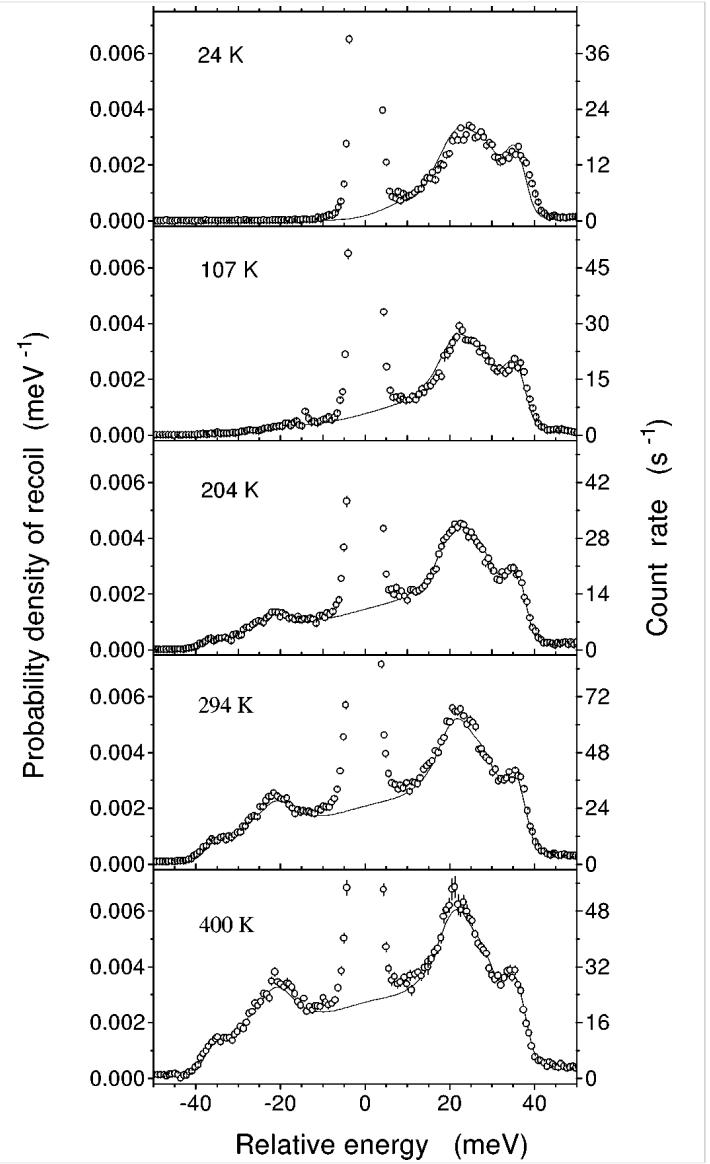

Chumakov, et al, Phys. Rev. B 54 (1996) 9596.

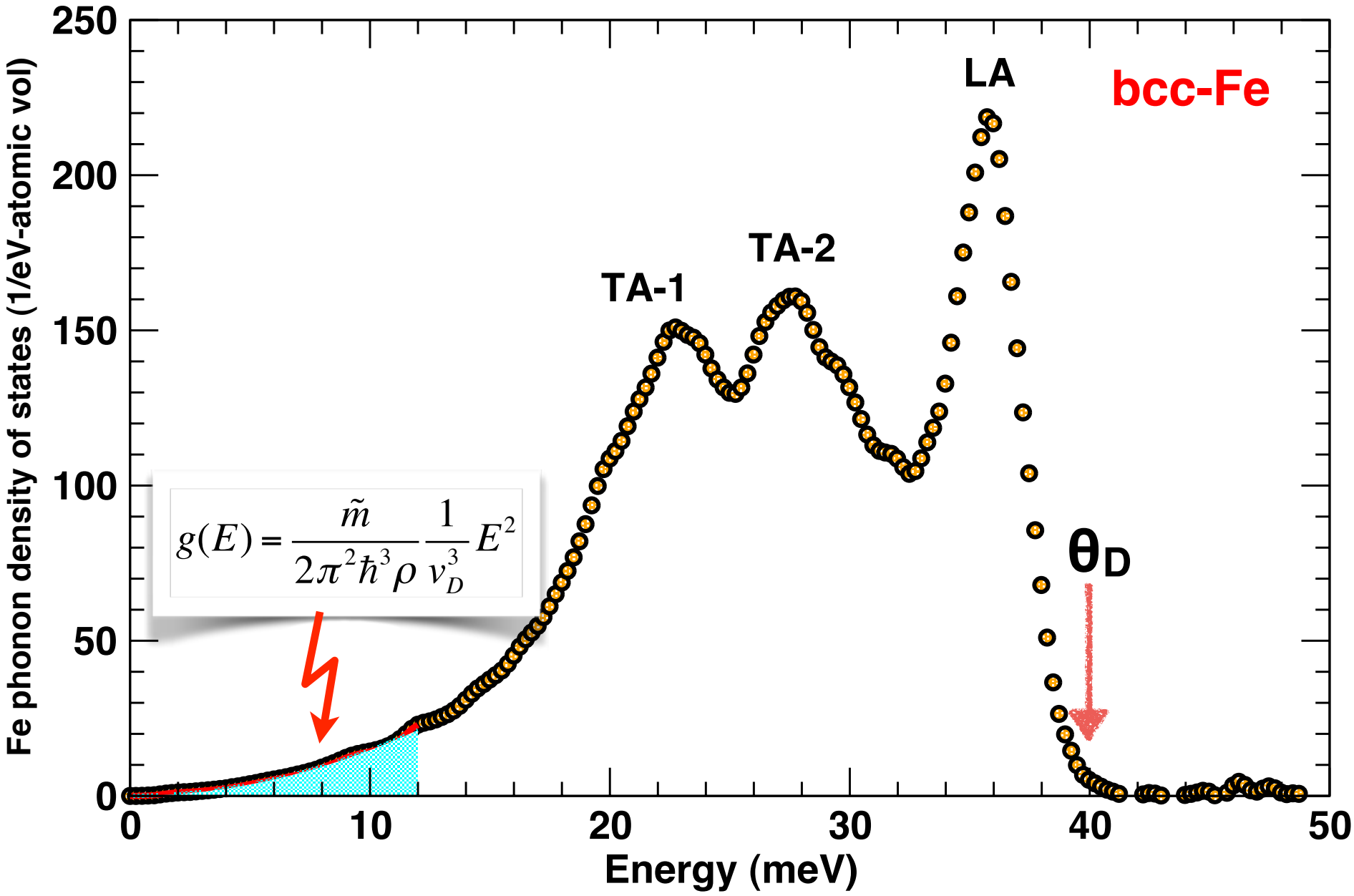
bcc-Fe
LA
TA-2
TA-1
θD
$g(E) = \frac{\tilde{m}}{2\pi^2\hbar^3\rho} \frac{1}{v_D^3} E^2$
Fe phonon density of states (1/eV-atomic vol)
Energy (meV)
0
50
100
150
200
250
0
10
20
30
40
50

Measurement of v_D, Debye sound velocity allows to resolve longitudinal and shear sound velocity, provided that bulk modulus and density, is independently and simultaneously measured by x-ray diffraction.

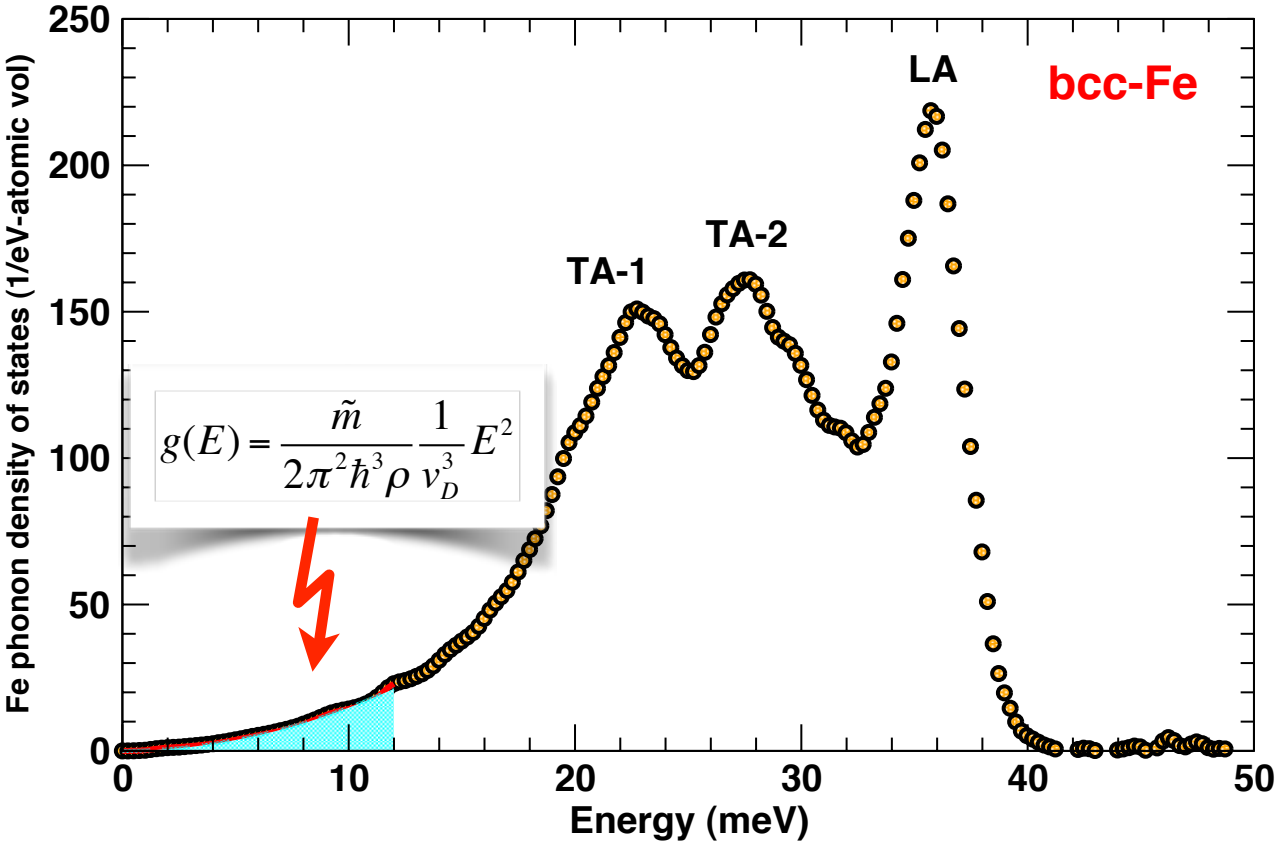

K (GPa)	ρ (g/cc)	V_D (m/s)	V_P (m/s)	V_S (m/s)	G (GPa)
165 ± 1	8.01	3510 ± 12	5813 ± 13	3146 ± 11	79.3 ± 0.6

$$\frac{K_S}{\rho} = V_P^2 - \frac{4}{3}V_S^2$$

$$\frac{G}{\rho} = V_S^2$$

$$\frac{3}{V_D^3} = \frac{1}{V_P^3} + \frac{2}{V_S^3}$$

K_S : adiabatic bulk modulus
G : shear modulus
V_P : compression wave velocity
V_S : shear wave velocity
V_D : Debye sound velocity
P : density

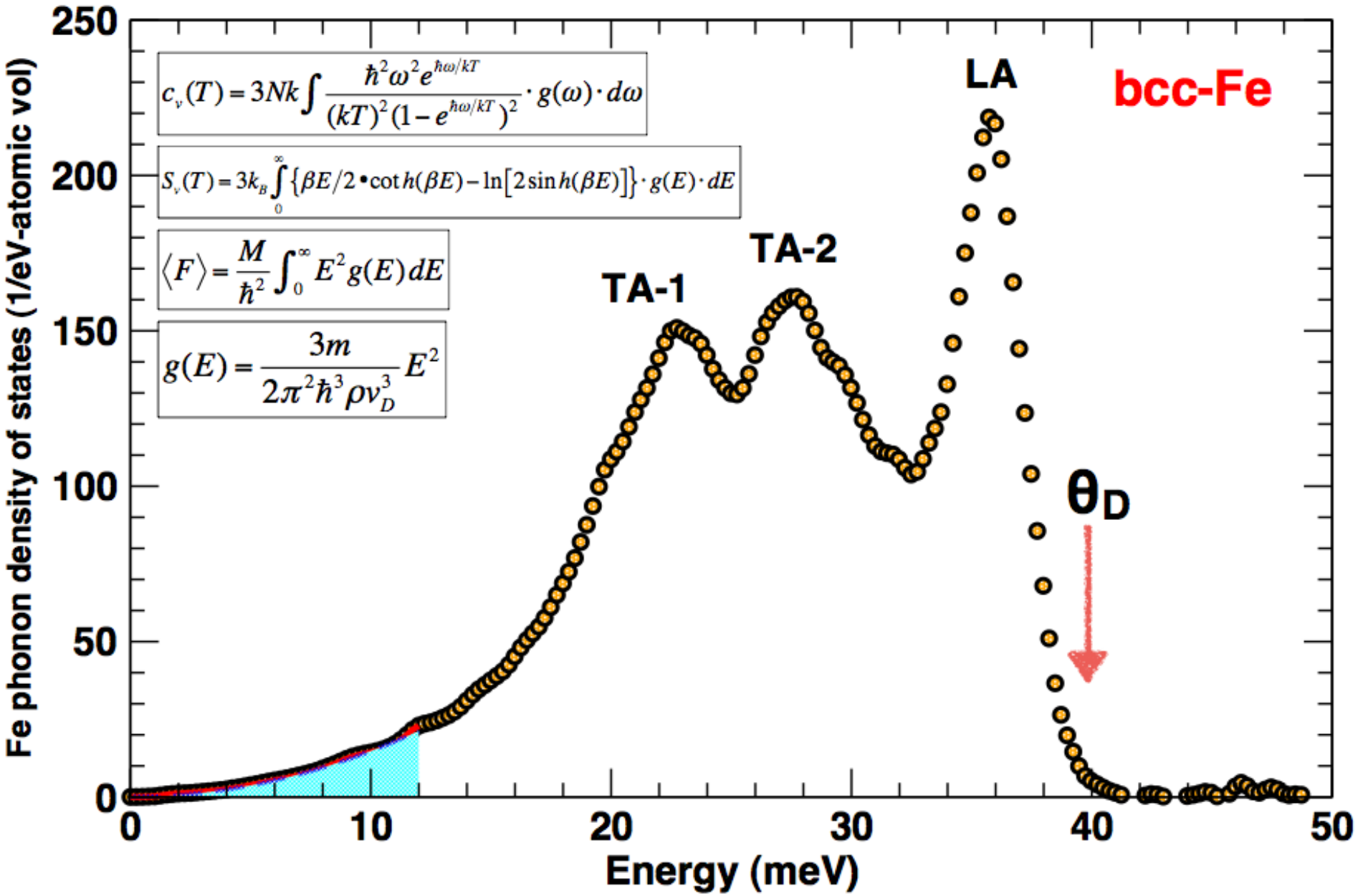
$c_v(T) = 3Nk \int \frac{\hbar^2 \omega^2 e^{\hbar\omega/kT}}{(kT)^2 (1 - e^{\hbar\omega/kT})^2} \cdot g(\omega) \cdot d\omega$
$S_v(T) = 3k_B \int_0^\infty \{\beta E/2 \bullet \cot h(\beta E) - \ln[2 \sin h(\beta E)]\} \cdot g(E) \cdot dE$
$\langle F \rangle = \frac{M}{\hbar^2} \int_0^\infty E^2 g(E) dE$
$g(E) = \frac{3m}{2\pi^2 \hbar^3 \rho v_D^3} E^2$
LA
bcc-Fe
TA-2
TA-1
θ_D
Fe phonon density of states (1/eV-atomic vol)
Energy (meV)
0
50
100
150
200
250
0
10
20
30
40
50

Thermodynamic properties as an additive function of phonon density of states

Lamb-Mössbauer factor

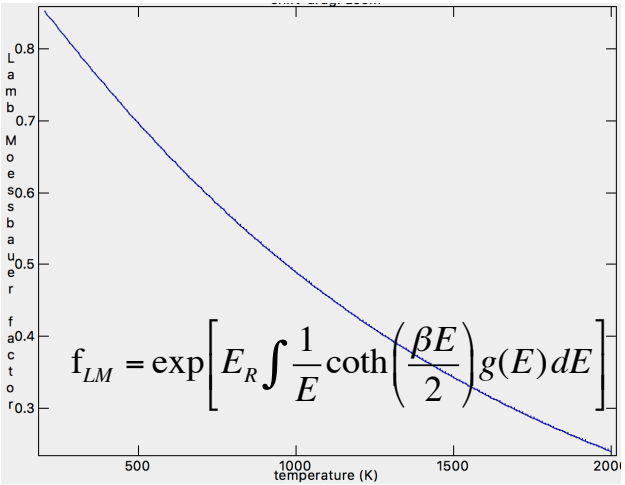

$$f_{LM} = \exp\left[E_R \int \frac{1}{E} \coth\left(\frac{\beta E}{2}\right) g(E)\,dE\right]$$

Vibrational entropy

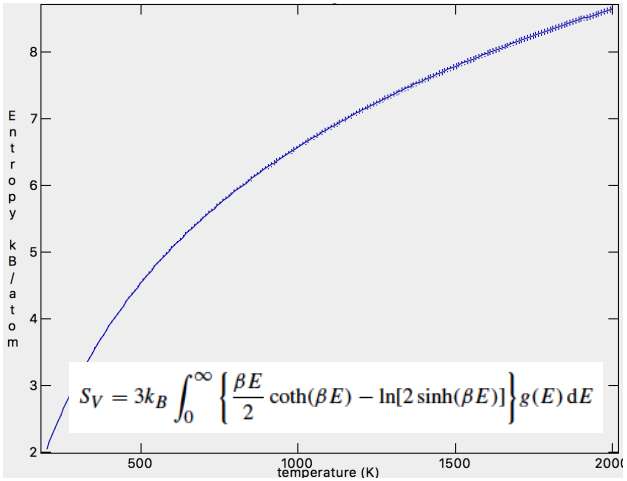

$$S_V = 3k_B \int_0^\infty \left\{\frac{\beta E}{2}\coth(\beta E) - \ln[2\sinh(\beta E)]\right\} g(E)\,dE$$

Specific heat

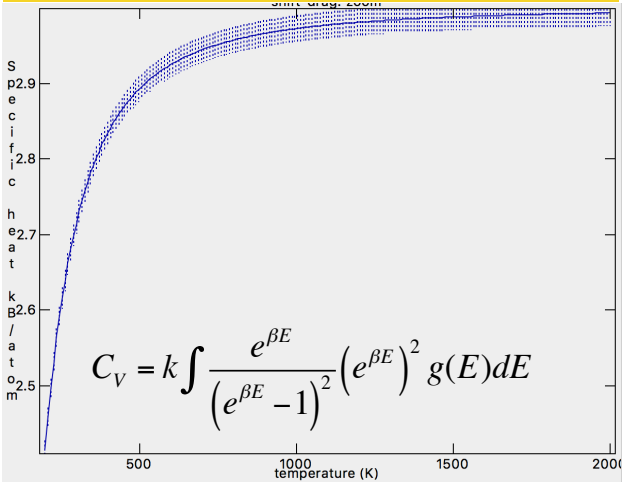

$$C_V = k \int \frac{e^{\beta E}}{\left(e^{\beta E} - 1\right)^2} \left(e^{\beta E}\right)^2 g(E)\,dE$$

Helmholz free energy

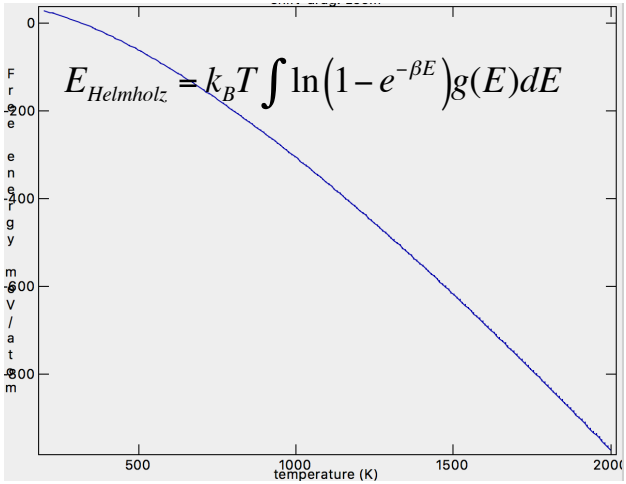

$$E_{Helmholz} = k_B T \int \ln\left(1 - e^{-\beta E}\right) g(E)\,dE$$

Kinetic energy

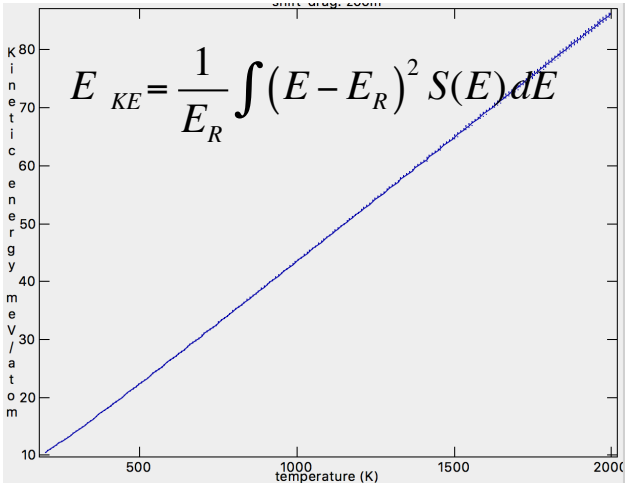

$$E_{KE} = \frac{1}{E_R} \int \left(E - E_R\right)^2 S(E)\,dE$$

Isotope fractionation

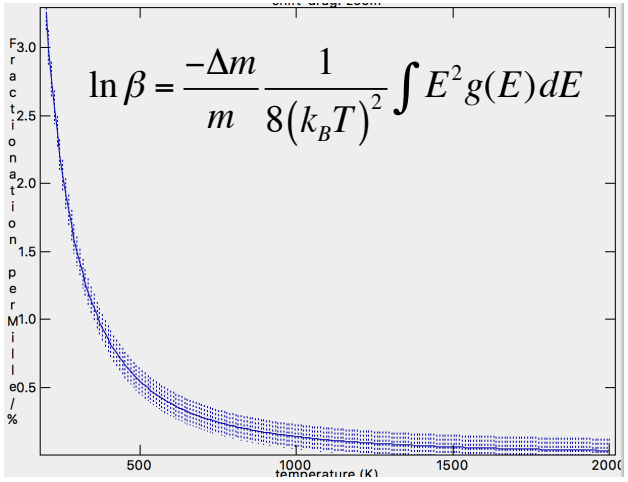

$$\ln\beta = \frac{-\Delta m}{m} \frac{1}{8\left(k_B T\right)^2} \int E^2 g(E)\,dE$$

Information from NRIXS spectra:

- directly from the data, S(E)
  - ⇨ temperature
    $$T = -\frac{E}{k_B} \ln\left[\frac{S(-E)}{S(E)}\right]$$
  - ⇨ mean square displacement
    $$\langle u^2 \rangle = -\frac{1}{k^2} \ln\left[1 - \int \{S(E) - S(0)\}\, dE\right]$$
  - ⇨ kinetic energy
    $$E_{kin} = \frac{1}{4E_R} \int (E - E_R)^2 S(E) dE$$
  - ⇨ average force constant
    $$D = \frac{k^2}{2E_R^2} \int (E - E_R)^3 S(E) dE$$

- quasi-harmonic lattice model
  - ⇨ partial phonon density of states
    $$\mathcal{D}(E)$$
  - ⇨ Debye sound velocity
    $$v_D = \left(\frac{M}{2\rho\pi^2\hbar^3} \frac{E^2}{\mathcal{D}(E \to 0)}\right)^{1/3}$$
  - ⇨ Grüneisen parameter
    $$\gamma_D = \frac{1}{3} + \frac{\rho}{v_D} \left(\frac{\partial v_D}{\partial \rho}\right)_T$$
  - ⇨ isotope fractionation
    $$\ln \beta = -\frac{\Delta m}{M} \frac{1}{8(k_B T)^2} \int E^2 \mathcal{D}(E)\, dE$$

k ~ wave number of nuclear transition
E_R ~ recoil energy
ρ ~ mass density

M ~ mass of resonant isotope
Δm ~ isotope mass difference
k_B ~ Boltzmann's constant
T ~ temperature

Courtesy: W. Sturhahn

Phonon density of states

$$g(k)\,\mathrm{d}k = \frac{V}{(2\pi)^3}\,4\pi k^2\,\mathrm{d}k.$$

Number of wave vectors in a spherical shell of radius k per unit volume of reciprocal space.

$$g(\omega) = \frac{3V}{2\pi^2 c^3}\omega^2$$

Phonon density of states has a quadratic dependence on frequency, and inversely proportional to the cube of sound velocity.

Debye model

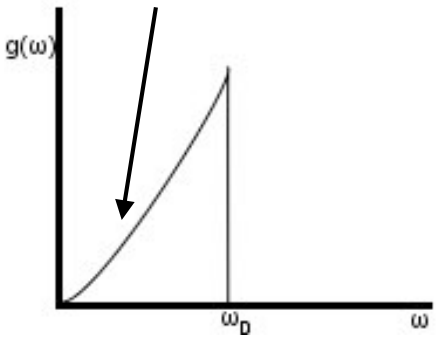

pure iron

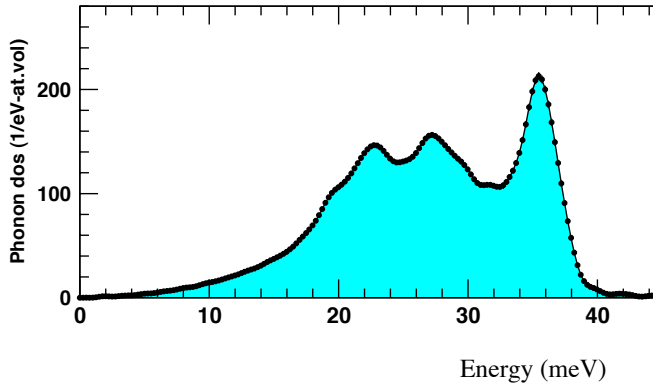

Fe-TPP-NO

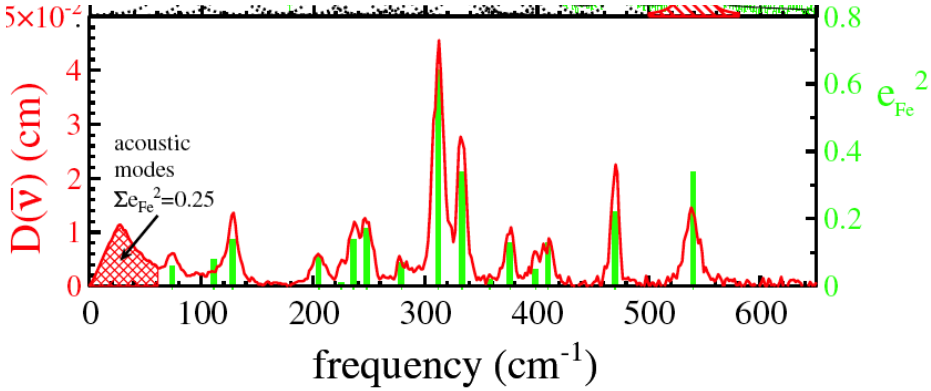

$DyFe_3$

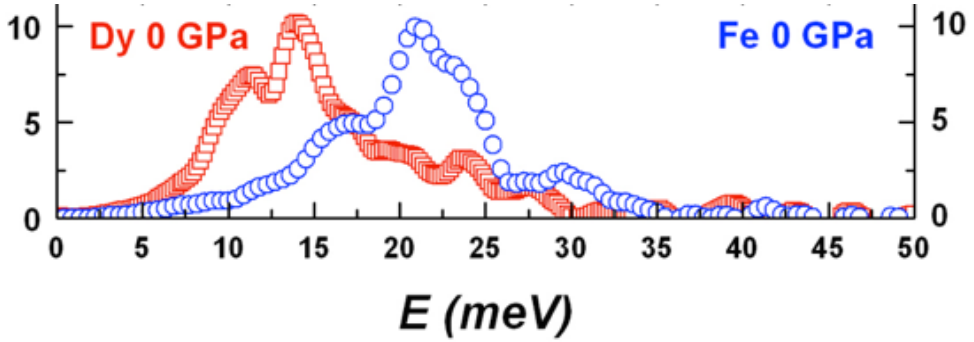

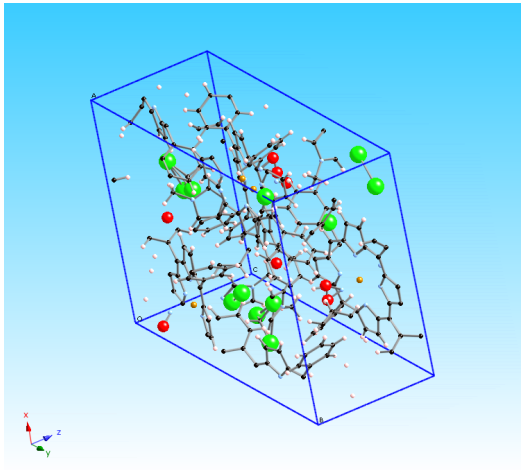

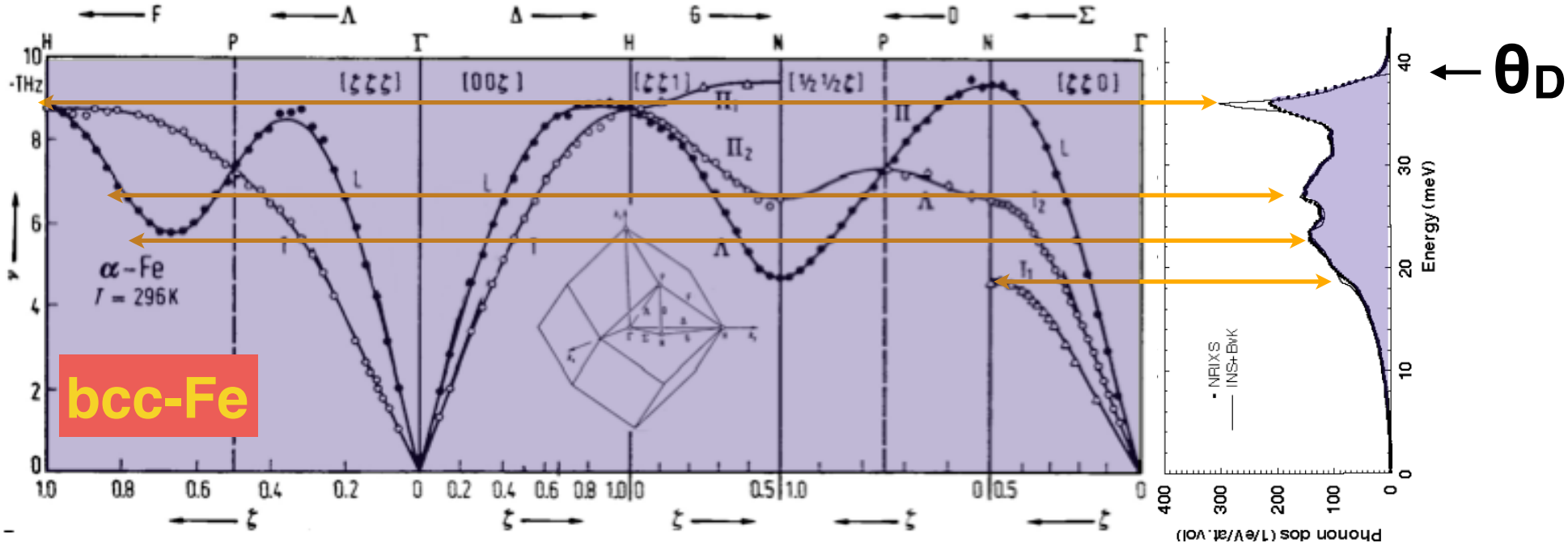

$\leftarrow \theta_D$

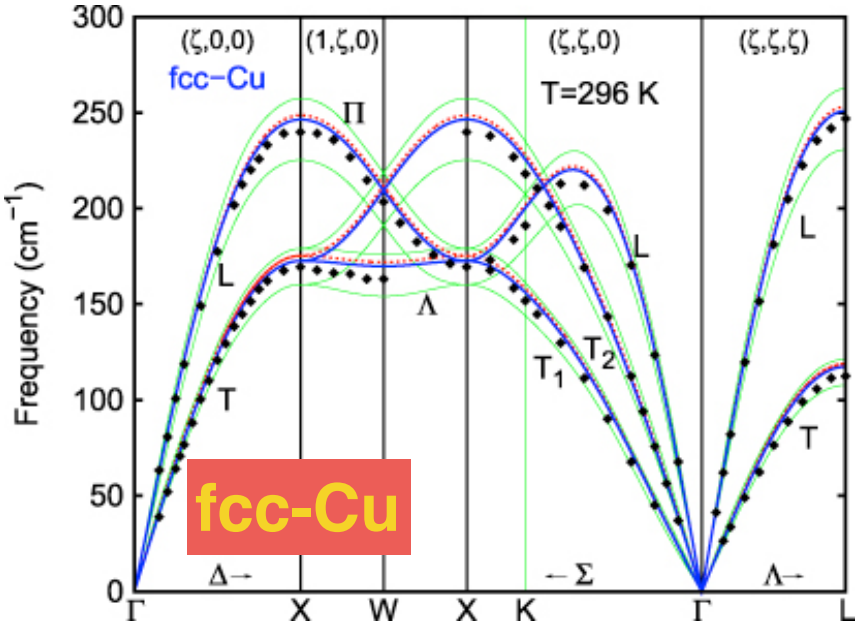

Let's assume that the acoustic modes have a linear relationship between frequency and wave vector:

$\omega = ck$, where ***c*** is average sound velocity

Maximum frequency cut off is at Debye energy: e.g. for Cu, this frequency is 240 cm^{-1} (~ 30 meV). Considering 1 meV = 11.605 K=8.065 cm^{-1}, this corresponds to 348 K, which is close to 344 K.

For Fe, the measured cut-off value is ~ 39.5 meV, which corresponds to 458 K, very close to reported 460 K.

Phonon density of states of iron under high pressure

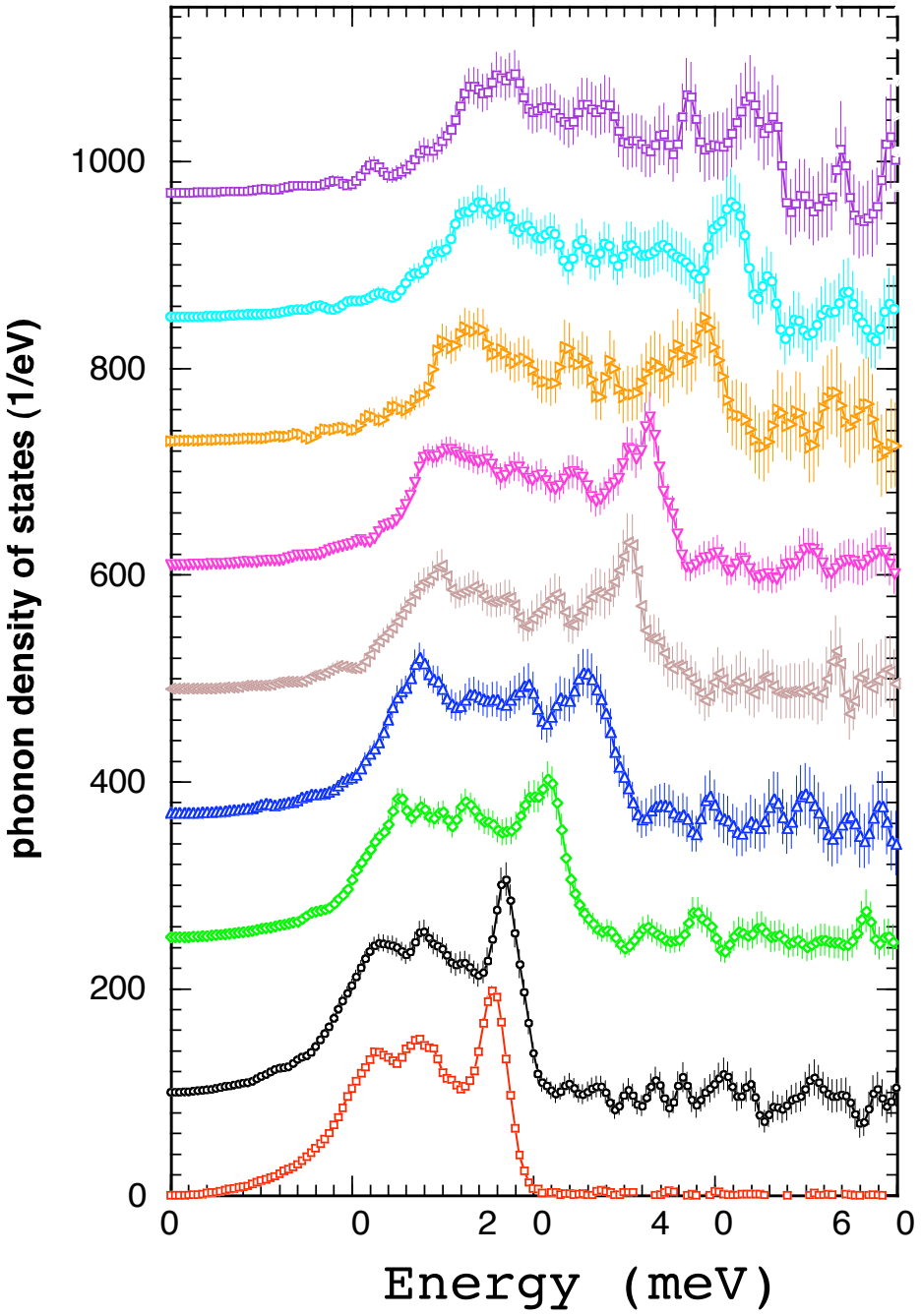

153 GPa

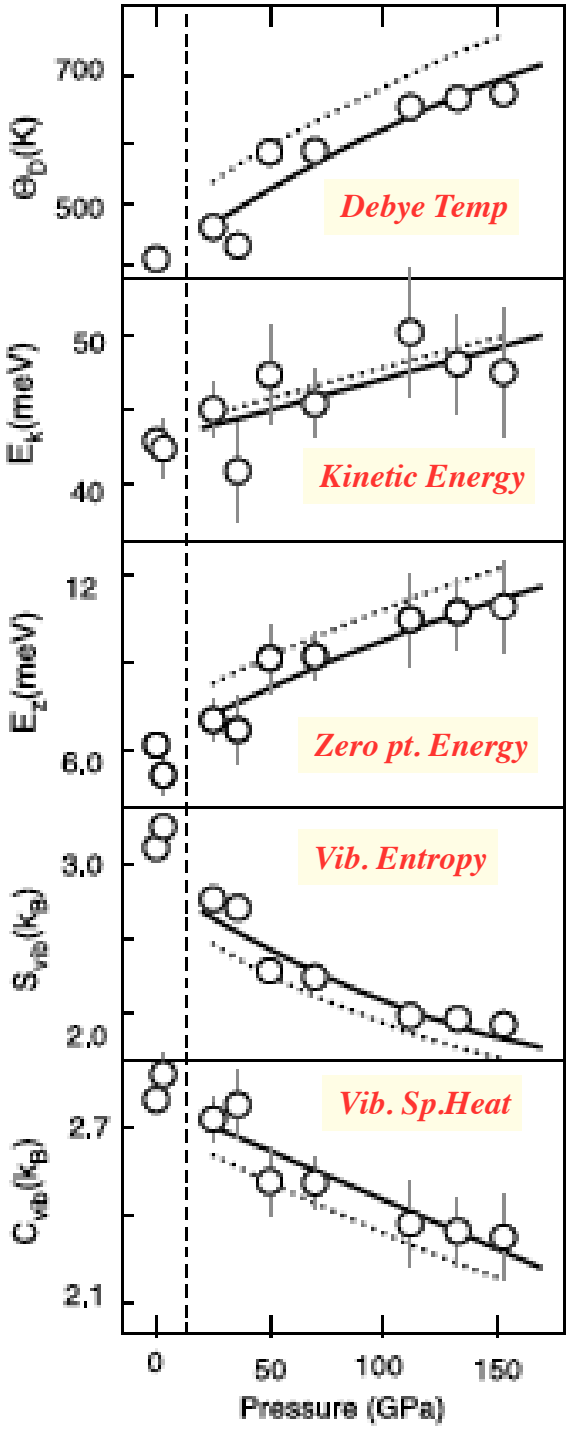

H.K. Mao, et al, Science, 292 (2001) 914

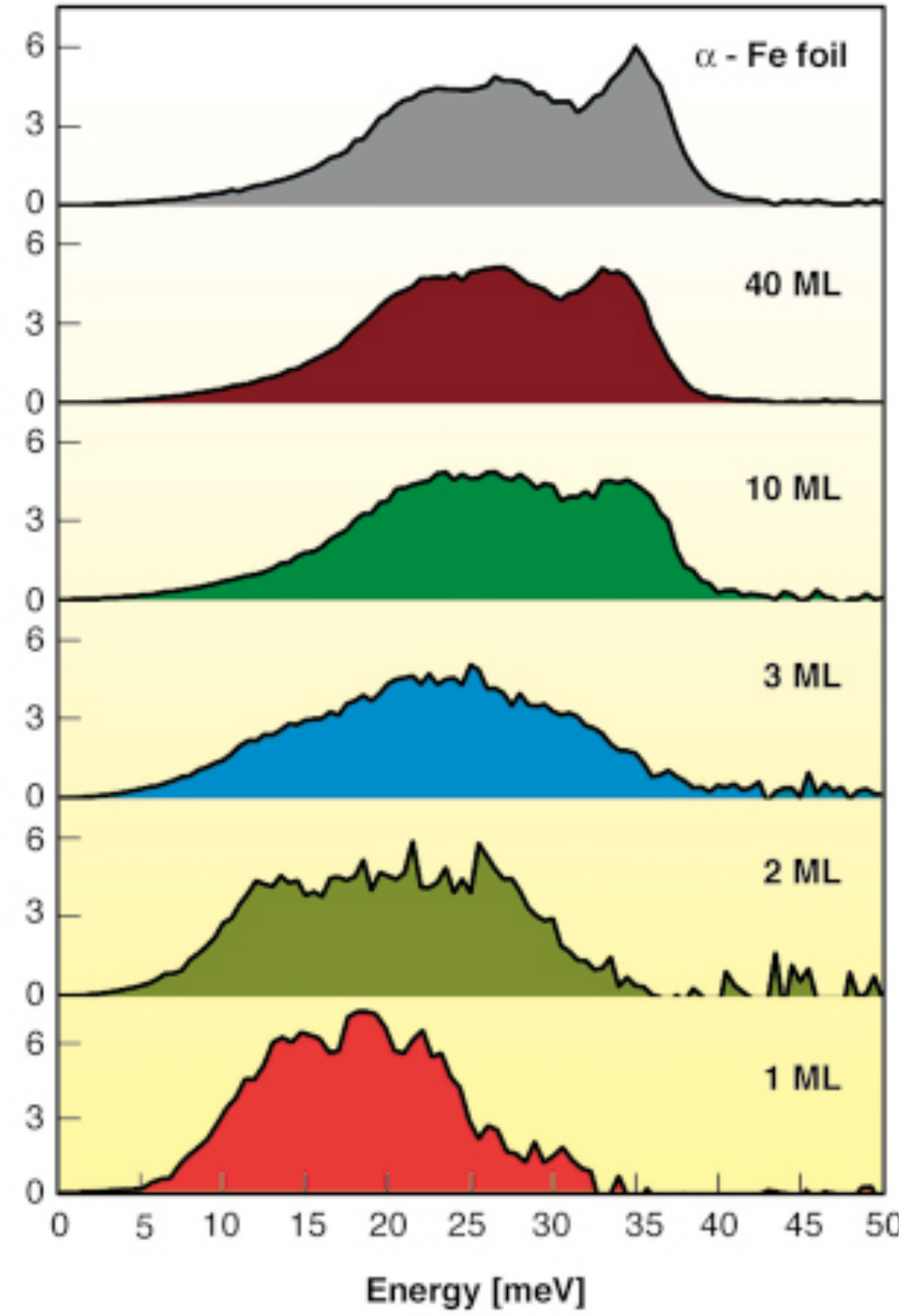

Fe films deposited on W(110)

Transition from the bulk to a single iron monolayer

S. Stankov, R. Röhlsberger, T. Slezak, M. Sladecek, B. Sepiol, G. Vogl, A. I. Chumakov, R. Rüffer, N. Spiridis, J. Lazewski, K. Parlinski, and J. Korecki,

ESRF Highlights 2006

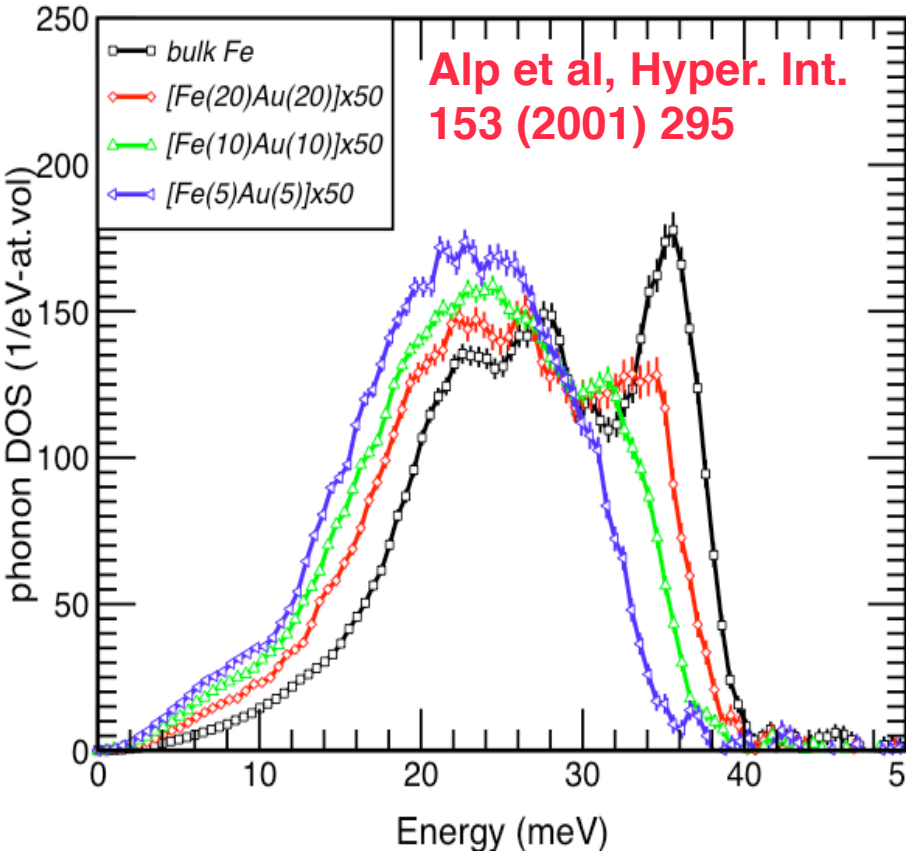

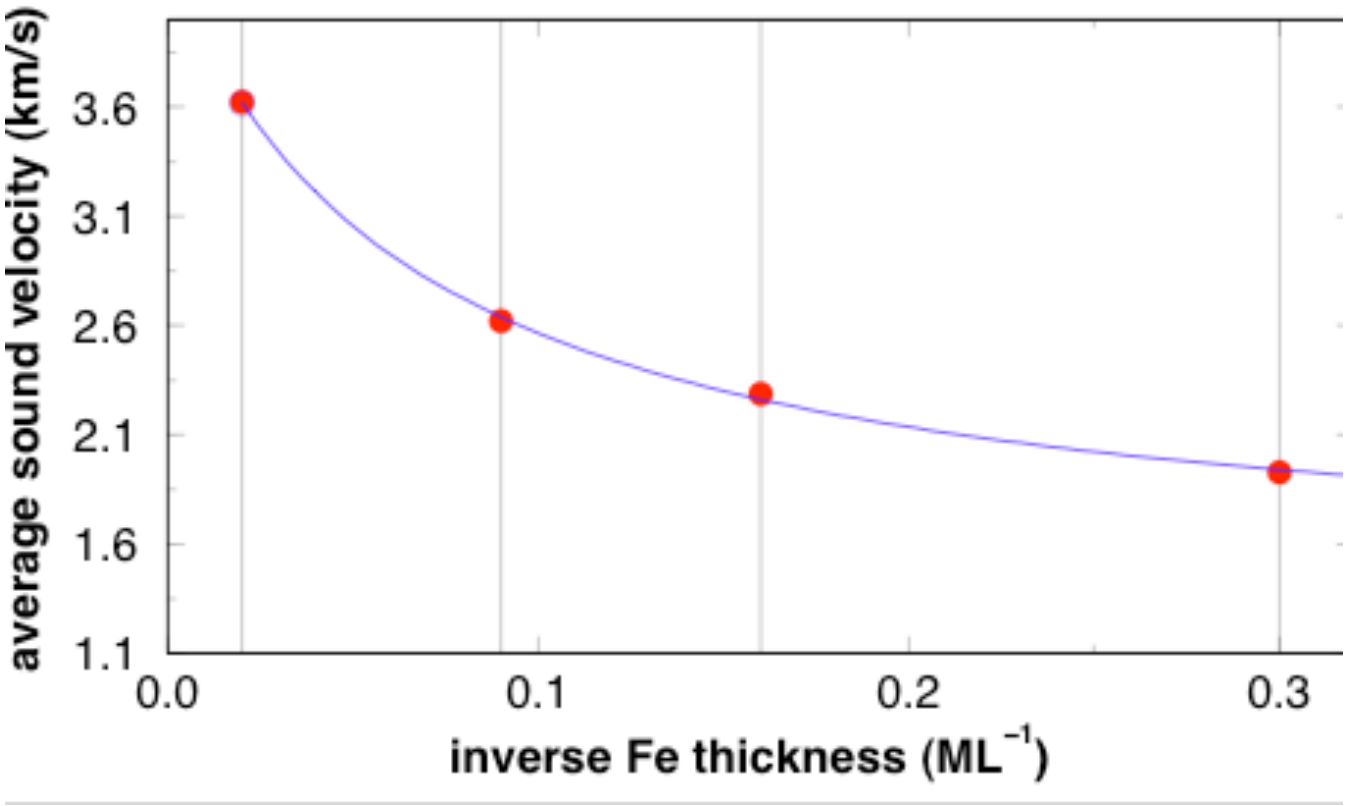
average sound velocity (km/s)
3.6
3.1
2.6
2.1
1.6
1.1
0.0
0.1
0.2
0.3
inverse Fe thickness (ML^{-1})

1. Thermoelectric materials: always something new !..

Skutterudites

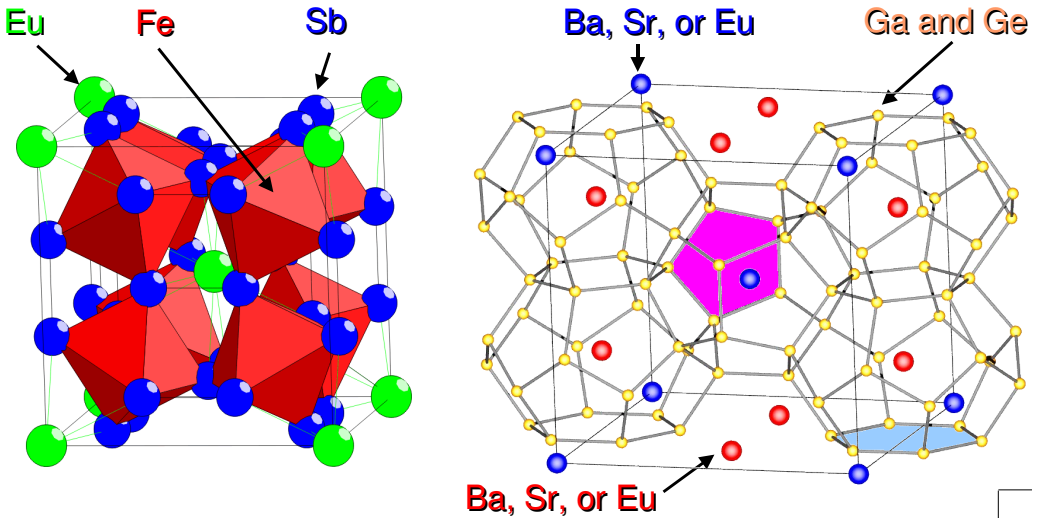

$EuFe_4Sb_{12}$

The loosely bound guests affect the characteristics of the vibrations, and change the thermal conductivity

Many elements in modern thermolelectric materials include **Fe**, rare-earth atoms like **Eu, Sm, Dy**, as well as **Sb**, and **Te**. These are all proper Mössbauer resonances we can exploit, and we do..

Wille, et al, PRB 76 (2007) 140301

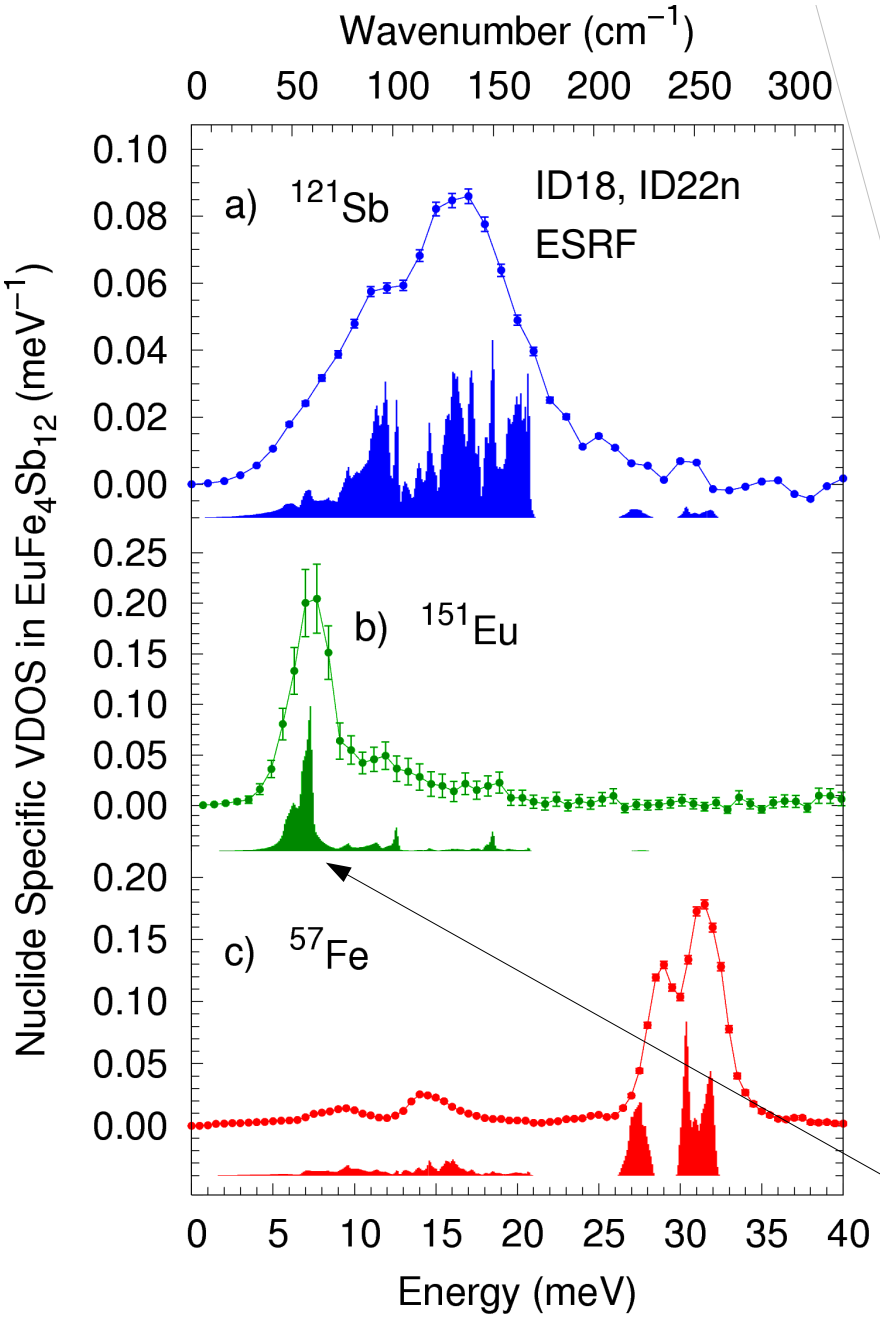

Vibrational dynamics of the host framework in Sn clathrates

Bogdan M. Leu,[1,*] Mihai Sturza,[2] Michael Y. Hu,[1] David Gosztola,[3] Volodymyr Baran,[4] Thomas F. Fässler,[4] and E. Ercan Alp[1]

$K_8Zn_4Sn_{42}$

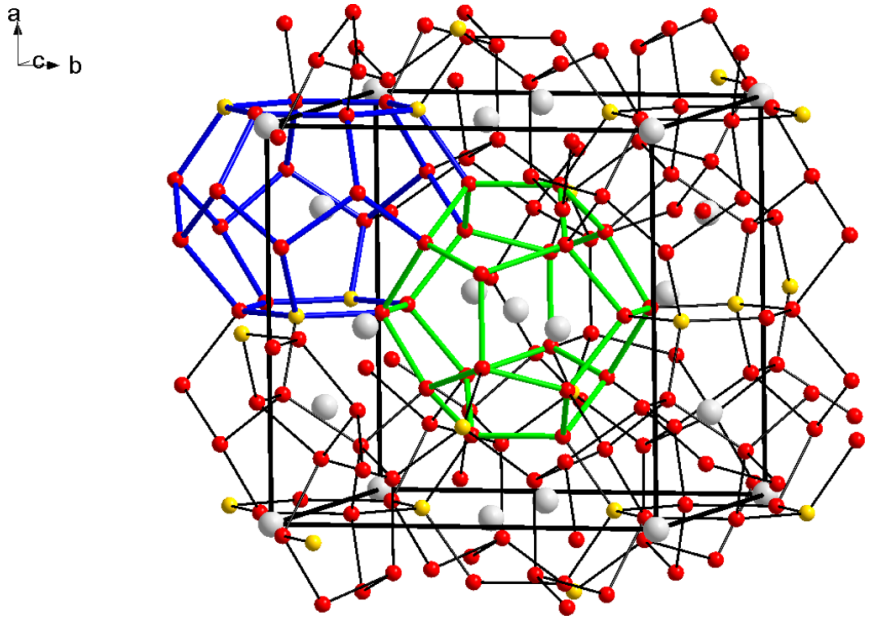

FIG. 1. (Color online) Structure of type-I clathrate $K_8Zn_4Sn_{42}$. Color scheme: gray = K, yellow = Zn/Sn, red = Sn. One small (pentagonal dodecahedron) and large (tetrakaidecahedron) host framework cage are highlighted in green and blue, respectively.

$Ba_8Ga_4Sn_{30}$

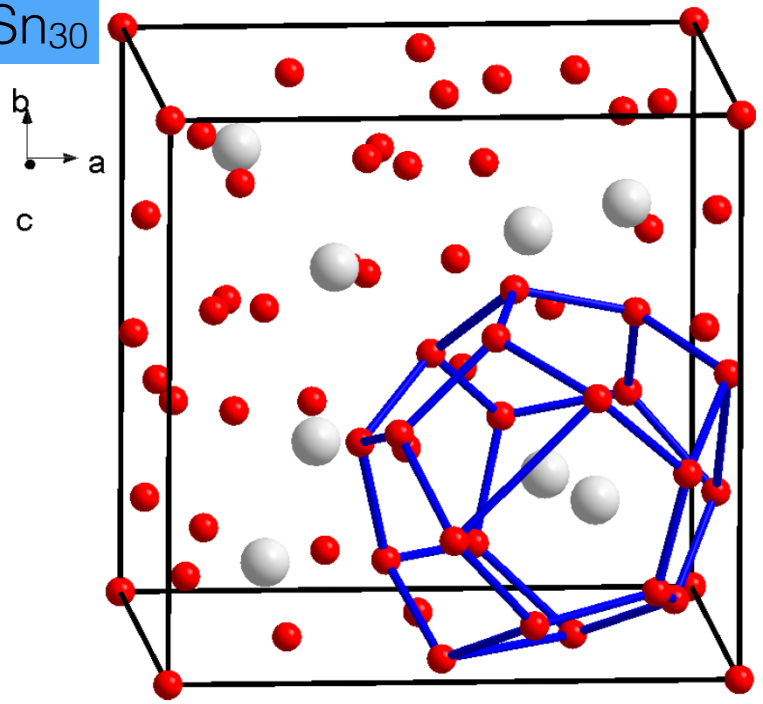

FIG. 2. (Color online) Structure of type-VIII clathrate $Ba_8Ga_{16}Sn_{30}$. Color scheme: gray = Ba, red = Sn/Ga. One host framework cage (pentagonal dodecahedron) is highlighted in blue.

type-I clathrate: pentagonal dodecahedra and tetrakaidecahedra alternating in a 1:3 ratio

type VIII : pentagonal dodecahedra; however, BGS adopts the type-I clathrate structure at high-temperature

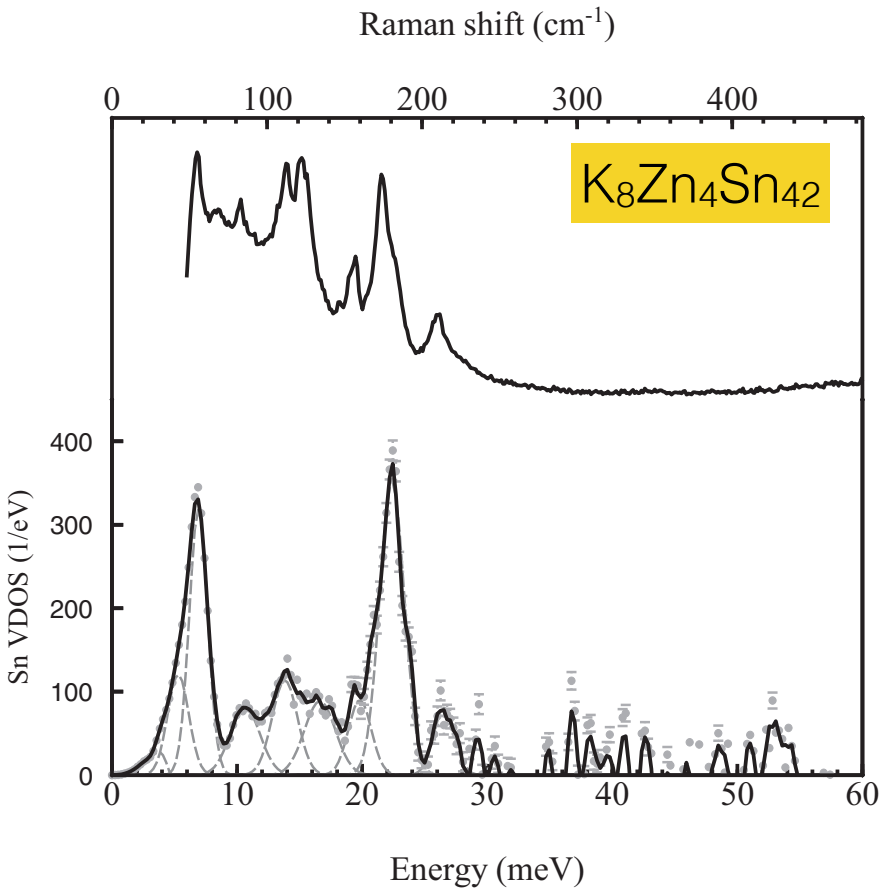

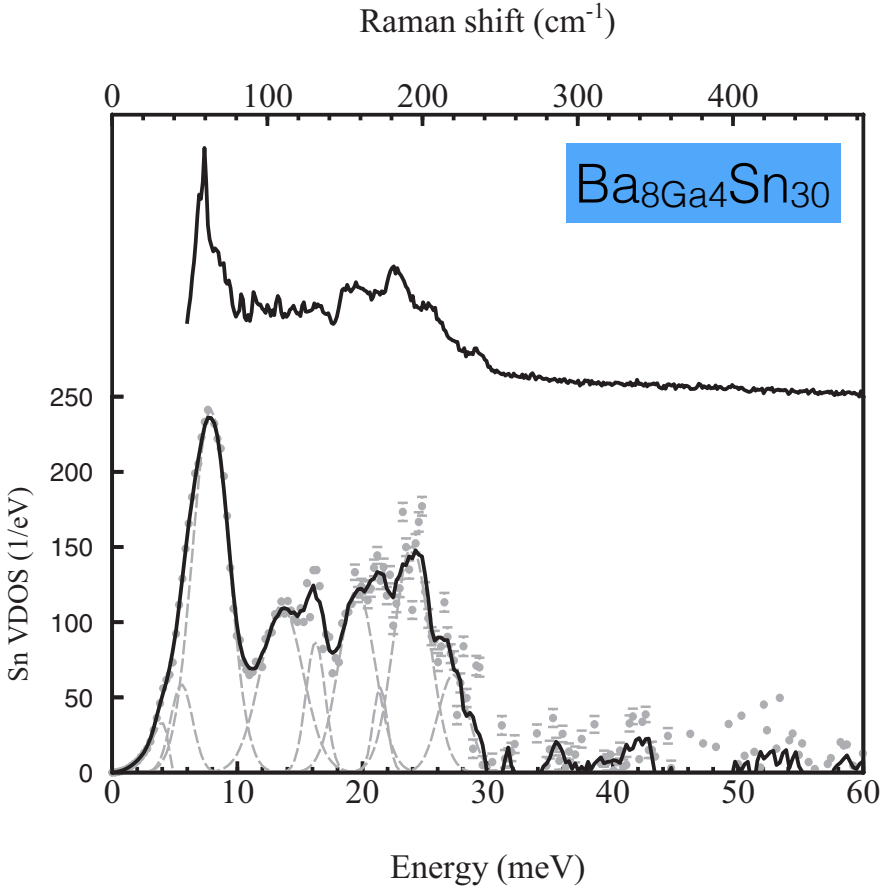

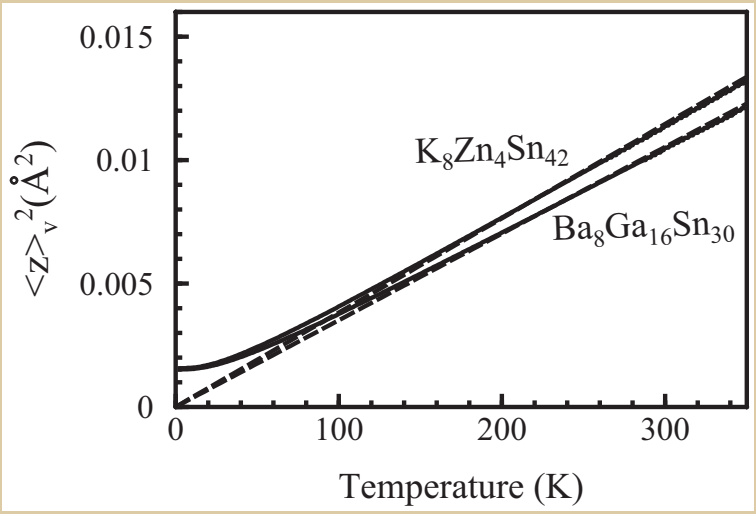

mean square displacement via phonon dos

$$\langle z^2 \rangle_v = \frac{1}{3k^2} \int [2\bar{n}(\bar{\nu}) + 1] \frac{\bar{\nu}_R}{\bar{\nu}} D(\bar{\nu}) d\bar{\nu},$$

3.8×10^{-5} Å^2/K for KZS and 3.5×10^{-5} Å^2/K for BGS.

H. Giefers, et al, Phys. Rev. Lett. 98 (2007) 245502

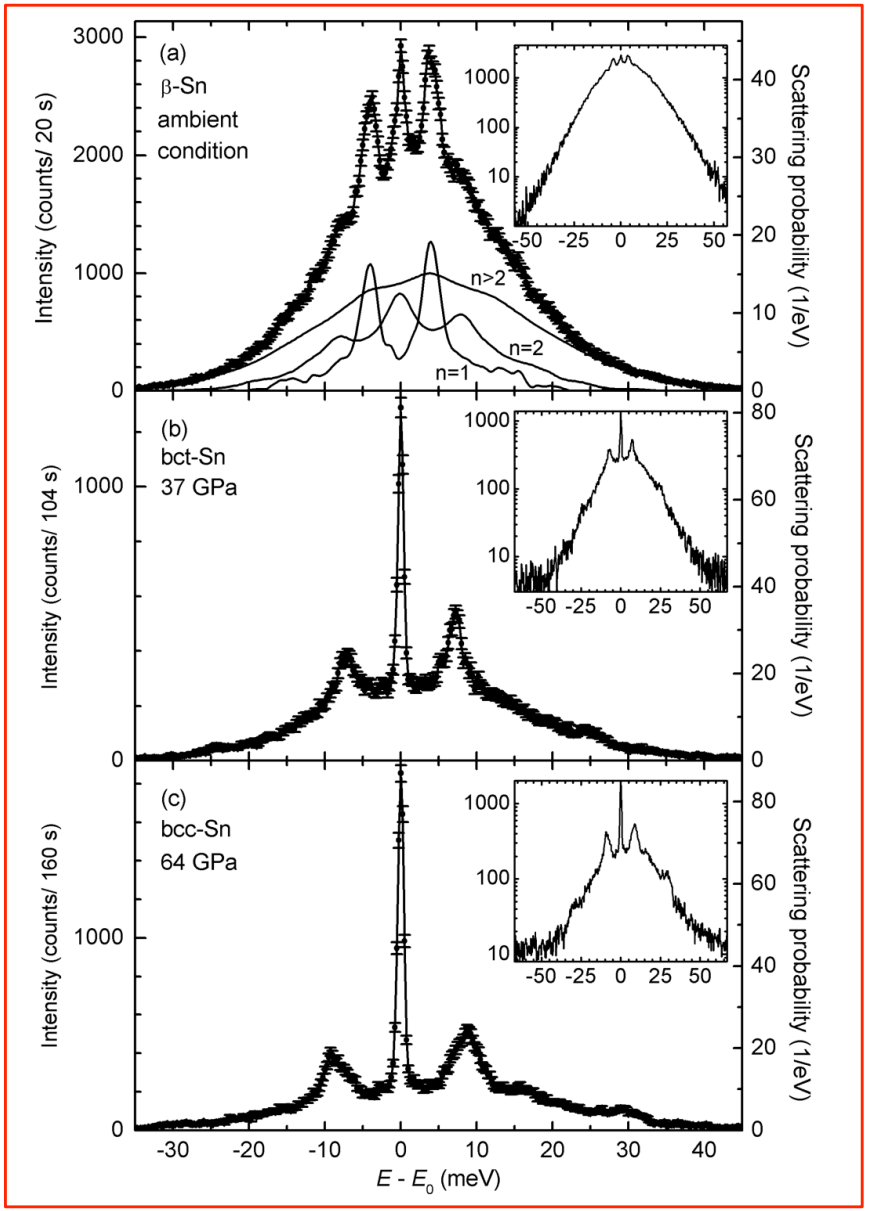

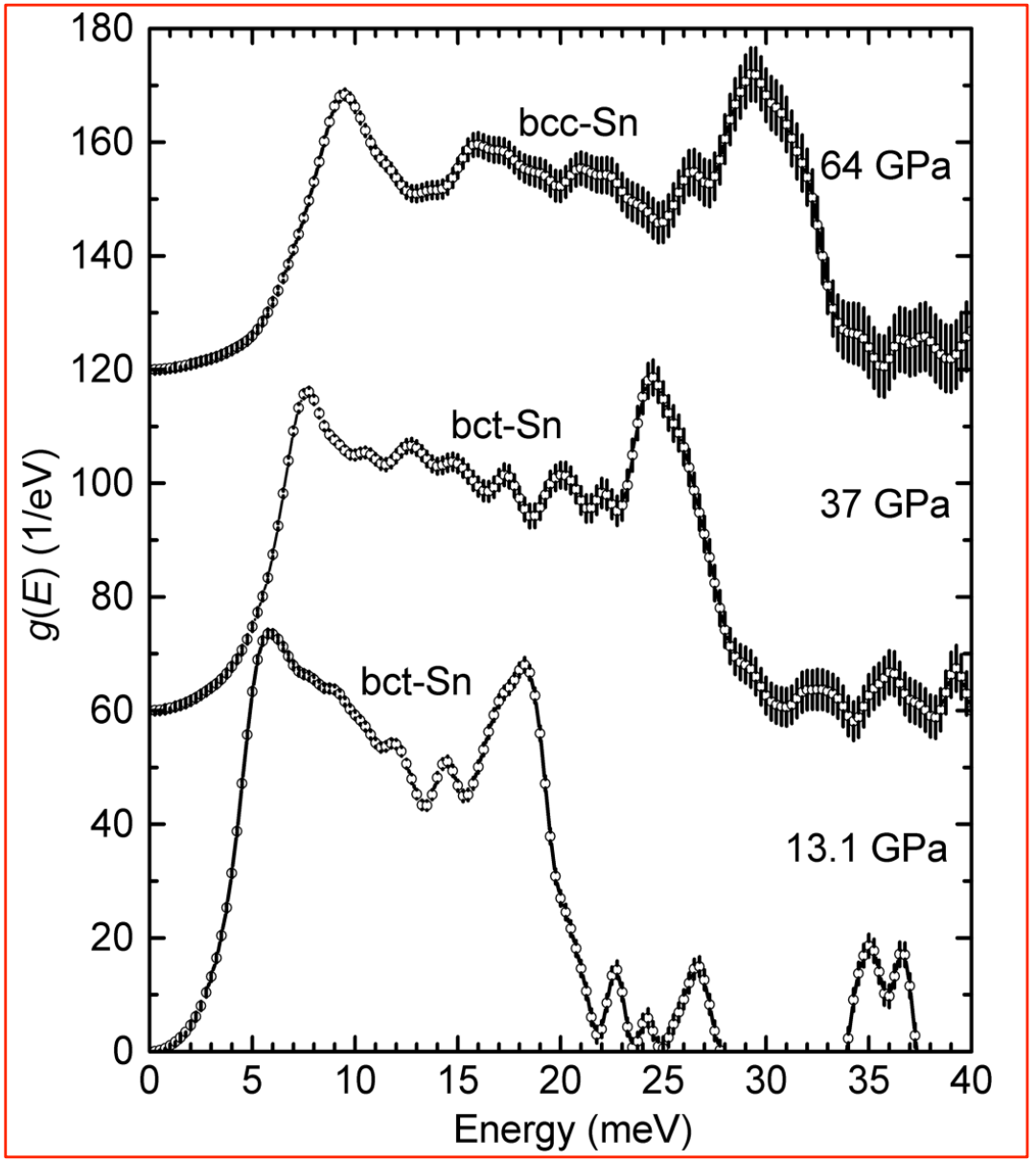

H. Giefers, et al, Phys. Rev. Lett. 98 (2007) 245502

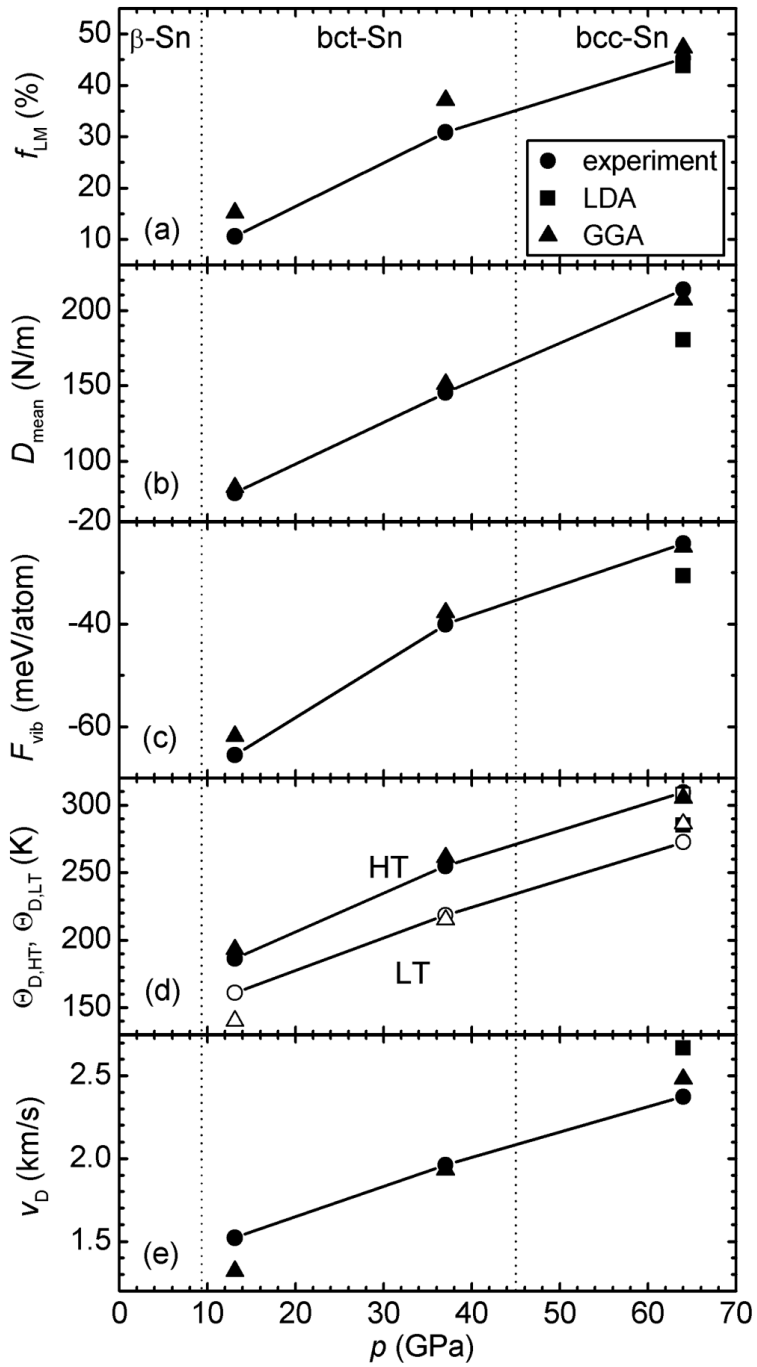

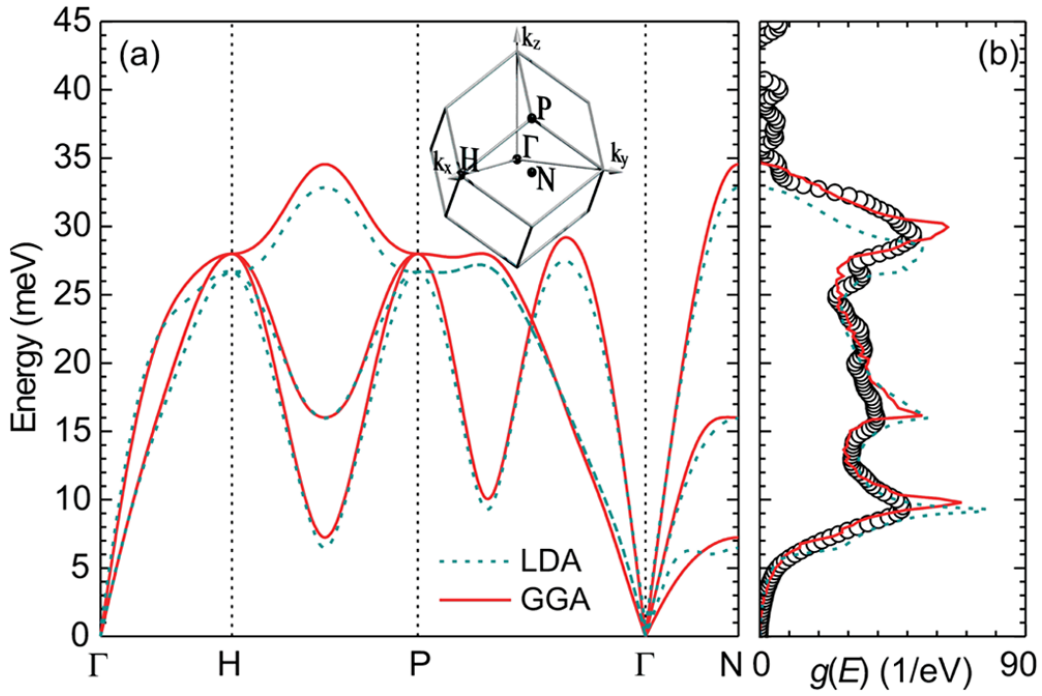

FIG. 3 (color online). (a) Theoretical phonon dispersion relation of bcc-Sn at 64 GPa. The inset shows the Brillouin zone of the bcc-Sn lattice. (b) Comparison between the theoretically calculated phonon DOS (lines) and the experimentally derived phonon DOS at 64 GPa (circles).

Biology & bio-inorganic chemistry

S. Cramer	University of California-Davis
E. Solomon	Stanford University
T. Sage	Northeastern University
E. Munck	University of Pittsburg
DeBeer George	Cornell University
Nicolai Lehnert	University of Michigan
R. Scheidt	University of Notre Dame

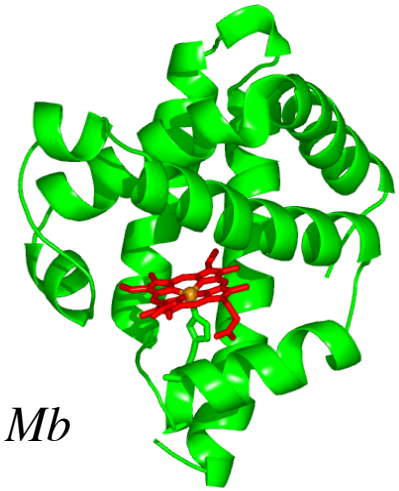

Mb

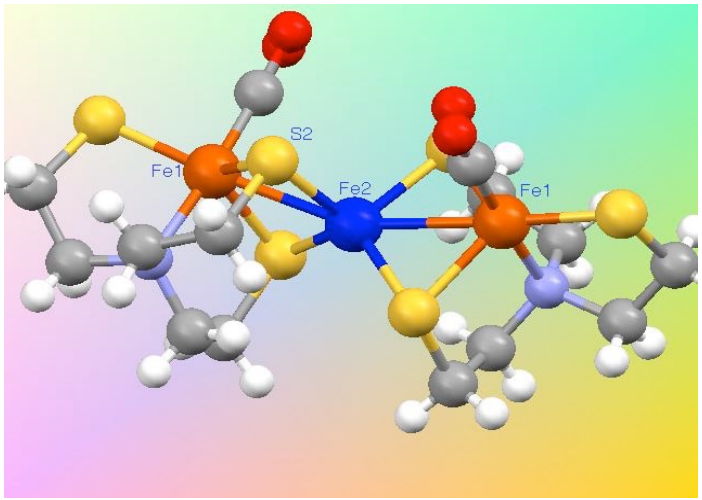

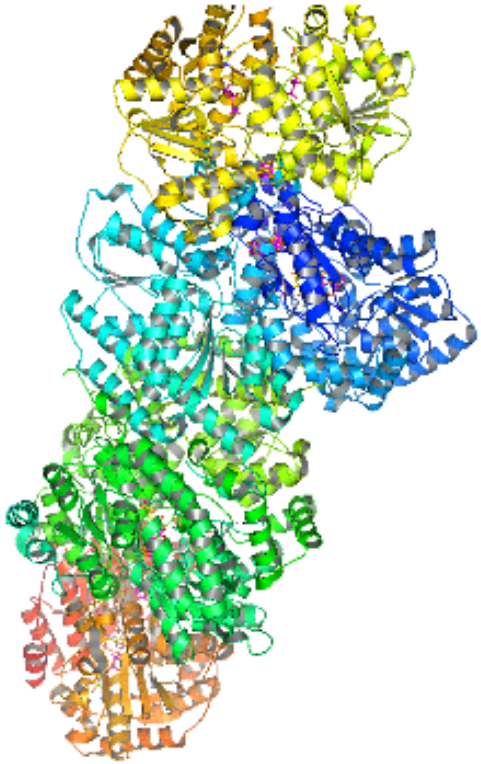

Vibrational spectroscopy of proteins, enzymes and biomimic model porphyrins and cubanes

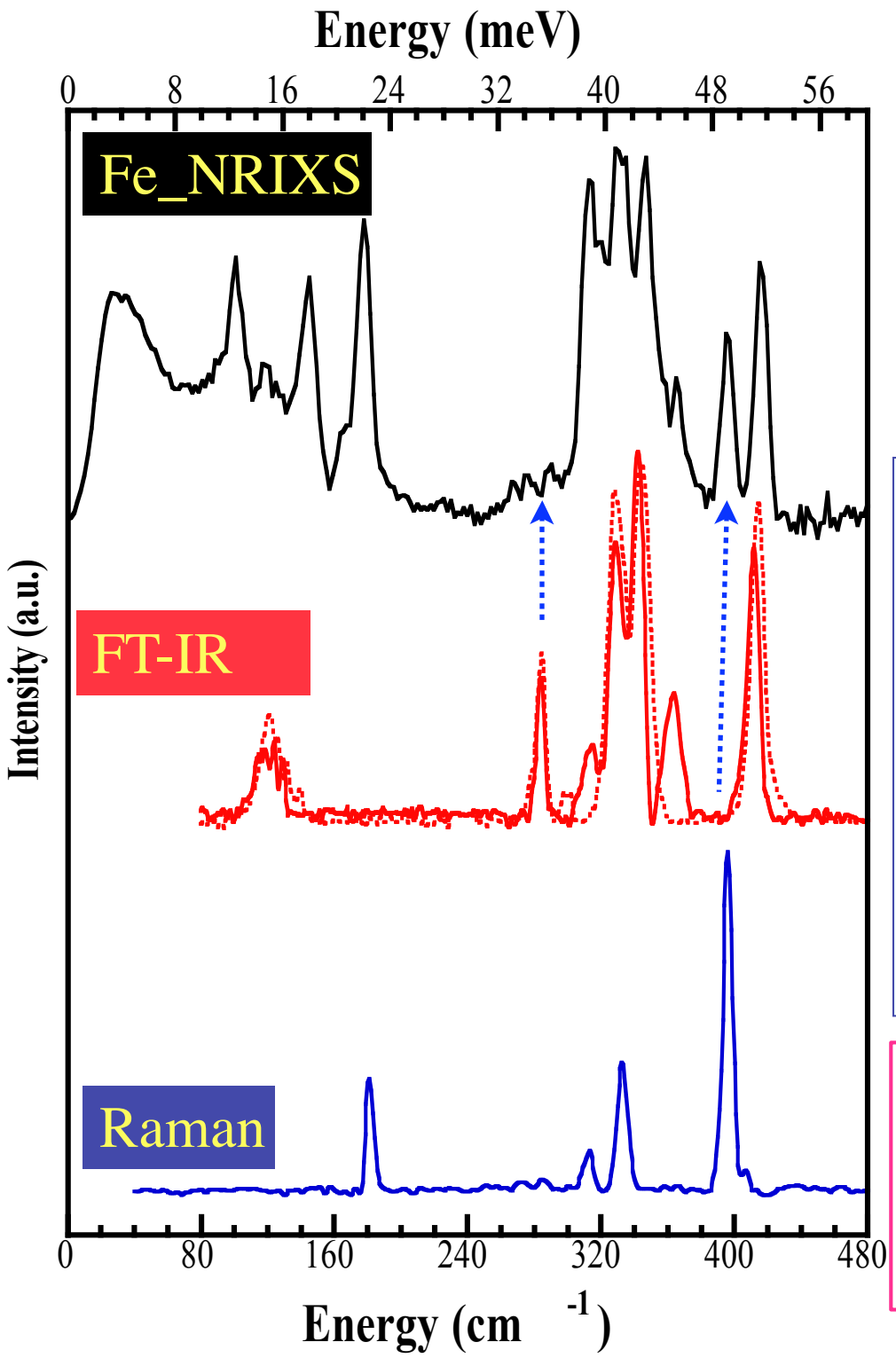

$[NEt_4]_2[Fe_2S_2Cl_4]$.

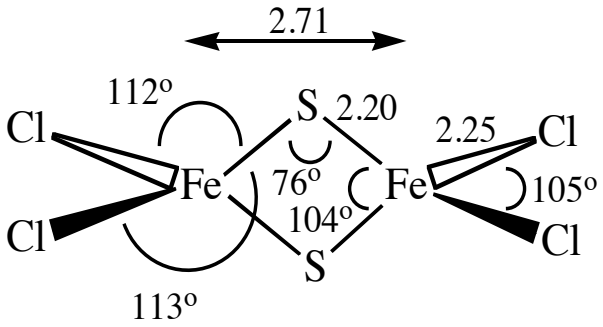

Some unique advantages of NRIXS

1. Low frequency motions: ~ total mass
2. No selection rule except motion of atoms along x-ray propagation
3. Peak intensity ~ mode participation ~ actual displacement
4. No matrix effects or limitations
5. Element and isotope selective
6. No unpredictable cancellations in scattering terms

$$\phi_\alpha = \frac{1}{3}\frac{\bar{\nu}_R}{\bar{\nu}_\alpha} e^2_{j\alpha}(\bar{n}_\alpha + 1) f$$

Matt Smith, et al, Inorganic Chemistry, 2005, 44,5562

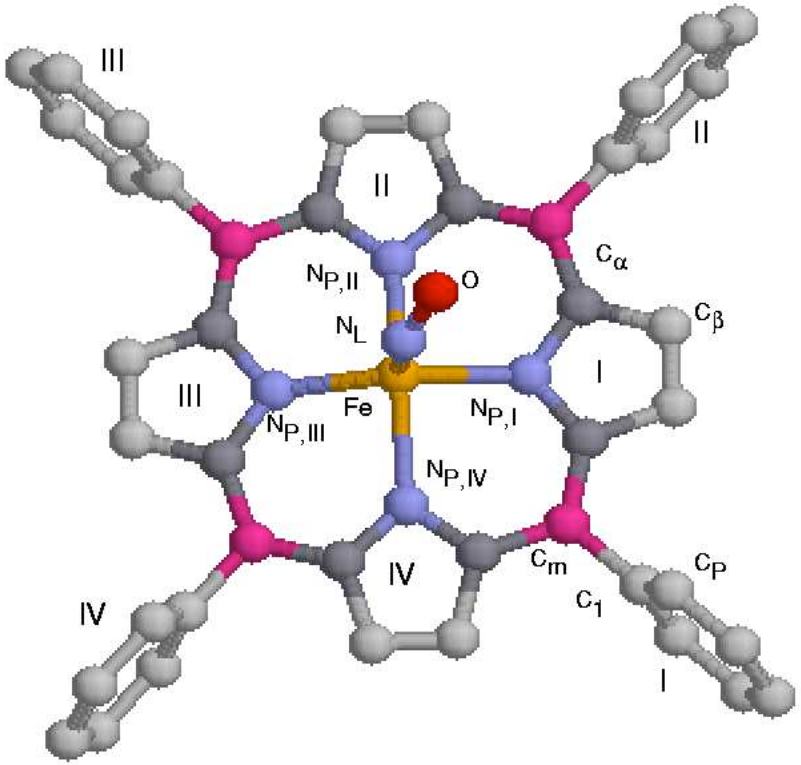

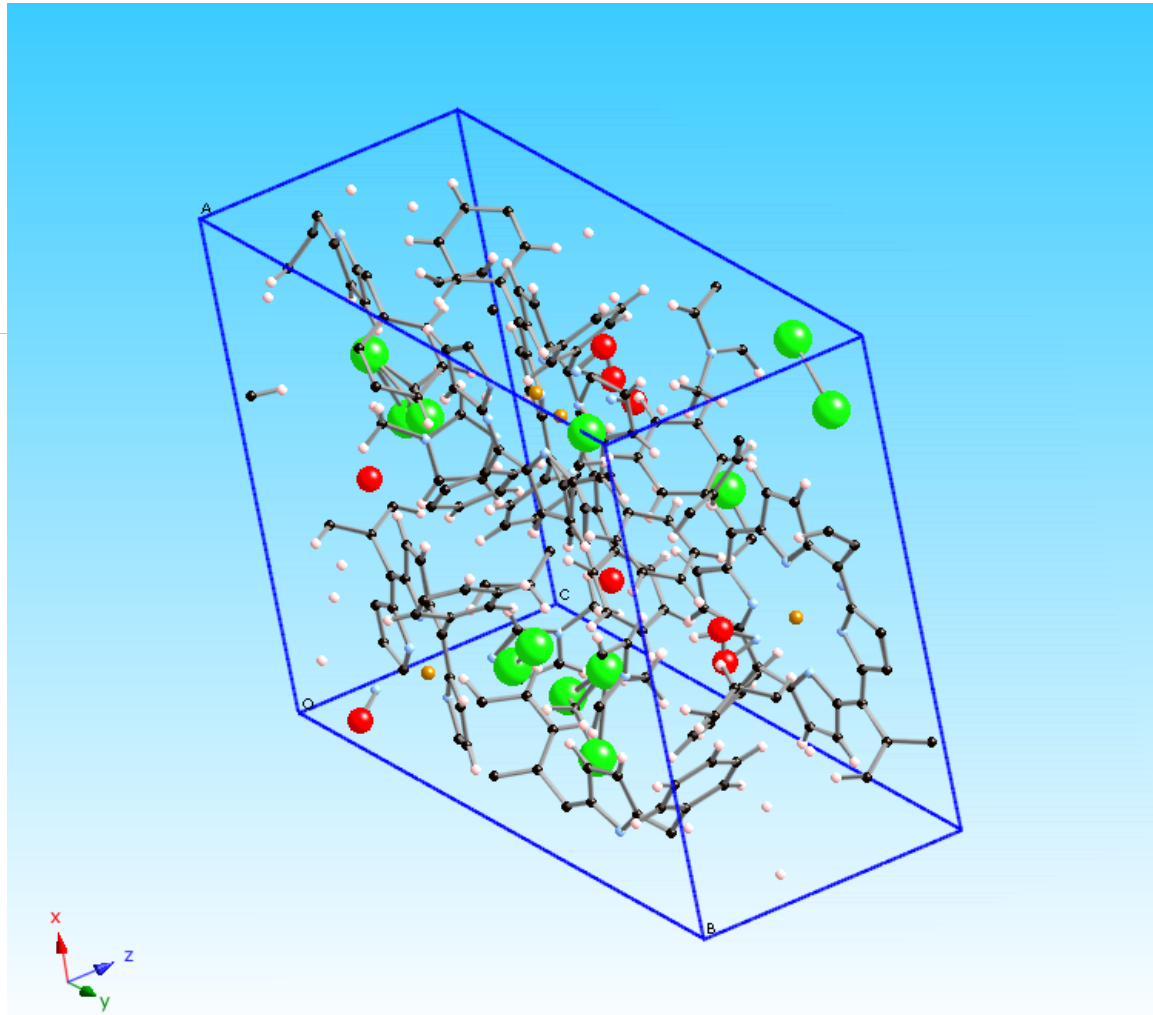

Porphyrins:	A	B
Tetraphenylporphyrin (TPP)	Phenyl	H
Octaethylporphyrin (OEP)	H	Ethyl

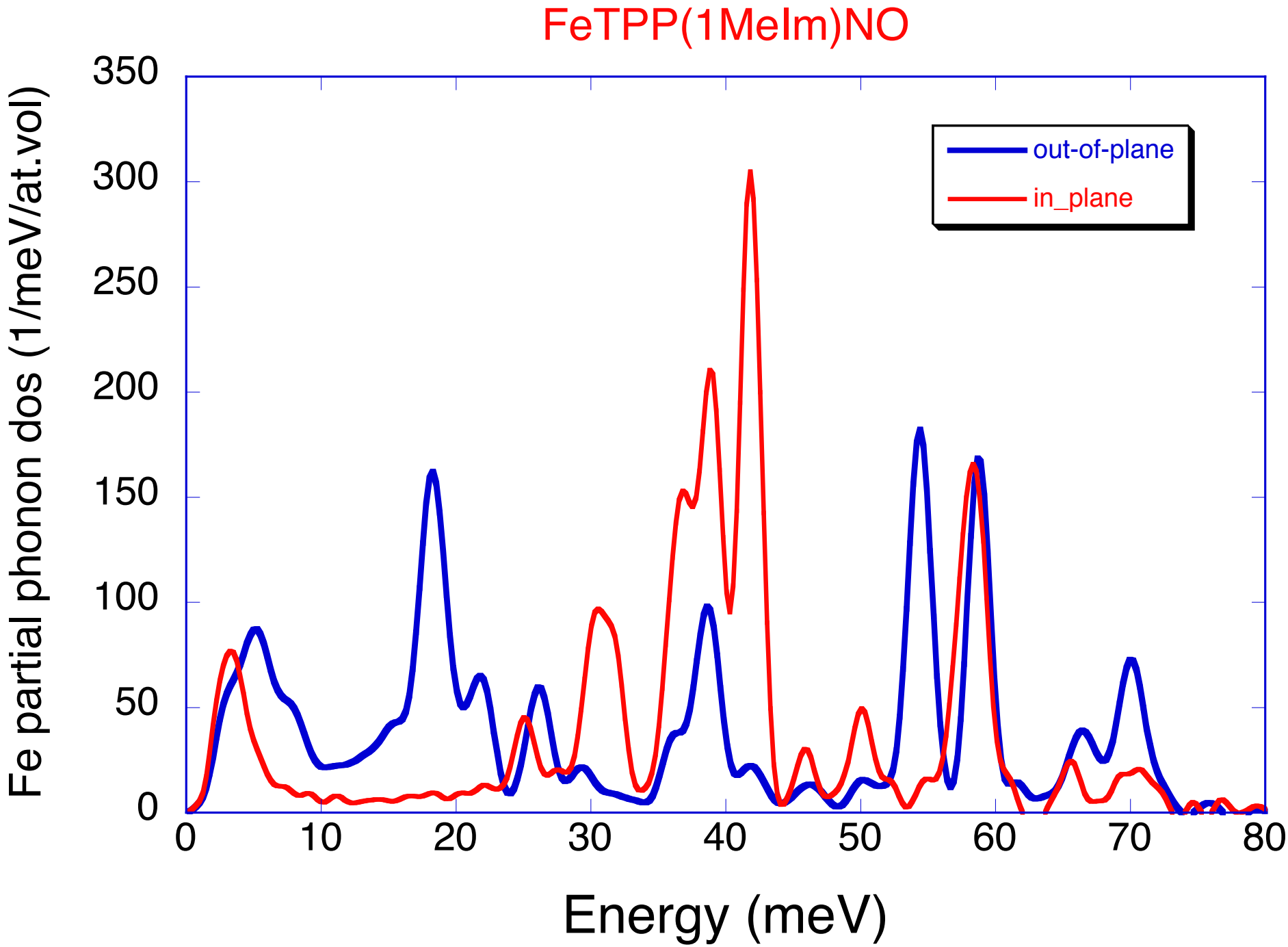
FeTPP(1MeIm)NO
Fe partial phonon dos (1/meV/at.vol)
Energy (meV)
out-of-plane
in_plane
0
50
100
150
200
250
300
350
0
10
20
30
40
50
60
70
80

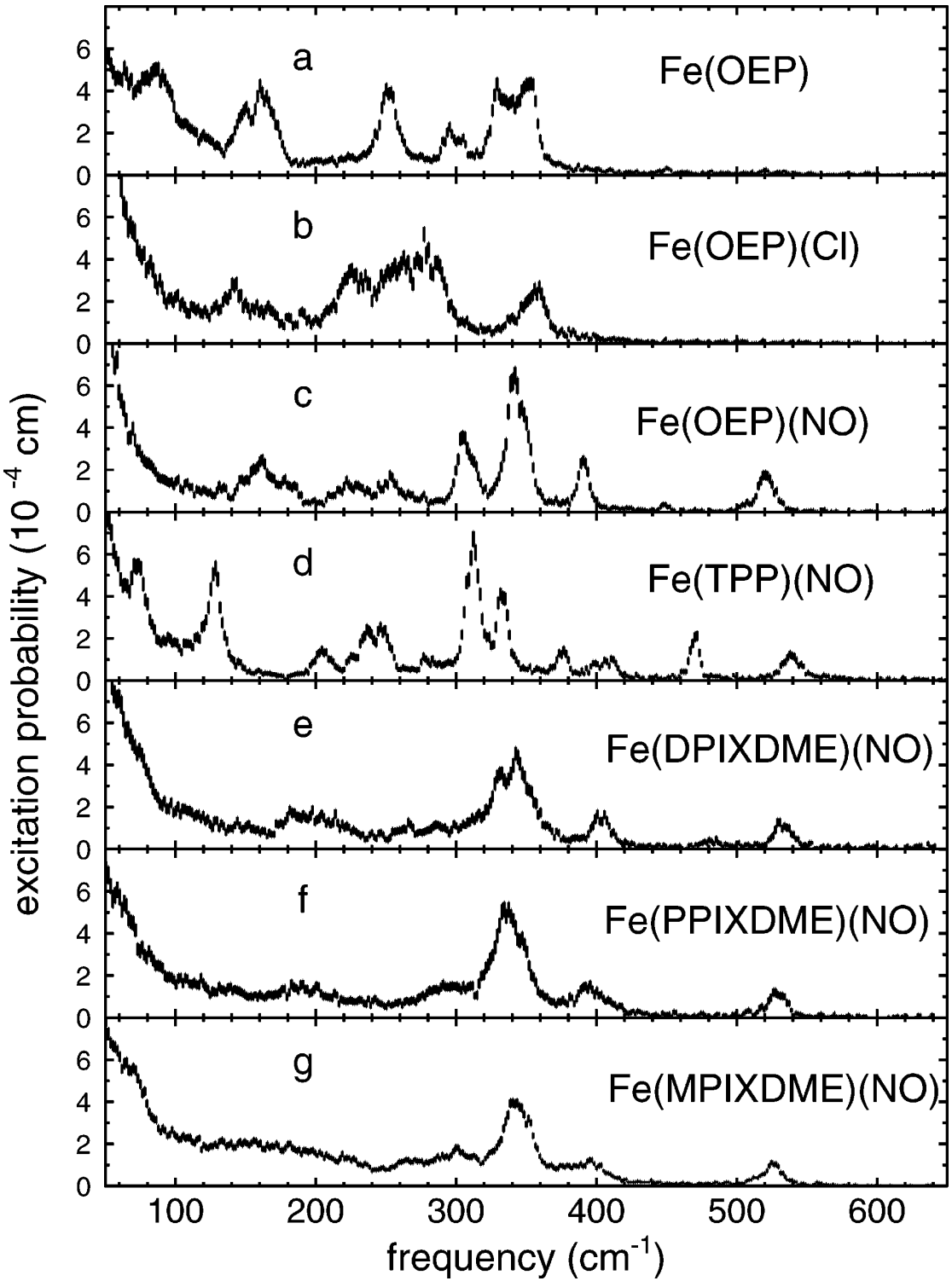

OEP: octaethylporphyrin;

TPP: Tetraphenylporphyrin

DPIXDME, deuteroporphyrin IX dimethyl ester

PPIXDME, protoporphyrin IX dimethyl ester

MPIXDME, mesoporphyrin IX dimethyl ester

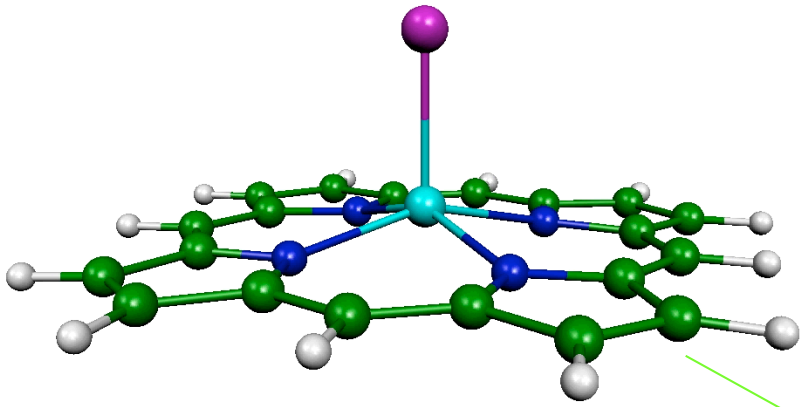

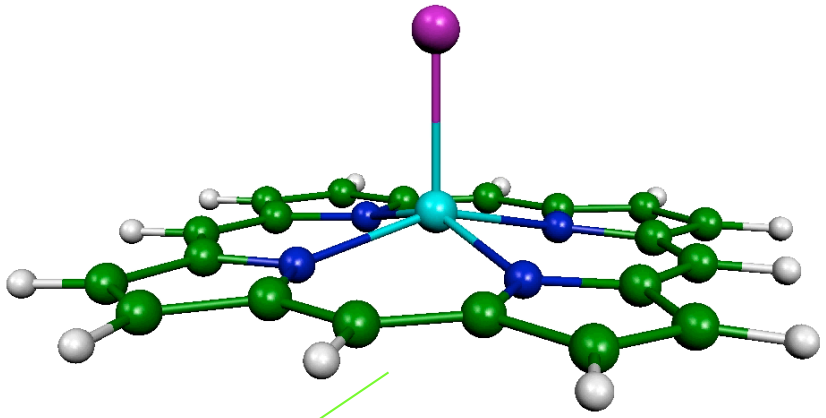

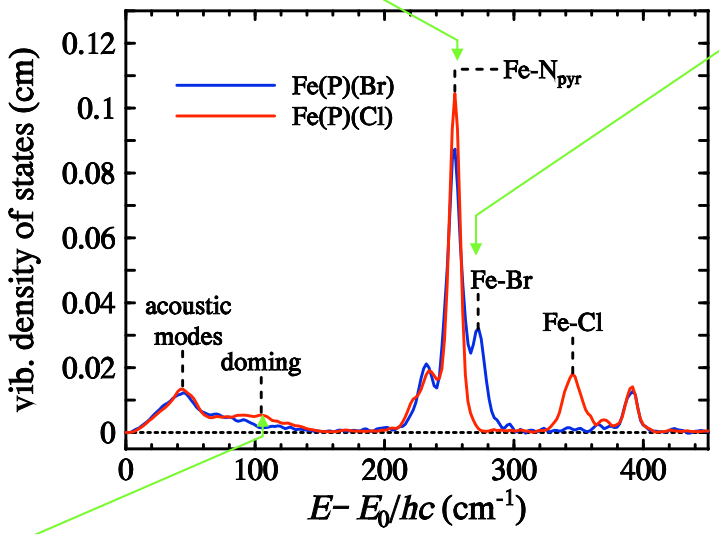
vib. density of states (cm)
0.12
0.1
0.08
0.06
0.04
0.02
0
Fe(P)(Br)
Fe(P)(Cl)
Fe-N$_{pyr}$
Fe-Br
Fe-Cl
acoustic
modes
doming
0
100
200
300
400
$E - E_0/hc$ (cm^{-1})

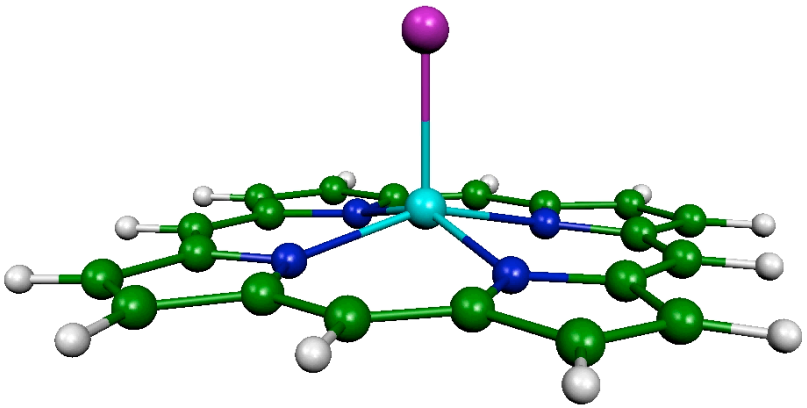

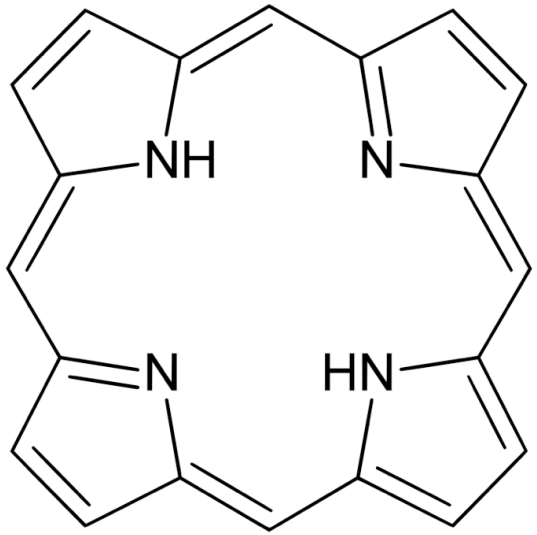
NH
N
N
HN

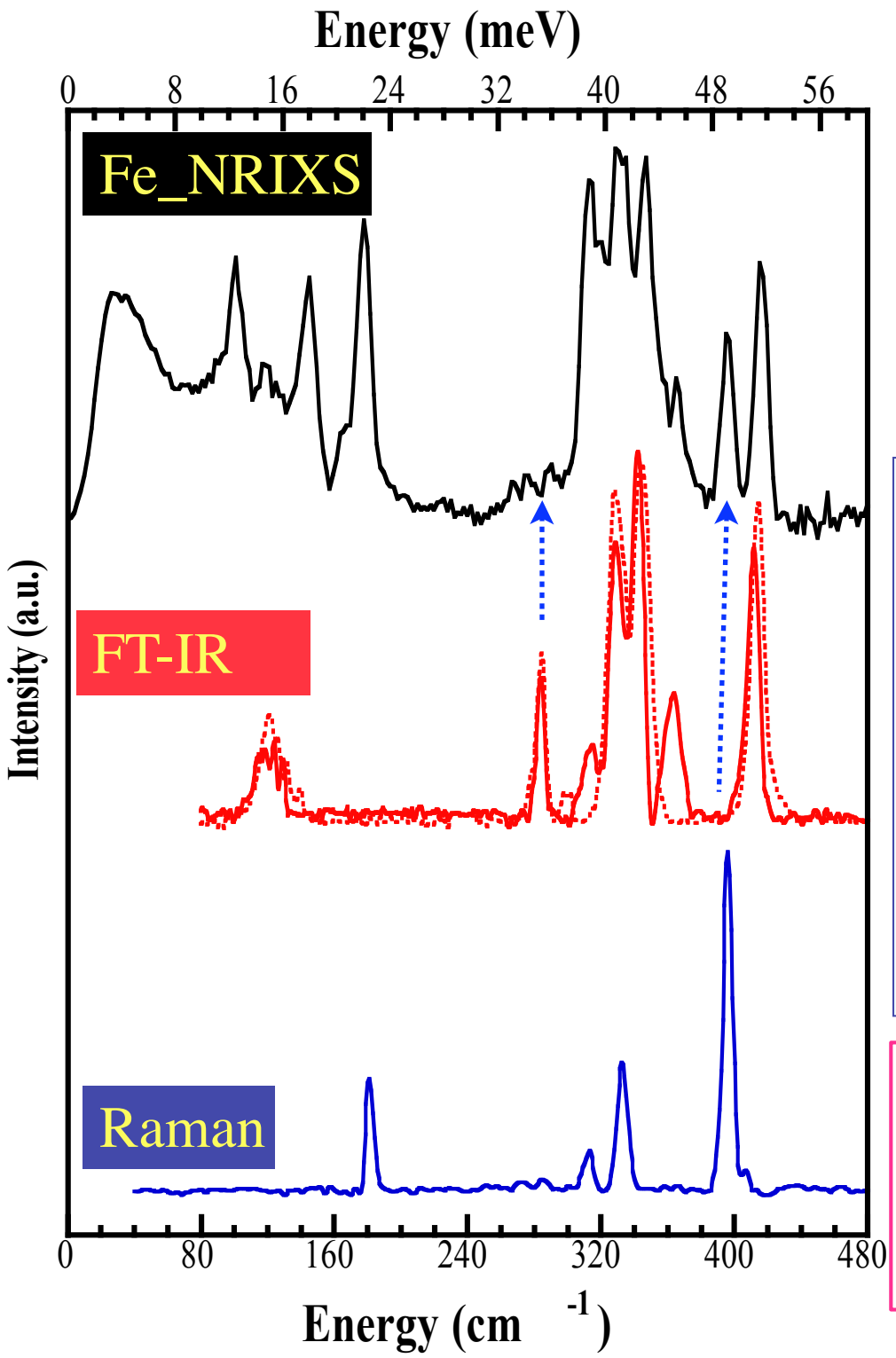

$[NEt_4]_2[Fe_2S_2Cl_4]$.

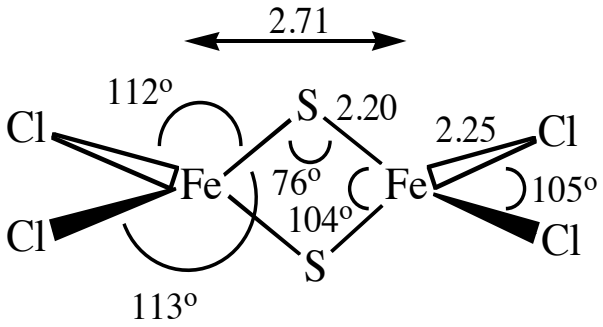

Some unique advantages of NRIXS

1. Low frequency motions: ~ total mass
2. No selection rule except motion of atoms along x-ray propagation
3. Peak intensity ~ mode participation ~ actual displacement
4. No matrix effects or limitations
5. Element and isotope selective
6. No unpredictable cancellations in scattering terms

$$\phi_\alpha = \frac{1}{3}\frac{\bar{\nu}_R}{\bar{\nu}_\alpha} e^2_{j\alpha}(\bar{n}_\alpha + 1) f$$

Matt Smith, et al, Inorganic Chemistry, 2005, 44,5562

~ 0.1meV, all-vacuum high resolution monochromator

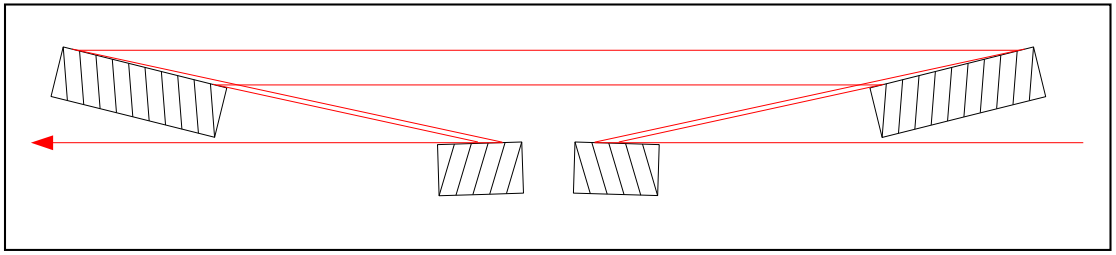

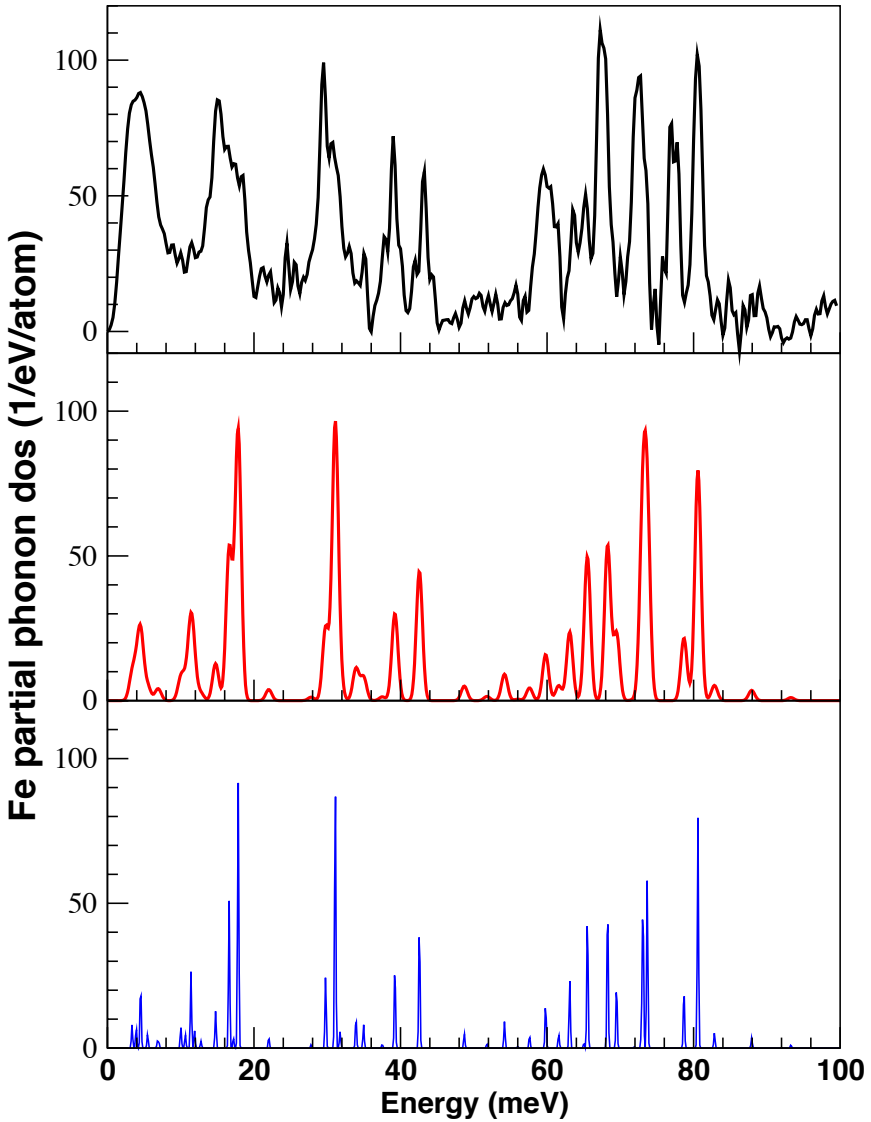

Protonation state of oxo-ligand in heme protein intermediates:

J|A|C|S COMMUNICATIONS

Published on Web 01/18/2008

Synchrotron-Derived Vibrational Data Confirm Unprotonated Oxo Ligand in Myoglobin Compound II

Weiqiao Zeng,† Alexander Barabanschikov,† Yunbin Zhang,† Jiyong Zhao,‡ Wolfgang Sturhahn,‡ E. Ercan Alp,‡ and J. Timothy Sage*,†

J. AM. CHEM. SOC. 2008, *130*, 1816−1817

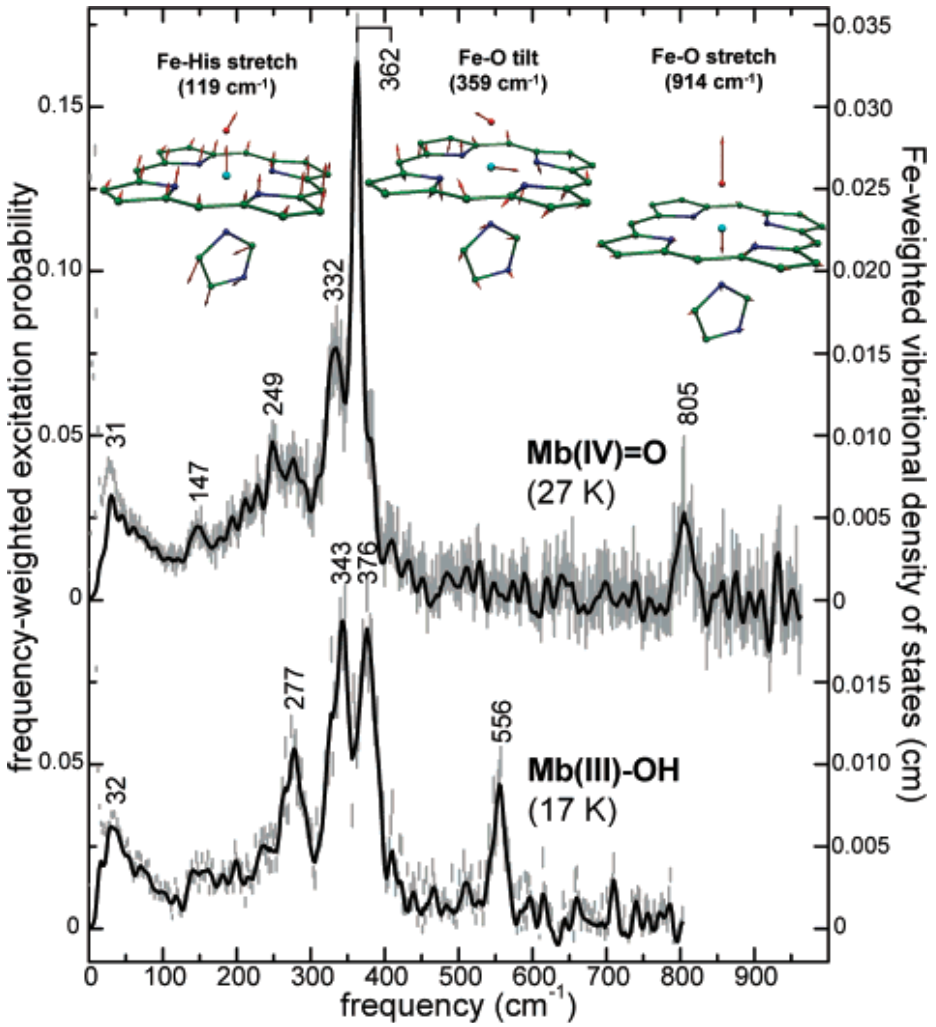

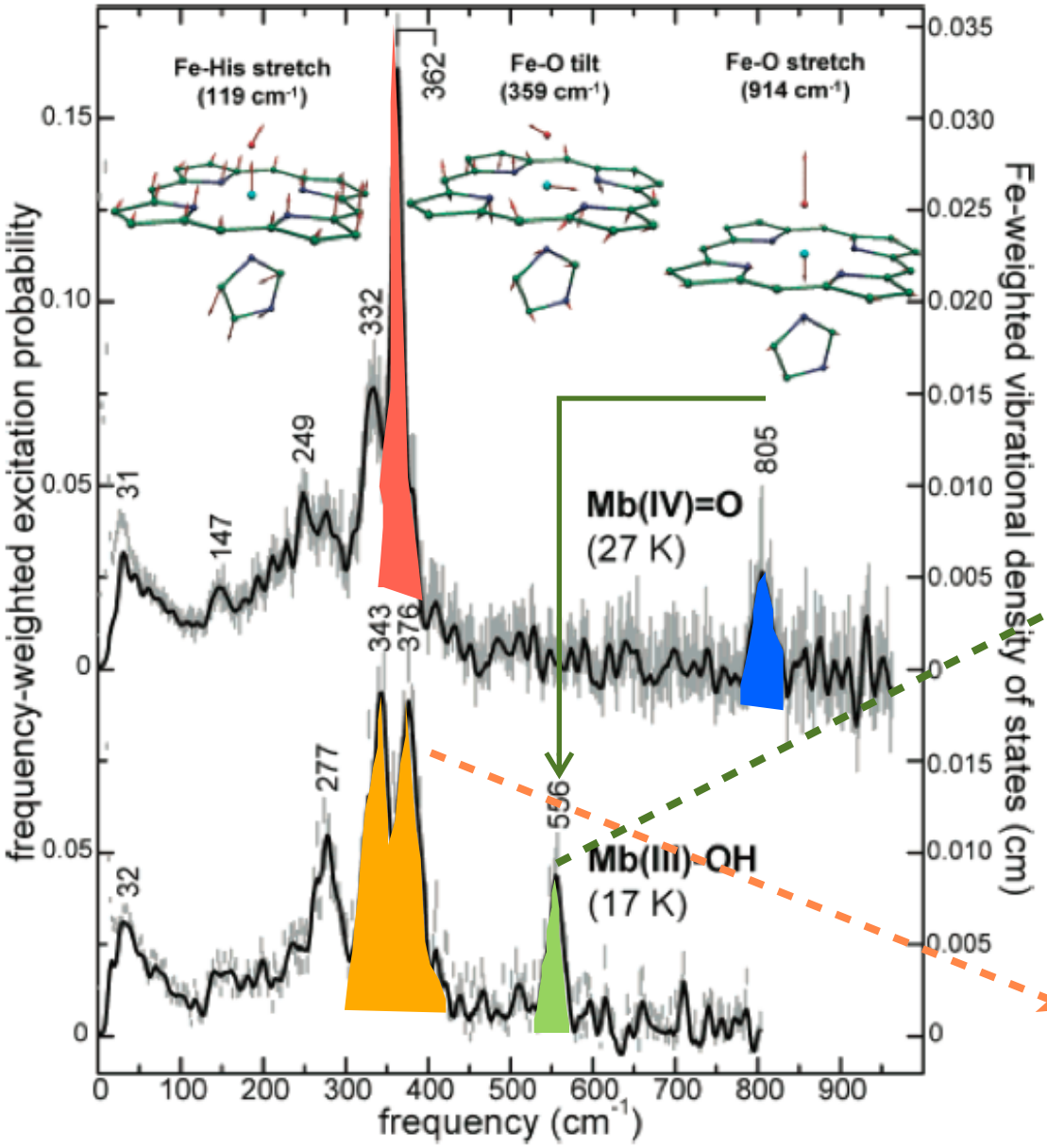

Figure 1. Vibrational dynamics of the heme Fe reveal an unprotonated oxo ligand in Mb(IV)=O, in contrast with the bound hydroxyl group in Mb(III)−OH. Protonation of the oxo ligand results in a downshift of the Fe−O stretching frequency from 805 cm^{-1} to 556 cm^{-1}, and splits the Fe−O tilting vibrations, which are degenerate near 362 cm^{-1} in Mb(IV)=O, but are separated by 33 cm^{-1} in the asymmetrically protonated heme Mb(III)−OH complex. Error bars represent the normalized experimental signal,

Fe-O stretching

Fe-O tilting

Fe-O tilting

Downshift of Fe-O stretching frequency by protonation of oxo-ligand

Lifting of degeneracy of tilting frequency by protonation of the oxo-ligand

The Mössbauer isotopes observed with synchrotron radiation (1985-2016)

Isotope	Energy (eV)	Half-life (ns)	ΔE (neV)	Tabulated E (eV)
^{181}Ta	6215.5	9800.	0.067	6238
^{169}Tm	8401.3	4.	114.0	8409.9
^{83}Kr	9403.5	147.	3.1	9400
^{187}Os	9776.8	2.16	211.	
^{57}Fe	14412.5	97.8	4.67	14413
^{151}Eu	21541.4	9.7	47.0	21532
^{149}Sm	22496.	7.1	64.1	22490
^{119}Sn	23879.4	17.8	25.7	23870
^{161}Dy	25651.4	28.2	16.2	25655
^{129}I	27770.	16.8	27.2	27800
^{40}K	29834.	4.25	107.0	29560
^{125}Te	35460	1.48	308.0	35491.9
^{121}Sb	37129.	4.53	100.0	37133.
^{129}Xe	39581.3	1.465	311.2	39578.
^{61}Ni	67419.	5.1	89.0	67400
^{73}Ge	68752	1.86	245.	68752
^{176}Hf	88349.	1.43	319.4	83000
^{99}Ru	89571.	28.8	15.8	89651.8
^{67}Zn	93300.	9200.	0.049	

Thank you ....